AD-A127 785 DOMAINS AND BOUNDARIES OF PSEUDO-STATIONARY OBLIQUE SHOCK-WAVE REFLECTION. (U) TORONTO UNIV DOWNSVIEW (ONTARIO) INST FOR AEROSPACE STUDIES J LEE ET AL. 1/1

UNCLASSIFIED JUN 82 UTIAS-262 AFOSR-TR-83-0368 F/G 20/4 NL

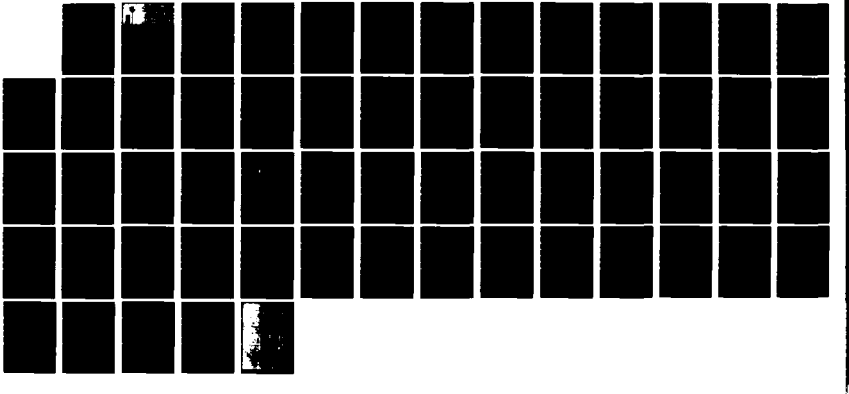

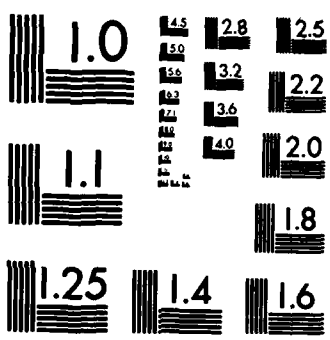

UTIAS

FOR

AEROSPACE STUDIES

UNIVERSITY OF TORONTO

DOMAINS AND BOUNDARIES

OF PSEUDO-STATIONARY UNIQUE SHOCK-WAVE REFLECTIONS IN AIR

by

T. [illegible] and I. I. Glass

REPORT DOCUMENTATION PAGE

READ INSTRUCTIONS BEFORE COMPLETING FORM

1. REPORT NUMBER **AFOSR-TR- 83-0368**	2. GOVT ACCESSION NO. AD-A127785
3. RECIPIENT'S CATALOG NUMBER	
4. TITLE (and Subtitle) DOMAINS AND BOUNDARIES OF PSEUDO-STATIONARY OBLIQUE SHOCK-WAVE REFLECTIONS IN AIR	5. TYPE OF REPORT & PERIOD COVERED Interim
	6. PERFORMING ORG. REPORT NUMBER UTIAS Report No. 262
7. AUTHOR(s) J.-H. Lee and I. I. Glass	8. CONTRACT OR GRANT NUMBER(s) AFOSR 82-0096
9. PERFORMING ORGANIZATION NAME AND ADDRESS University of Toronto, Institute for Aerospace Studies, 4925 Dufferin St., Downsview, Ontario, Canada, M3H 5T6	10. PROGRAM ELEMENT, PROJECT, TASK AREA & WORK UNIT NUMBERS 61102F 2307/A1
11. CONTROLLING OFFICE NAME AND ADDRESS Air Force Office of Scientific Research/NA Bldg. 410, Bolling Air Force Base, DC 20332	12. REPORT DATE June 1982
	13. NUMBER OF PAGES
14. MONITORING AGENCY NAME & ADDRESS(if different from Controlling Office)	15. SECURITY CLASS. (of this report) Unclassified
	15a. DECLASSIFICATION DOWNGRADING SCHEDULE

16. DISTRIBUTION STATEMENT (of this Report)

Approved for public release; distribution unlimited.

17. DISTRIBUTION STATEMENT (of the abstract entered in Block 20, if different from Report)

18. SUPPLEMENTARY NOTES

19. KEY WORDS (Continue on reverse side if necessary and identify by block number)

1. Oblique shock-wave reflections; 2. Domains and transition boundaries; 3. Perfect and real-gas effects; 4. Shock-tube flows.

20. ABSTRACT (Continue on reverse side if necessary and identify by block number)

The reflection of oblique shock waves in air in pseudo-stationary flow was investigated analytically and numerically. The transition boundaries between the four types of shock-wave reflection (regular RR, single Mach SMR, complex Mach CMR and double Mach DMR) were established up to $M_S = 20$ for both perfect and imperfect air in thermodynamic equilibrium (rotation-vibration coupling, vibrational excitation, dissociation, electronic excitation and ionization). In

addition, an analysis was made for perfect gases with differing γ, in order to clarify the effects of the specific-heat ratio γ, on the shock-wave configurations. It was verified that the reflected wave angle ω' was a very sensitive function of γ, and a decrease in γ lowered the value of ω' significantly and even shifted the value of ω' towards negative values under certain conditions of Mach reflection. This phenomenon occurred in a perfect gas with γ less than 1.4 and in imperfect air. However, it was absent in perfect air with $\gamma = 1.4$. An examination of the perfect and imperfect air results shows no crossings of transition lines and removes the conjecture of possible triple-Mach reflection. The present analytical results were compared with the available experimental data for air and nitrogen for shock Mach numbers up to 10. From the available experimental cases, it was clarified, by examining the relaxation lengths behind the shock waves, that the flow states behind the shock fronts, which determined the wave systems for the shock-wave reflection, were frozen or nearly frozen regarding vibrational excitation and dissociation. Consequently, in general, the present perfect-gas analysis agreed with experiment. However, RR persisted, to some extent, below the perfect-gas termination line determined by the detachment criterion, and SMR and DMR did sometimes occur outside their analytically predicted domains. The development of more accurate transition criteria, improvements in the methods of predicting the first triple-point trajectory angle, accurate locations of the kink and triple points along with possible boundary-layer effects on the persistence of regular reflection are problems to be resolved in the future.

DOMAINS AND BOUNDARIES

OF PSEUDO-STATIONARY OBLIQUE SHOCK-WAVE REFLECTIONS IN AIR

by

J.-H. LEE and I. I. GLASS

Submitted April 1982

August, 1982

UTIAS Report No. 262
CN ISSN 0082-5255

Acknowledgements

We are grateful to Mr. R. Deschambault for providing us with some of his excellent experimental results and part of his computational program for his M.A.Sc. thesis. We wish to thank Dr. K. Takayama and Dr. G. Ben-Dor for their advice on the numerical calculations. The assistance received from Mr. M. Shirouzu with some of the calculated results is appreciated.

The financial support received from the U.S. Air Force under Grant AF-AFOSR-82-0096, the U.S. Army Research Office, and the Natural Sciences and Engineering Research Council of Canada is acknowledged with thanks.

Summary

The reflection of oblique shock waves in air in pseudo-stationary flow was investigated analytically and numerically. The transition boundaries between the four types of shock-wave reflection (regular RR, single Mach SMR, complex Mach CMR and double Mach DMR) were established up to $M_s = 20$ for both perfect and imperfect air in thermodynamic equilibrium (rotation-vibration coupling, vibrational excitation, dissociation, electronic excitation and ionization). In addition, an analysis was made for perfect gases with differing γ, in order to clarify the effects of the specific-heat ratio γ, on the shock-wave configurations. It was verified that the reflected wave angle ω' was a very sensitive function of γ, and a decrease in γ lowered the value of ω' significantly and even shifted the value of ω' towards negative values under certain conditions of Mach reflection. This phenomenon occurred in a perfect gas with γ less than 1.4 and in imperfect air. However, it was absent in perfect air with $\gamma = 1.4$. An examination of the perfect and imperfect air results shows no crossings of transition lines and removes the conjecture of possible triple-Mach reflection.

The present analytical results were compared with the available experimental data for air and nitrogen for shock Mach numbers up to 10. From the available experimental cases, it was clarified, by examining the relaxation lengths behind the shock waves, that the flow states behind the shock fronts, which determined the wave systems for the shock-wave reflection, were frozen or nearly frozen regarding vibrational excitation and dissociation. Consequently, in general, the present perfect-gas analysis agreed with experiment. However, RR persisted, to some extent, below the perfect-gas termination line determined by the detachment criterion, and SMR and DMR did sometimes occur outside their analytically predicted domains. The development of more accurate transition criteria, improvements in the methods of predicting the first triple-point trajectory angle, accurate locations of the kink and triple points along with possible boundary-layer effects on the persistence of regular reflection are problems to be resolved in the future.

Contents

Notation

A	RR $\rightleftharpoons$ MR transition line for perfect air
B	RR $\rightleftharpoons$ MR transition line for imperfect air
C	CMR $\rightleftharpoons$ DMR transition line for perfect air
CMR	complex Mach reflection
D	CMR $\rightleftharpoons$ DMR transition line for imperfect air
DMR	double Mach reflection
DMR^+	double Mach reflection with positive reflection angle
DMR^-	double Mach reflection with negative reflection angle
E	SMR $\rightleftharpoons$ CMR transition line for perfect air
F	SMR $\rightleftharpoons$ CMR transition line for imperfect air
G	line $M_1 = 1.0$ for perfect air
H	line $M_1 = 1.0$ for imperfect air
I	incident shock wave
K	kink of reflected shock wave
L	horizontal distance between first-triple-point and vertex of wedge
ℓ	horizontal distance between first-triple-point and kink (or second-triple-point)
ℓ^*	relaxation length
M, M'	Mach stems
M_1	flow Mach number in region (1)
M_{2T}	flow Mach number in region (2) with respect to first-triple-point
M_{2K}	flow Mach number in region (2) with respect to kink
MR	Mach reflection
NR	no reflection
P	reflection point, or pressure
P*	CMR $\rightleftharpoons$ DMR transition line in $(M_s - \chi, \chi')$ plane
Q*	line $\omega' = 0$ in $(M_s - \chi, \chi')$ plane
R	reflected shock wave
R'	second reflected shock wave
R*	$DMR^+ \rightleftharpoons DMR^-$ transition line for imperfect air
RR	regular reflection
S, S'	slipstreams
SMR	single Mach reflection
T	first-triple-point, or temperature
T'	second-triple-point

t	time
x	x-coordinate
y	y-coordinate
α_{O_2}	dissociation degree of O_2
α_{N_2}	dissociation degree of N_2
β	ionization degree of O and N
γ	specific-heat ratio
θ	flow deflection angle
θ_m	maximum deflection angle
θ_s	sonic angle
θ_w	actual wedge angle
θ'_w	$= \theta_w + \chi$, effective wedge angle
ρ	flow density
ϕ	incident angle between flow and shock wave
χ	first-triple-point-trajectory angle
χ'	second-triple-point-trajectory angle
ω'	reflection angle

Subscripts

(0)	flow ahead of incident shock wave I
(1)	flow behind incident shock wave I
(2)	flow behind reflected shock wave R
(3)	flow behind Mach stem M

1. INTRODUCTION

When a planar moving-incident shock wave impinges on a sharp compressive corner in a shock tube, different types of reflection take place depending on the incident shock Mach number M_s and the corner wedge angle θ_w. The four possible types of reflection in pseudo-stationary flows are illustrated in Fig. 1: (a) regular reflection (RR), (b) single Mach reflection (SMR), and in Fig. 2: (a) complex Mach reflection (CMR), and (b) double Mach reflection (DMR). A RR consists of a two-shock configuration (the incident shock wave I and the reflected shock wave R), as shown in Fig. 1(a). However, a SMR has an additional third shock M, referred to as a Mach stem, and a slipstream S, across which pressure and flow direction are continuous but all other flow properties are discontinuous [Fig. 1(b)]. The confluence point T of the four discontinuities in Fig. 1(b) is referred to as the (first) triple point. The CMR wave system is characterized by a kinked reflected shock wave [Fig. 2(a)], whereas the DMR has two reflected shock waves (R and R'), two Mach stems (M and M') and two slipstreams (S and S'), as shown in Fig. 2(b).

In steady supersonic wind-tunnel experiments only RR and SMR have been observed and this distinguishes such flows from nonstationary one-dimensional flows. Ben-Dor and Glass [Refs. 1, 2, 3] concluded that the shock-wave reflections in nonstationary flows also depend on the flow-deflection process over the wedge and this is the prime reason for the existence of CMR and DMR. The incident shock wave is reflected by the wedge surface, whereas the induced nonstationary flow behind it is deflected by the wedge surface. The interaction between these two processes, which take place simultaneously, causes CMR and DMR to occur in nonstationary flows in addition to RR and SMR observed in steady flows.

Extensive studies on the transitions between various types of shock-wave reflections have been done by many researchers in the past. Griffith [Ref. 4] has given a recent review. Von Neumann [Ref. 5] studied theoretically the RR $\rightleftarrows$ MR transition for an inviscid, perfect-gas flow under the concept of self-similarity. He deduced the well-known detachment criterion, i.e., the transition from RR to MR occurs when the flow deflection angle θ_1 through the incident shock wave exceeds the maximum flow deflection angle θ_{2m} through the reflected shock wave.

Henderson and Lozzi [Ref. 6] proposed the alternative criterion, which is referred to as the mechanical-equilibrium criterion for the RR $\rightleftarrows$ MR transition. They investigated the RR $\rightleftarrows$ MR transition problem by using both a wind tunnel and a shock tube. This criterion is attributed to the consideration that the pressure change in the system should be gradual at the transition from RR to MR; in other words, the system remains in *mechanical equilibrium* during the transition. Recently, Hornung, Oertel and Sandeman [Ref. 7] tried to introduce a new criterion with a length scale in the system. However, their criterion and the length scale have not been substantiated. According to the sonic criterion proposed by Hornung et al [Ref. 7], the RR $\rightleftarrows$ MR transition takes place at the sonic deflection angle, the angle of deflection at which the flow behind the reflected shock wave is just sonic relative to the reflection point. Note that the sonic deflection angle and the maximum deflection angle are very close [see Ref. 8]. Therefore, the transition lines predicted by the detachment and the sonic criteria are almost identical and are difficult to resolve experimentally.

The experimental data of Ben-Dor [Ref. 1], Henderson and Lozzi [Ref. 6], Hornung et al [Ref. 7], Smith [Ref. 9], White [Ref. 10] and others support the mechanical equilibrium criterion as the correct RR $\rightleftarrows$ MR transition criterion for steady flows; meanwhile the detachment criterion is accepted as the correct transition criterion for the nonstationary case. Smith [Ref. 9] performed intensive shock-tube experiments for shock-wave reflections. Bleakney and Taub [Ref. 11] revised Smith's data and mapped out the region of RR (two-shock pattern) and Mach reflection MR (three-shock pattern). Some disagreement between the detachment criterion and Smith's experimental results were found, i.e., RR persisted beyond the limit determined by the detachment criterion at low incident shock-wave Mach numbers. This persistence of RR beyond the theoretical limit was observed by Henderson and Siegenthaler [Ref. 12] at similar conditions and a cross-over at a higher pressure ratio.

The attempt of Henderson and Lozzi [Ref. 6] to substantiate the mechanical equilibrium criterion revealed a *remarkable anomaly* between their results from wind-tunnel and shock-tube experiments. They found that RR continued to exist in the shock-tube experiments beyond the limit predicted by both the detachment and the mechanical equilibrium criteria. They resolved the anomaly by postulating that the RR configurations observed beyond the theoretical limit were undeveloped DMR configurations in which all the shock waves, slipstreams and triple-points typical of a well-developed DMR were too close together to be observed. Ben-Dor and Glass [Refs. 2, 3] and Ando [Ref. 13] criticized this hypothesis. based on the experimental results, as doubtful.

If a moving-incident shock wave encounters concave or convex wedges instead of a sharp wedge, a transient effect arises in the RR $\rightleftarrows$ MR transition phenomenon. Since the wedge angle θ_w varies along concave and convex wedges, then the entire process will be transient and the flow is truly nonstationary. The existing criteria (detachment and mechanical equilibrium) for the RR $\rightleftarrows$ MR transition cannot be applied to the truly nonstationary case, since they were based on stationary flow. Ben-Dor and Glass [Ref. 2] hypothesized that in truly nonstationary flows there existed a hysteresis between the RR $\rightarrow$ MR and the MR $\rightarrow$ RR transitions. Ben-Dor et al [Ref. 14] and Itoh et al [Ref. 15] investigated the RR $\rightleftarrows$ MR transition in truly nonstationary flows and confirmed this hypothesis.

When RR terminates, three different types of Mach reflection can occur in pseudo-stationary flows. They are CMR and DMR, in addition to SMR. As noted previously, CMR first noticed by Smith [Ref. 9], and DMR first observed by White [Ref. 10], take place as a result of the interaction between the reflection process at the wedge surface and the flow-deflection process over the wedge corner, which is peculiar to time-dependent flows in a

shock tube. White [Ref. 10] investigated the additional reflection patterns (CMR and DMR) and noticed that both of them were associated with the flow behind the reflected shock wave which was supersonic relative to the triple-point T (i.e., $M_{2T} > 1.0$). A CMR is characterized by a straight reflected shock wave at the triple-point T that is connected to a curved bow wave through a smooth or sharper kink K [Fig. 2(a)]. This pattern is distinguished from that of SMR which has no kink in the reflected shock wave over its entire region [Fig. 1(b)]. A DMR also has a straight reflected shock wave at T, and a secondary reflected shock wave R' emanating from a sharp kink T', a secondary Mach stem M', and a secondary slipstream S' originating at the second-triple-point T' [Fig. 2(b)]. Henderson and Lozzi [Ref. 6] suggested that a *band of compression waves* must exist in a CMR. These compression waves finally converge to a shock wave and DMR occurs when the flow behind the reflected shock wave with respect to the first-triple-point T is supersonic. Gvozdeva et al [Ref. 16, 17] investigated the mechanism for the formation of DMR and erroneously suggested that DMR occurs as a result of the excitation of internal degrees of freedom of the gas molecules behind the reflected shock wave and the Mach stem. Bazhenova et al [Ref. 18] obtained the transition boundary lines for SMR, CMR and DMR experimentally. However, their experimental data were limited to lower Mach number and did not cover a wide range of interest.

Ben-Dor [Ref. 1] and Ben-Dor and Glass [Refs. 2, 3] established the transition criteria which were initiated by Law and Glass [Ref. 19] for the SMR $\rightleftarrows$ CMR and the CMR $\rightleftarrows$ DMR transitions. They suggested that the SMR $\rightleftarrows$ CMR transition occurred when the flow behind the reflected shock wave R was sonic with respect to the first-triple-point T (i.e., $M_{2T} = 1.0$) and that the CMR $\rightleftarrows$ DMR transition took place when the flow behind the reflected shock wave R was sonic relative to the kink K (i.e., $M_{2K} = 1.0$). It must be noted that the kink K, or the second-triple-point T', is formed as a result of the interaction between the shock reflection and the flow-deflection processes. Since the above mentioned criteria for the SMR $\rightleftarrows$ CMR and the CMR $\rightleftarrows$ DMR transitions are deduced without considering that interaction process explicitly, their physical interpretations are still somewhat ambiguous, even though the transition lines predicted by these criteria agree quite well with experimental data for some gases.

Ben-Dor [Ref. 1] and Ben-Dor and Glass [Refs. 2, 3] mapped out analytically the regions of RR, SMR, CMR and DMR in the $(M_S-\theta_W')$-plane, where M_S is the incident shock Mach number and θ_W' the effective wedge angle ($\theta_W' = \theta_W + \chi$, where χ is the triple-point-trajectory angle). They conducted the experiments for the various types of reflection in nitrogen (as a diatomic gas) and argon (as a monatomic gas) over the range of M_S from 1.9 to 8.0. Following the work of Ben-Dor and Glass, Ando [Ref. 13] delineated the regions of the various types of reflection for carbon dioxide (as a linear triatomic gas) in the $(M_S-\theta_W)$-plane and performed the experiments over the range of M_S from 1.8 to 10.2.

It is natural to consider that the real-gas effects due to the excitation of the internal degrees of freedom, vibration, dissociation and ionization may influence the shock-wave system in case of strong shock waves. Gvozdeva et al [Ref. 16] studied Mach reflection in various perfect gases with different specific-heat ratios γ, and in vibrationally excited carbon-dioxide and air. They noted that an increase of the incident shock velocity led to a decrease of the reflection angle ω' [Figs. 1, 2], and becoming negative under certain conditions. Hornung et al [Ref. 7] investigated the RR $\rightleftarrows$ MR transition for dissociating nitrogen and carbon dioxide, and ionizing argon. In addition to real-gas effects, they gave an explanation for the persistence of RR beyond the limit predicted by the detachment criterion in terms of the displacement thickness of the boundary layer on the wall surface in pseudo-stationary flow.

Ben-Dor [Ref. 1] and Ben-Dor and Glass [Refs. 2, 3] studied analytically and experimentally the domains and boundaries between various types of reflection patterns in dissociating nitrogen and ionizing argon under equilibrium conditions. They concluded that real-gas effects had a significant influence on the size of the regions and their boundaries; hence the shock-wave pattern depended on the initial thermodynamic state of the gas (i.e., temperature T_o and pressure P_o) in addition to M_S and θ_W. They conducted shock-tube experiments covering a wide range of M_S and θ_W; however these experiments were not directed sufficiently towards the transition lines of the various types of reflection. Ando [Ref. 13] calculated the regions corresponding to the four types of reflection in carbon dioxide using five models of the equation of state from complete dissociational-vibrational equilibrium to a perfect (frozen) gas. Based on his experimental results in the $(M_S-\theta_W)$-plane, he concluded that real-gas effects played no part in predicting the boundaries between various types of reflection, and hence all transition boundaries had to be determined on the basis of a perfect gas. Ando and Glass [Ref. 20] hypothesized to explain this as follows: The shock fronts in the various wave systems instantly responded to the existing state of the gas. Any further vibrational or dissociational excitation required appropriate relaxation times and if large would not be a contributing factor to the immediate shock shapes at the point of reflection P or triple-point T. Their explanation appears reasonable for nitrogen or even air where the relaxation lengths are large. However, for carbon dioxide this is not the case. Yet, the best agreement in the $(M_S-\theta_W)$-plane occurred for CO_2 as a perfect gas. This casts some doubt on the accuracy of the present criteria, even though they are the best available to date. This will be discussed further by Shirouzu and Glass [Ref. 36] in the near future.

Note that if the relaxation length (i.e., the distance behind the shock wave in which the gas reaches equilibrium and depends on the gas and the initial thermodynamic state) is small compared with the available flow length, the flow is in equilibrium. On the other hand, if the relaxation length is large compared with the region of interest, the flow is frozen. If the relaxation length is comparable to the available flow length, the flow will be in nonequilibrium. Consequently, real-gas effects could affect the location of K and T', or R and R', and awaits analytical and experimental verification.

Several numerical techniques have been proposed

to solve and numerically simulate the full flow fields involving the multiple shock-wave configurations. Auld and Bird [Ref. 21], Schneyer [Ref. 22], Kutler and Shankar [Ref. 23] and Shankar et al [Ref. 24] performed numerical studies on regular and single-Mach reflections using different numerical techniques. Recently Booen and Needham [Ref. 25], Book et al [Ref. 26], Glaz [Ref. 27] and Champney et al [Ref. 28] presented results of numerical calculations simulating complex and double-Mach reflections. The earlier calculated results [Ref. 22-24] showed satisfactory agreement with the actual experimental results in the overall wave shapes and systems. However, they gave rather poor predictions for the flow properties such as the isopycnics and fair agreement for the density profiles along the wall [see Ben-Dor and Glass, Ref. 29]. The later results [Refs. 25-28] show much better agreement for the density along the wall, and improved though still not satisfactory isopycnic shapes and locations. Even though intensive efforts are required to improve the numerical techniques for obtaining solutions with acceptable costs, the numerical methods which are presently evolving will be valuable assets in predicting such complex shock-wave flows in the near future.

The objectives of the present study were as follows:

(1) To predict the domains and transition boundaries of the various types of reflection for perfect and imperfect air in thermodynamic equilibrium in the $(M_s-\theta_w)$-plane.

(2) To clarify the effects of the specific-heat ratio γ on the transition boundaries and the shock-wave configurations.

(3) To investigate the validity and the restrictions of existing transition criteria for the various types of reflection.

(4) To estimate the contribution of real-gas effects to the shock-wave configurations by comparing the analytical results with the available experimental data.

2. ANALYTICAL CONSIDERATION

2.1 Analysis for Pseudo-Stationary Flow

Since the planar incident shock wave I [Figs. 1 and 2] moves with constant velocity along the wedge surface, the entire reflection phenomenon can be considered to be pseudo-stationary in a frame of reference attached to the confluence point of the shock waves. That is, instead of three independent variables x, y and t, the phenomenon may be described in terms of x/t and y/t, and the flow is now self-similar [Bleakney and Taub, Ref. 11]. The variables x and y may be measured relative to any point moving with constant velocity with respect to the wedge corner, and time t is measured from the instant the incident shock wave has passed through the point.

In a pseudo-stationary flow, the entire shock-wave configuration remains similar and grows linearly with time from the instant the incident shock wave collides with the wedge corner. If we pay attention to the flow fields in the vicinity of the confluence point [the reflection point P for RR, Fig. 1(a), or the triple-point T for MR, Fig. 1(b)], the calculations for obtaining the flow properties of each region only require the use of oblique-shock-wave relations for each shock wave. This is based on the assumption that in the angular regions around the confluence point the flow is in a uniform state. The necessary boundary condition for regular reflection (two-shock theory) is that the flow deflections across the incident and reflected shock waves must be equal and opposite, i.e.,

$$\theta_1 + \theta_2 = 0 \tag{1}$$

The boundary conditions for Mach reflection (three-shock theory) are that the total flow deflection across the incident and reflected shock waves must be equal to the flow deflection across the Mach stem, and that the pressures across the slipstream are equal, i.e.,

$$\theta_3 = \theta_1 \pm \theta_2 \tag{2}$$

$$P_2 = P_3 \tag{3}$$

In a MR, it is necessary to give a value to the triple-point-trajectory angle χ as an initial condition in order that the system of equations be closed [Ben-Dor, Ref. 1]. Law and Glass [Ref. 19] proposed an empirical method for predicting the value of χ based on experimental observations. They assumed a straight Mach stem normal to the wedge surface and introduced an additional independent geometrical relation as:

$$\phi_3 = 90° - \chi \tag{4}$$

The above assumption is good in the range $5° \leq \theta_w \leq 45°$ [Ben-Dor, Ref. 1]. However, it is not valid for $M_s < 2$ and $\theta_w \leq 5°$. This restriction will be explained subsequently.

Since the analytical formulations of the two-shock and three-shock theories and the calculation procedures are well known [see Ben-Dor, Ref. 1, and Law and Glass, Ref. 19], none of the details will be given here.

Calculations were performed for the following two cases:

(1) Perfect air with a specific-heat ratio $\gamma = 7/5$.

(2) Thermodynamic equilibrium imperfect air, taking into account rotation-vibration coupling, vibrational excitation, dissociation, electronic excitation and ionization. In this case, the equilibrium calculation of air was made by using the *equilibrium-constant technique* of Hansen [Ref. 30] with 7 species (N_2, O_2, N, O, N^+, O^+, e^-). The mole fractions of other species except nitric-oxide NO are of the order of 0.1 percent, or less in high-temperature air [see Gilmore, Ref. 31, and Laird and Heron, Ref. 32]. The mole fraction of NO may become as much as 10 percent at a pressure of 10 atmospheres and a temperature of about 5000 K. However, this nitric-oxide does not strongly influence the resulting thermodynamic properties of air. Therefore, NO was neglected in the present equilibrium calculation for simplicity. The mole fractions of molecular oxygen and nitrogen in air

at room temperature were assumed to be 0.2 and 0.8, respectively. For the imperfect-air case, the gas is considered to reach a new equilibrium state immediately behind each shock wave around a confluence point.

2.2 Formation and Termination Criteria for the Various Types of Reflection

In order to predict the transition boundaries and the regions of the various types of shock-wave reflection, the following transition criteria were utilized as the most reasonable criteria (confirmed by experiments) to date.

The detachment criterion proposed by von Neumann [Ref. 5] was used for the termination criterion of RR. This criterion is attributed to the concept that the transition from RR to MR occurs when the flow-deflection angle θ_1, through the incident shock wave exceeds the maximum flow deflection angle θ_{2m}, through the reflected shock wave. Analytically, this can be expressed as

$$\theta_1 + \theta_{2m} = 0 \tag{5}$$

For the SMR $\rightleftarrows$ CMR and the CMR $\rightleftarrows$ DMR transitions, the criteria established by Ben-Dor [Ref. 1] and Ben-Dor and Glass [Refs. 2, 3] were applied. They suggested that the SMR $\rightleftarrows$ CMR transition occurred when the flow behind the reflected shock wave R was sonic with respect to the first-triple-point T, and that the CMR $\rightleftarrows$ DMR transition took place when the flow behind the reflected shock wave R was sonic with respect to the kink K. Therefore the SMR $\rightleftarrows$ CMR transition criterion is expressed as

$$M_{2T} = 1.0 \tag{6}$$

and the CMR $\rightleftarrows$ DMR transition criterion as

$$M_{2K} = 1.0 \tag{7}$$

In addition, it is necessary to predict the location of the kink K, in order to obtain the flow velocity behind the reflected shock wave with respect to the kink. Law and Glass [Ref. 19] assumed that the kink K moved with the same horizontal velocity as the induced flow behind the incident shock I. As a result, the ratio ℓ/L, where ℓ is the horizontal distance between the first-triple-point T and the kink K (or the second triple-point T'), and L is the distance between T and the vertex of the wedge [see Fig. 2], becomes equal to the density ratio across the incident shock wave irrespective of the wedge angle θ_w, that is

$$\frac{\ell}{L} = \frac{\rho_o}{\rho_1} \tag{8}$$

where, ρ_o/ρ_1 is the density ratio across the incident shock wave I.

Bazhenova et al [Ref. 18] investigated the ratio ℓ/L experimentally in argon, air and carbon dioxide and found that the relation (8) was valid only in the range $\theta_w < 40°$. Their experimental data for $\theta_w > 40°$ showed that the ratio ℓ/L decreased and approached zero as θ_w increased. This fact was confirmed experimentally by Ando and Glass [Ref. 20]. They concluded that the ratio ℓ/L vanished at the critical wedge angle corresponding to the RR $\rightleftarrows$ MR transition, because the first triple-point T and the kink K (or the second triple-point T') coincided at the RR $\rightleftarrows$ MR transition boundary. Consequently, the SMR $\rightleftarrows$ CMR transition line and the CMR $\rightleftarrows$ DMR transition line must merge at the RR $\rightleftarrows$ MR transition boundary. Further analysis for the prediction of the location of K (or T') at higher wedge angle θ_w is still required in order to analytically modify the CMR $\rightleftarrows$ DMR transition line C [Fig. 3(a)].

3. RESULTS AND DISCUSSIONS

3.1 Analytical Results and Discussions

The transition boundary lines between various types of nonstationary oblique-shock-wave reflection were calculated based on the two-shock and three-shock theories. The aforementioned formation and termination criteria for RR, SMR, CMR and DMR were used along with the basic assumption for the shock-wave configurations.

Figures 3(a) and 3(b) show the domains and transition boundaries for various types of reflection in the $(M_S\text{-}\theta_w')$-plane. Note that the effective wedge angle θ_w' is the sum of the actual wedge angle θ_w and the first triple-point-trajectory angle χ [see Figs. 1, 2]. In the following, the solid boundary lines are for perfect air with $\gamma = 7/5$, while the dashed lines are for air in thermodynamic equilibrium (rotation-vibration coupling, vibrational excitation, dissociation, electronic excitation and ionization) at the *given initial pressure P_o = 15 torr and temperature T_o = 300 K*. The initial values were chosen to correspond to previous work and experimental data. Lines A and B show the RR $\rightleftarrows$ MR transition lines ($\theta_1 + \theta_{2m} = 0$) for perfect and imperfect air, respectively. Lines C and D are the CMR $\rightleftarrows$ DMR transition line ($M_{2T} = 1.0$), while lines E and F are the SMR $\rightleftarrows$ CMR transition lines ($M_{2K} = 1.0$). Lines G and H show the lines of $M_1 = 1.0$, below which no reflection (NR) can occur. It is clear from these figures that the boundary lines for perfect air (lines A, C, E and G) are monotonic and smooth. As the incident shock Mach number M_S increases, these lines level out and become almost independent of M_S. This will be explained subsequently.

It is evident from Figs. 3(a) and 3(b) that real-gas effects shift every boundary line downwards in the $(M_S\text{-}\theta_w')$-plane. That is, the imperfect boundaries begin to drop from their perfect-gas values even at very low incident shock-wave Mach number M_S, owing to vibrational excitation. The line B, for instance, starts to separate from line A at $M_S = 1.40$ and decreases as M_S increases. It must be noted that real-gas effects for air appear more clearly than for pure nitrogen because of the presence of about 20% oxygen, whose internal energy is excited at lower shock Mach numbers than that of nitrogen. Dissociation also occurs at lower shock Mach number in oxygen compared to nitrogen. At higher values of M_S, dissociation of oxygen in air occurs first, followed by nitrogen. Electronic excitation and ionization of dissociated atoms becomes significant at still higher shock Mach numbers. Due to these real-gas effects, the imperfect lines (B, D, F and H) in air have quite different features from those of the perfect-gas lines (A, C, E and G). The imperfect-gas lines

not only decrease but also, in some ranges, increase with increasing M_S, i.e., the lines undulate as M_S increases. The general tendency of the imperfect boundary lines can be understood by considering the density ratio across each shock wave. The density ratio across a normal shock wave in imperfect air increases rapidly but undulates within certain ranges of shock Mach number. This trend becomes significant at lower initial pressures. The same behaviour can be seen in imperfect nitrogen at much higher shock Mach numbers. The first undulation of the density ratio across a normal shock wave occurs at shock Mach numbers of about 10.0 [Ref. 33] in imperfect air. This value depends on the initial pressure. The same undulation, however, takes place at shock Mach numbers of about 19.0 in imperfect nitrogen [Ref. 34].

It must be noted that the steady flow incident Mach number is given by the relation $M_O = M_S/\sin\phi_O = M_S/\cos\theta_w'$ [Fig. 1]. Consequently, M_O becomes stronger with increasing θ_w' for fixed M_S. However, the normal flow Mach number to the incident shock wave is the same as M_S. Therefore, the flow state in the region behind the incident shock wave (region 1) is the same for a given M_S for every type of reflection as shown in Table 1. It is clear from Table 1 that the flow states in the regions behind the reflected shock wave (region 2) and the Mach stem (region 3) depend on the type of reflection. It was estimated that oxygen and nitrogen begin to dissociate at $M_S = 6.1$ and $M_S = 12.8$, respectively, in region 1 at $P_O = 15$ torr and $T_O = 300$ K. In region 2 behind the reflected shock wave, dissociations of oxygen and nitrogen occur at $M_S = 5.0$ and $M_S = 10.0$, respectively, along line B (RR $\rightleftarrows$ MR transition line for imperfect air). On the other hand, the dissociations begin at $M_S = 6.0$ and $M_S = 12.6$, respectively, along line D (CMR $\rightleftarrows$ DMR transition line for imperfect air). Ionization of oxygen atoms and nitrogen atoms (we assumed the same ionization energy for O and N) does not occur until $M_S = 20.0$ in region 1, but it takes place at $M_S = 19$ 5 in region 2 only along line B.

It should be emphasized that for a reflected shock wave R to occur, the flow behind the incident shock wave I must be supersonic with respect to the reflection point P (in the case of RR), or the first triple-point T (in the case of MR). Lines G and H are the lines corresponding to $M_1 = 1.0$ for perfect and imperfect air, respectively. Under these lines, i.e., in the NR domain, shock-wave reflection does not exist. It is reasonable to consider that these lines coincide with the lines $\theta_w = 0$, where the first-triple-point trajectory angle χ has its maximum value χ_{max} for a fixed M_S. If M_S is fixed, χ is a decreasing function with increasing θ_w' (or θ_w), and approaches zero at $\theta_w' = \theta_w = \theta_{wRR\text{-}MR}$ (the critical wedge angle for the RR $\rightleftarrows$ MR transition). Consequently, the NR domain does not exist in practice. That is, MR occurs even when the value of θ_w is very close to zero. We will explain this later in detail in relation to the variation of χ with θ_w. Lines E and F represent the SMR $\rightleftarrows$ CMR transition boundary lines for perfect and imperfect air, respectively. The imperfect line F approaches the imperfect NR line H (where $M_1 = 1.0$) for $M_S > 10.0$. This means that the flow Mach number M_1 behind the incident shock wave decreases to nearly 1.0 (but must be greater than 1.0), and the reflected shock wave becomes a very weak shock wave. For instance, $M_1 = 1.039$ at $M_S = 10.0$ and $M_1 = 1.023$ at $M_S = 16.0$ along the line F.

It is convenient for experimental purposes to draw the boundaries and domains corresponding to the various types of reflection in terms of the incident shock Mach number M_S, and the actual wedge angle θ_w, i.e., in the $(M_S\text{-}\theta_w)$-plane. The formation and termination criteria for RR, SMR, CMR and DMR in the $(M_S\text{-}\theta_w)$-plane are shown in Figs. 4(a) and 4(b). The solid lines are for perfect air with $\gamma = 1.40$, while the dashed lines are for imperfect air at $P_O = 15$ torr and $T_O = 300$ K. As might be expected, every boundary line for imperfect air is shifted down from its perfect-gas value in the $(M_S\text{-}\theta_w)$-plane owing to real-gas effects. This result is analogous to the results for gases with lower values of γ [cf. Figs. 5, 6]. The same type of undulations of the imperfect gas lines occur in the $(M_S\text{-}\theta_w)$-plane as in the $(M_S\text{-}\theta_w')$-plane. The divergence between the perfect and imperfect boundary lines becomes greater with increasing M_S. For example, at $M_S = 5.0$, the corresponding actual wedge angle θ_w to the CMR $\rightleftarrows$ DMR transition boundary is 27.7° for perfect air and is 24.7° for imperfect air or 22.7° for perfect air and 13.0° for imperfect air at $M_S = 10.0$. At higher Mach numbers (especially beyond $M_S = 10.0$), the perfect-gas lines level out so that they become nearly independent of M_S. This can best be understood by referring to the shock polar in the $(\phi\text{-}\theta)$-plane [see Liepmann and Roshko, Ref. 35]. It is seen that for $M_O \rightarrow \infty$ at detachment the deflection angle has a value $\theta_m = 45.6°$ and the wave angle $\phi\theta_m = 67.7°$ for $\gamma = 1.4$. For $M_O > 10$ these values remain almost the same. However, for a reflected wave, $M_2 > 1$, then a new polar has to be drawn for state 2, which must have the same deflection or $\theta_1 = \theta_2$. Consequently, $\theta_w = 90° - \phi_O$ will achieve a limiting value when $\theta_w \sim 50°$ at $M_S > 10$. Under these conditions, $M_S = 6.43$, $M_O = 10.0$, $\theta_1 = \theta_2 = 30.7°$, $\phi_O = 40°$, $M_2 = 2.6$ and $\phi_1 = 65°$. The imperfect-gas lines are strongly dependent on M_S due to real-gas effects. Every imperfect-gas boundary line in the $(M_S\text{-}\theta_w)$-plane, as shown in Figs. 4(a) and 4(b), begins to undulate at high Mach number but they are always located below the corresponding perfect-gas boundary line.

It is worth noting that the SMR $\rightleftarrows$ CMR transition line ($M_{2T} = 1.0$) for imperfect nitrogen at $P_O = 15$ torr and $T_O = 300$ K will be found in the $(M_S\text{-}\theta_w)$-plane between the corresponding line for a perfect diatomic gas with $\gamma = 1.40$ and the line for imperfect air at $P_O = 15$ torr and $T_O = 300$ K. However, the SMR $\rightleftarrows$ CMR and CMR $\rightleftarrows$ DMR transition lines for imperfect nitrogen at $P_O = 15$ torr and $T_O = 300$ K obtained by Ben-Dor [Refs. 1, 2] were drawn incorrectly [see also Ref. 36].

In order to clarify the effects of real gases on the oblique shock-wave-reflection configurations, it is instructive to examine the following perfect-gas cases: (1) monatomic gas ($\gamma = 1.667$), (2) diatomic gas ($\gamma = 1.40$), (3) triatomic gas (CO_2 with $\gamma = 1.290$), and (4) polyatomic gas (SF_6 with $\gamma = 1.093$). It is well known [Ref. 37] that an analogy can be made between real gases and perfect gases with lower values of γ. It will be seen that the boundary lines for real gases and those for lower γ exhibit significant similarities.

Figure 5 shows the RR $\rightleftarrows$ MR transition lines and the SMR $\rightleftarrows$ CMR transition lines in the $(M_S\text{-}\theta_w)$-

plane for perfect gases with different γ, and imperfect air. The CMR $\rightleftarrows$ DMR transition lines are shown in Fig. 6. It is evident from these figures that each transition line for a perfect gas drops significantly with decreasing γ. This can also be understood by referring to the shock polar in the (ϕ-θ)-plane [Ref. 35]. If γ is reduced then the deflection angle θ_m increases and the wave angle $\Phi\theta_m$ also rises until, at $\gamma = 1$, hypothetically the shock wave lies on the body and $\theta_m = \Phi\theta_m = 90°$. However, this time the limiting $M_2 \to 0$. Consequently, as γ is reduced in value θ_w is also reduced in order to meet the condition $\theta_1 = \theta_2$ for the lowered value of M_2. This effect is clearly illustrated in Figs. 5 and 6. All perfect-gas lines level out at higher Mach numbers resulting in a situation in which the perfect-gas lines are nearly independent of M_s. As M_s increases, the specific-heat ratio in imperfect air decreases due to the vibrational excitation and the imperfect lines, as a result, begin to drop from their perfect-gas values with $\gamma = 1.40$. At higher M_s dissociation of oxygen and nitrogen proceeds and the specific-heat ratio (and the equilibrium γ_e) of imperfect air decreases further. The behaviour of the imperfect air lines reveals this tendency very well as can be seen in Figs. 5 and 6. Consequently, the lines are shifted downward with increasing M_s and decreasing γ.

It is worthwhile to examine in detail the first triple-point trajectory angle χ (in the cases of SMR, CMR and DMR), and the second triple-point-trajectory angle χ' (in the case of DMR). We have used the best available analytical methods to date for the prediction of χ developed by Law and Glass [Ref. 19] and for obtaining χ' developed by Ben-Dor [Ref. 38]. In their analyses, they assumed that the Mach stem M was straight and perpendicular to the wedge surface, and that the second triple-point T', with respect to the first triple-point T, moved with the same horizontal velocity as the induced flow behind the incident shock wave I. These assumptions were deduced empirically based on the geometrical relation for the Mach stem and on an approximation for the relative motion of the second triple-point. It must be pointed out, however, that these two assumptions do not hold over the entire ranges of θ_w and M_s as mentioned in Chapter 2.

The values of χ and χ' as a function of M_s, with the actual wedge angle θ_w as a parameter, are shown in Figs. 7(a) and 7(b) up to $M_s = 20.0$ for perfect air with $\gamma = 1.40$. In the following figures, the line P* represents the line $M_{2K} = 1.0$, i.e., DMR does not exist in the region above the line P*. The values of χ' in this region were merely obtained analytically and have no physical meaning. Figures 7(a) and 7(b) show that χ' is, in general, a decreasing function with increasing θ_w and M_s. However, χ' becomes nearly independent of M_s at higher Mach numbers. The same tendency can be seen for χ at actual wedge angles θ_w less than 30°. At wedge angles greater than 30°, the value of χ becomes almost constant over the entire region of M_s. Apparently, χ and χ' are simple functions of the actual wedge angle θ_w at higher Mach numbers, i.e., $\chi = \chi(\theta_w)$ and $\chi' = \chi'(\theta_w)$. It can be clearly seen that for a given θ_w the value of χ' is always greater than that of χ for perfect air with $\gamma = 1.40$.

The dependence of χ and χ' on the incident shock Mach number M_s, for constant θ_w for imperfect air at $P_o = 15$ torr and $T_o = 300$ K, is shown in Figs. 8(a) and 8(b). At low Mach numbers the value of χ and χ' approach those of perfect air with $\gamma = 1.40$. The imperfect-air values of χ and χ' decrease significantly with increasing M_s due to real-gas effects. Undulations are seen again in the values of χ and χ' at higher shock Mach numbers. It is evident that the perfect-air values of χ and χ' are greater than the imperfect-air values. The value of χ' decreases much more rapidly than that of χ as M_s increases, and becomes smaller than the value of χ at higher M_s in the case of imperfect air. As noted above the line P* represents where $M_{2K} = 1$ and along the line Q*, $\omega' = 0$, as explained below.

The reflection angle ω' is defined as an angle between the wall surface and the reflected shock wave in the case of RR [Fig. 1(a)], and as an angle between the trajectory path of the first triple-point and the reflected shock wave in the case of MR [Figs. 1(a), 2(a), 2(b)]. The reflection angle ω' is given as:

$$\omega' = \phi_1 - \theta_1 \qquad (9)$$

where ϕ_1 is the incident flow angle to the reflected shock wave, and θ_1 is the flow-deflection angle behind the incident shock wave. The reflection angle ω' is always positive for RR, SMR and CMR. The shift of ω' from a positive to a negative value with increasing M_s occurs only in the DMR domain for imperfect air or gases with low values of γ. Figures 9(a) and 9(b) show ω' as a function of M_s with θ_w as a parameter for perfect air with $\gamma = 1.40$. It is evident from these figures that ω' is a decreasing function of M_s at lower Mach numbers and becomes independent of M_s at higher Mach numbers. It should be noted that ω' always has a positive value in the case of perfect air with $\gamma = 1.40$. However, quite different features of ω' can be seen for imperfect air. Figures 10(a) and 10(b) show the variation of ω' with M_s up to $M_s = 20.0$ for imperfect air. At lower shock Mach numbers, the variation of ω' is similar to the perfect-air case. However, as M_s increases, ω' decreases rapidly and becomes negative especially for larger θ_w. The constant θ_w lines undulate and cross over owing to real-gas effects. These lead to changes in the incident and flow-deflection angles, which are less sensitive to real-gas effects.

Calculations were performed for χ, χ' and ω' as a function of M_s with θ_w as a parameter for perfect gases with different γ. Figure 11 shows the variation of χ and χ' with M_s for a monatomic gas with $\gamma = 1.667$. The same tendencies which appeared for a diatomic gas with $\gamma = 1.40$ can be seen in Fig. 11. The line P* represents the line $M_{2K} = 1.0$. It can be seen that the value of χ' is always greater than that of χ, i.e., the reflection angle ω' is always positive over the entire range of M_s, as shown in Fig. 12. However, the values of χ' become less than those of χ, and ω' has a negative value above some Mach numbers in the case of a triatomic gas (CO_2 with $\gamma = 1.290$), as shown in Figs. 13 and 14. This tendency becomes more significant with decreasing γ. As can be seen in Figs. 15 and 16, χ' becomes less than χ and ω' has a negative value for a polyatomic gas (SF_6 with $\gamma = 1.093$) at smaller M_s for the same actual wedge angle θ_w, compared with the triatomic gas case. The reflection angle ω' is

shown in Fig. 17 as a function of θ_w for a given Mach number M_s = 10.0. From this figure it is clear that the reflection angle ω' is a very sensitive function of γ and a decrease in γ lowers the value of ω' significantly and shifts the value of ω' into the negative region. An increase in M_s for a constant γ has the same tendency except that ω' reaches a minimum value for a given M_s and γ. However, for a perfect gas with γ larger than or equal to 1.40, ω' cannot become negative. The variation of ω' was made clear by Gvozdeva et al [Ref. 16]. They calculated the reflection angle ω' as a function of the incident shock velocity U_o, and the angle of incidence ϕ_o for several perfect gases with different γ, and for vibrationally excited CO_2 and air.

Here we may classify DMR into two types and define these as follows: DMR with positive ω', as illustrated in Fig. 18(a), is defined as a DMR$^+$ and DMR with negative ω', as illustrated in Fig. 18(c), is defined as DMR$^-$. In DMR$^-$ the second triple-point T' is located below the first triple-point trajectory path. The case where $\chi = \chi'$ or $\omega' = 0$ appears in Fig. 18(b). Figure 18(d) would represent a hypothetical case where $\omega' < 0$ and $\chi' = 0$. The calculated results in the present study may be summarized as follows: DMR$^+$ occurs all the time for perfect gases for $\gamma \geq 1.40$, i.e., in a perfect diatomic gas and a perfect monatomic gas. On the other hand, the transition from DMR$^+$ to DMR$^-$ takes place with increasing M_s in a perfect triatomic gas and in a perfect polyatomic gas. The same transition can be observed in the case of an imperfect diatomic gas owing to real-gas effects at high M_s.

Table 2 shows the shock Mach number M_s corresponding to $\omega' = 0$ [Fig. 18(b)] with θ_w as a parameter. It is clear from Table 2 that the smaller γ gives a smaller M_s corresponding to $\omega' = 0$ for a given actual wedge angle θ_w. Line Q* in Figs. 8(a), 13 and 15 represents the line of $\omega' = 0$ in the ($M_s - \chi$, χ')-planes. The lines of $\omega' = 0$, i.e., the transition lines between DMR$^+$ and DMR$^-$ are shown in the (M_s-θ_w)-plane in Fig. 19 for perfect CO_2, perfect SF_6 and imperfect air at P_o = 15 torr and T_o = 300 K. It must be emphasized that this DMR$^+ \not\rightleftarrows$ DMR$^-$ transition line does not appear in the (M_s-θ_w')-plane or the (M_s-θ_w)-plane for perfect air. The line R* in Figs. 3(a) and 4(a) represents the DMR$^+ \not\rightleftarrows$ DMR$^-$ transition line for imperfect air. This is an important fact that may be valuable in estimating the contribution of real-gas effects to the shock-wave configuration in the case of air. The DMR$^+ \not\rightleftarrows$ DMR$^-$ transition occurs at decreasingly lower shock Mach numbers as γ decreases [see Fig. 19]. Ben-Dor [Ref. 38] developed an analytical method for the prediction of the second-triple-point-trajectory angle χ', and calculated χ' for perfect nitrogen with γ = 1.40 and imperfect nitrogen. Unfortunately, he made a mistake in explaining his result for χ'. The solid lines in Figs. 7, 8, 9 and 11 of Ref. 38 must represent the results for perfect nitrogen, contrary to his explanation, and the dashed lines correspond to imperfect nitrogen at P_o = 15 torr and T_o = 300 K. The discussion which then ensues was based on this error, and the comparison between the values of χ' and χ was not made. However, we can estimate M_s corresponding to $\chi' = \chi$ (i.e., $\omega' = 0$), for a given θ_w, in the case of imperfect nitrogen by comparing the values of χ in Fig. 31 of Ref. 1 with the values of χ' in Fig. 9 of Ref. 38. The line of $\omega' = 0$ in the (M_s-θ_w)-plane for imperfect nitrogen at P_o = 15 torr and T_o = 300 K, as shown in Fig. 19, is located in a much higher M_s region for constant θ_w, compared with the present imperfect-air result.

From the facts described above, a diatomic gas, especially air, may be considered to be an appropriate test gas for estimating real-gas effects on the shock-wave configurations. If we can observe a DMR$^-$ experimentally at high M_s (for $M_s > 6$ at P_o = 15 torr and T_o = 300 K), which does not appear at all in the case of a perfect diatomic gas, it confirms real-gas effects on the shock-wave configurations.

As may be seen in Fig. 15, the second triple-point-trajectory angle χ' becomes zero at θ_w larger than 40° for $M_s < 10$ in the case of perfect SF_6 with γ = 1.093. This means, as illustrated in Fig. 18(d), that the second triple-point T' would attach to the wedge surface, i.e., the reflected shock wave R would strike the wedge surface and be reflected like a RR. The second triple-point T' attaches to the wedge surface at M_s = 6.5 for θ_w = 40° and at M_s = 5.0 for θ_w = 45°. However, it should be pointed out that these points are above the MR termination line in the (M_s-θ_w)-plane for perfect SF_6 as can be seen in Fig. 5. (θ_{wRR-MR} is 40.1° at M_s = 5.0 and θ_{wRR-MR} is 38.9° at M_s = 6.5, where θ_{wRR-MR} is a critical angle for the RR $\not\rightleftarrows$ MR transition.) Therefore, a reflection of the type shown in Fig. 18(d) cannot exist in practice. This will be explained subsequently in relation to the two- and three-shock theories.

As noted previously, there are mainly two different criteria which exist for the termination of RR. The first one is known as the detachment criterion, and the second one is referred to as the mechanical equilibrium criterion which was found experimentally to be inapplicable to nonstationary flows. Note that the detachment criterion is based on the two-shock theory [Ref. 5] and the mechanical equilibrium criterion originates in the three-shock theory [Ref. 6]. In order to clarify the difference between these two criteria, the termination lines of RR(MR) in the (M_s-θ_w)-plane are drawn as a function of M_s in Fig. 20 for a perfect diatomic gas with γ = 1.40. As is evident from Fig. 20, the actual wedge angle θ_w corresponding to the mechanical equilibrium criterion is larger than the detachment criterion over the entire range of M_s. In the region between the detachment and mechanical equilibrium criteria, MR may exist if we apply the mechanical equilibrium criterion as the MR termination criterion. In other words, we can obtain analytically MR with a finite value of χ in this region using the three-shock theory. However, the detachment criterion must be applied as the MR termination criterion for nonstationary flows. Therefore, MR cannot exist above the MR termination line determined by the detachment criterion for the nonstationary case. Consequently, if M_s is fixed while increasing the actual wedge angle θ_w, the first triple-point-trajectory angle χ decreases monotonically and must drop to zero discontinuously at $\theta_w = \theta_{wRR-MR}$. Note that χ and χ' were calculated based on three-shock theory. The points corresponding to $\chi' = 0$ are above the MR termination line in the (M_s-θ_w)-plane [Fig. 5] and therefore they do not exist in practice.

On the other hand, if one starts at a fixed shock Mach number M_s and decreases the actual wedge angle θ_w, then the first triple-point-trajectory

angle χ increases monotonically, as can be seen in Figs. 7(a), 8(a), 11, 13 and 15. The values of χ as a function of M_S for very small θ_w are shown in Fig. 21* for a perfect diatomic gas with $\gamma = 1.40$. For fixed M_S, χ increases monotonically as θ_w decreases. A dot-dashed line in Fig. 21 represents the line of $M_1 = 1.0$, which corresponds to the critical line for the existence of a reflected shock wave R and also may be considered as the line for which the critical wedge angle $\theta_w = 0°$. Consequently, the line of χ for a given θ_w terminates at the $M_1 = 1.0$ line (the critical value of χ for $\theta_w = 0°$),and when $\theta_w \to 0°$ this line must merge with the $M_1 = 1.0$ line. As is evident in Fig. 21, the value of χ predicted by the method of Law and Glass [Ref. 19] monotonically approaches the $M_1 = 1.0$ line with decreasing θ_w for $M_S > 2.0$. However, the value of χ becomes larger than the $M_1 = 1.0$ line at M_S smaller than 2.0 for very small actual wedge angles ($\theta_w \lesssim 5°$). Ben-Dor [Ref. 1] proposed an alternative method to predict χ for very small wedge angle ($\theta_w \leq 4°$) empirically as follows:

$$\chi = \theta'_{wM_1=1.0} - \theta_w \qquad (10)$$

where $\theta'_{wM_1=1.0}$ is the effective wedge angle corresponding to $M_1 = 1.0$. This method, however, is quite an artificial one and is inconsistent with the method developed by Law and Glass [Ref. 19] for predicting χ. A better method for predicting the correct value of χ at smaller M_S and θ_w is still required.

3.2 Comparison of Analytical Results with Available Experimental Results

In the following, the present analytical results of pseudo-stationary oblique shock-wave reflection are compared with experiment. Figure 22 is a reproduction of Fig. 3(a) and represents the domains and transition boundaries for various types of reflection in the $(M_S\text{-}\theta'_w)$-plane. The solid lines are perfect air with $\gamma = 7/5$, while the dashed lines are for imperfect air with a given initial pressure $P_o = 15$ torr and a temperature $T_o = 300$ K. The experimental data of Deschambault for air [Ref. 39] and the data of Ben-Dor for nitrogen [Ref. 40] are plotted in Fig. 22 to check the present analysis for the transition boundaries. Deschambault [Ref. 39] conducted interferometric experiments for air in the UTIAS hypervelocity shock tube with a 10cm × 18cm cross-section. The initial temperatures T_o were nearly 300 K and pressures were in the range 5.0 torr $\leq P_o \leq$ 785.5 torr. The incident shock Mach number range covered was $1.2 \leq M_S \leq 10.3$ over a series of wedge angles $2.0° \leq \theta_w \leq 63.4°$. The initial conditions and the experimental results are summarized in Table 3. It is evident from Fig. 22 that the experimental data, except for RR and one or two other points, lie inside the domains predicted by the perfect-gas model. It can be seen that RR persists below the perfect RR $\rightleftarrows$ MR transition line determined by the detachment criterion. This persistence of RR at low shock Mach numbers was called "von Neumann's paradox" [Refs. 4, 9, 11]. It is clear from the experimental results for air that"von Neumann's paradox" also exists at higher shock Mach numbers.

The possibility exists that RR occurs below the analytical terminating boundary line for perfect air for all M_S. However, a detailed and careful set of experiments must be performed at higher M_S for $\theta_w < 50°$ to verify this point. A comparison of the experimental results show good agreement with all the other perfect-gas boundary lines, except for the perfect RR $\rightleftarrows$ MR transition line. It should be stressed that these results for θ'_w do not require the measurement of χ and can be considered more accurate than plots of θ_w [cf. Fig. 23].

The experimental results of Deschambault [Ref. 39] for air (see Table 3 for details) as well as the data of Ben-Dor [Ref. 40] for nitrogen are plotted in the $(M_S\text{-}\theta_w)$-plane in Fig. 23 [a reproduction of Fig. 4(a)]. It is noted from Fig. 23 that several SMR points lie in the domain corresponding to CMR. For air, SMR were observed at $M_S = 3.0$ for $\theta_w = 20°$ and at $M_S = 6.41$ for $\theta_w = 10°$. Meanwhile, Ben-Dor reported SMR for $\theta_w = 10°$ at $M_S = 5.92$, 6.79 and 7.58. On the other hand, several of the data points for air lie below the perfect CMR $\rightleftarrows$ DMR transition line. That is, Deschambault observed DMR configurations at $M_S = 3.79$ for $\theta_w = 30°$, at $M_S = 3.84$ and 4.77 for $\theta_w = 27°$, and at $M_S = 8.85$ for $\theta_w = 20°$. It was not possible to redo some of these experiments to check their repeatability at high M_S owing to possible damage to the interferometric-quality windows. Some experimental points for air even lie below the imperfect CMR $\rightleftarrows$ DMR transition line. These facts suggest that the existing criteria for the SMR $\rightleftarrows$ CMR transition ($M_{2T} = 1.0$) and the CMR $\rightleftarrows$ DMR transition ($M_{2K} = 1.0$) might be necessary but not sufficient conditions for these transitions [see Ref. 36]. Further investigation regarding this point is necessary. Apart from this disagreement and the persistence of RR below the detachment criterion, the experimental points, in general, lie inside of their domains predicted by the perfect-gas model in the $(M_S\text{-}\theta_w)$-plane [Fig. 23]. Consequently, the analysis as given in Refs. 1-3 is reasonable, if not precise, in modelling the actual physics of the problem.

Figure 24 shows the experimental data in the $(M_S\text{-}\theta_w)$-plane for air, nitrogen and oxygen from several sources [Refs. 9, 18, 19, 39 and 40] in the range $1.0 < M_S \leq 3.0$. It is evident from the data of Smith [Ref. 9] that RR persists even below the imperfect detachment line at $P_o = 15$ torr and $T_o = 300$ K. Note that the contribution of real-gas effects is merely due to vibrational excitation of oxygen and nitrogen molecules in this shock Mach number range. Although Smith had noticed a CMR configuration, he did not distinguish between SMR and CMR, and referred to them as MR. Except for RR, the experimental points appear to lie well inside of the analytically predicted domains for $M_S \leq 3.0$. However, had Smith distinguished between SMR, CMR and DMR we might have seen some discrepancies. For example, Deschambault [Ref. 39] observed a DMR configuration at $M_S = 2.08$ for $\theta_w = 49°$, in which the data point was located in the CMR domain. This fact supports the hypothesis of Ando and Glass [Ref. 20] for results in CO_2 that the SMR $\rightleftarrows$ CMR and CMR $\rightleftarrows$ DMR transition lines meet at the RR $\rightleftarrows$ MR transition boundary. However, more experimental data in the CMR domain for $\theta_w \geq 40°$ are required in order to have additional evidence.

Figure 25 shows the predicted values of χ and χ' versus M_S for $\theta_w = 27°$ and 40° and their

*The authors are grateful to Mr. M. Shirouzu for performing the calculation of χ for $\theta_w \lesssim 5°$.

comparison with experiment. In this figure the solid lines are for perfect air with $\gamma = 7/5$, while the dashed lines are for imperfect air at $P_o = 15$ torr and $T_o = 300$ K. The experimental results for air from Ref. 39 and nitrogen from Ref. 40 are plotted. It is clear from Fig. 25 that the experimental data of χ and χ' for $\theta_w = 27°$ agree reasonably well with the perfect-gas values over the entire range of M_s. However, for $\theta_w = 40°$ the agreement is only good for $M_s < 6$. For the range $M_s \geq 6$ the agreement becomes worse, and the experimental values of χ and χ' deviate from the values predicted by the perfect-gas model. It is worth mentioning that the method for predicting χ proposed by Law and Glass [Ref. 19] is only good in the range $\theta_w < 40°$ [Bazhenova et al, Ref. 18], and that the values of χ and χ' are relatively small at higher wedge angles which might lead to noticeable experimental error. The calculated and measured values of reflection angle ω' are plotted as a function of M_s for $\theta_w = 27°$ and $40°$ in Fig. 26. The experimental points for air lie close to the solid lines (perfect gas) with $\gamma = 7/5$. It should be noted that DMR^-, which may occur in imperfect air, and the $DMR^+ \not\rightleftarrows DMR^-$ transition ($\omega' = 0$) depend on the initial thermodynamic conditions. Such transitions were not observed in experiments in air [Ref. 39] or nitrogen [Ref. 40] in the range $M_s \leq 10$. That is, χ' is always greater than χ, and therefore ω' is always positive [see Table 3 of present report and Table 2(a) of Ref. 40], again confirming that real-gas effects were not significant.

As mentioned previously, the transition from DMR^+ to DMR^- occurs with increasing M_s in a perfect gas with γ less than 1.40. The calculated values of reflection angle ω' for a perfect gas with $\gamma = 1.290$ were compared with the available experimental data for CO_2 [Table 2 of Ref. 13] in Fig. 27. It is evident from Fig. 27 that the experimental data for the reflection angle ω' decreases rapidly and becomes negative for $M_s \gtrsim 4$. Ando plotted the difference $\Delta\omega'$ between the predicted and measured ω' for CO_2 [see Appendix F of Ref. 13]. He showed that the predicted value of ω' based on the perfect-gas model with $\gamma = 1.290$ deviated from the measured values significantly for $M_s \gtrsim 3.5$. The quasi-equilibrium models, taking into account the excitation of the vibrational modes, agreed best with experiment for ω' [Ref. 13], since real-gas effects contribute at $M_s \geq 3.5$ in CO_2.

This is confirmed in Ref. 36 where the vibrational effects on ω' are also plotted in a different form. The experimental data is in good agreement with this plot, as shown in Fig. 27 for the case of ω' for a set of wedge angles of 20°, 30° and 40° for CO_2 in vibrational equilibrium. Better agreement is obtained at the higher angles since the analytical curves lie closer together in that range. In addition, the fact that the plot has θ_w rather than θ_w' as a variable also adds to deviations since χ must be known to obtain θ_w but not θ_w'. Consequently, any errors in the analytical results for χ will also show up in this plot. On the whole though, the agreement is quite good. Consequently, even though the types of reflections agree best with $\gamma = 1.290$ in Ref. 13, the measurements of ω' are much more basic as they agree with the relaxation lengths. This raises a question as to the validity of the perfect-gas transition lines for CO_2 in the $(M_s\text{-}\theta_w')$ and $(M_s\text{-}\theta_w)$ planes.

It is worthwhile to examine the relaxation lengths behind the shock waves. The relaxation length for vibrational or dissociational excitation which depends on the gas used and the initial thermodynamic conditions, is an important factor in estimating the state of the gas behind the shock-front. If the relaxation length behind a shock wave is large compared with the shock thickness, which is on the order of a few gas mean-free-paths, the state of the gas at the shock front can be considered as frozen. On the other hand, if the relaxation length is negligibly small (order of mean-free-paths), the state of the gas behind the shock-front is in equilibrium. Various reports exist dealing with vibrational and dissociational relaxations in N_2, O_2 and air [Refs. 41-44]. The relaxation lengths behind a normal shock wave versus M_s are plotted in Fig. 28 for the various excitation modes (vibrational excitation for O_2 and N_2, and dissociational excitation for O_2, N_2 and overall air). These curves are for the initial conditions of $P_o = 10$ torr and $T_o = 300$ K, and were obtained on the basis of the above theoretical and empirical analyses [Refs. 41, 43, 44]. From Fig. 28, we can estimate the relaxation lengths behind shock waves for the experimental cases of air [Ref. 39] and nitrogen [Ref. 40]. Table 4 shows the vibrational and dissociational relaxation lengths behind the incident shock wave in the case of air [Table 3] for $M_s > 5$. It is evident from Table 4 that the relaxation lengths except for O_2 vibration are large. The shortest relaxation length for O_2 vibration is 0.05 mm (Exp. #416), and $\ell^*_{O_2 vib}$ of other cases are in the range of $0.15 \sim 13$ mm. Consequently, we can estimate that the state of the gas at the incident shock-front is nearly frozen. Only the O_2 vibrational mode may be partially excited. The mole fraction of oxygen molecules in air is about 20%; therefore, the partial excitation of O_2 vibration may not significantly influence the resulting thermodynamic state of air at the shock-front.

Table 5 shows the vibrational relaxation length $\ell^*_{N_2 vib}$ behind the incident shock wave for the case of nitrogen [Table 2(a) of Ref. 40] for $M_s > 5$. The relaxation lengths for N_2 vibrational excitation are quite large (the shortest $\ell^*_{N_2 vib}$ is 69 mm). The relaxation lengths behind the Mach stem (in the case of MR) can be considered to be of the same order of magnitude as those behind the incident shock wave.

The relaxation lengths behind the reflected shock wave are much shorter than those behind the incident shock wave owing to the two-step compressions through the incident and reflected shock waves. Even if we assume the relaxation lengths behind the reflected shock wave to be one order of magnitude less than those behind the incident shock wave, $\ell^*_{N_2 vib}$ behind the reflected shock wave is still large for N_2 experiments of Ben-Dor [Ref. [40]. In Deschambault's experiments in air [Ref. 39] $\ell^*_{O_2}$ is still small behind the reflected shock wave when $M_s > 5$ and $p_o > 30$ torr approximately (Table 4). From these estimates we can conclude that the state of the gas at each shock-front is frozen for N_2 experiments [Ref. 40] and is nearly frozen, except for O_2 vibrational excitation in some cases, for air experiments [Ref. 39]. Consequently, the shock shapes around the confluence point are determined at the frozen shock-fronts, and therefore the experimental data for air and nitrogen agree, in general, with the analytical results based on the perfect-gas model.

The discrepancy between the perfect-gas analysis and experiment, i.e., the persistence of RR below the detachment criterion and the disagreement of some experimental points with the SMR $\not\geq$ CMR and CMR $\not\geq$ DMR transitions, are probably due to the criteria themselves rather than to real-gas effects suggested earlier in Refs. 1-3, or possibly displacement effects of the boundary layer on the wall as suggested by Hornung et al [Ref. 7]. However, the latter effect has hardly been verified and is considered in some detail in Ref. 36.

4. CONCLUSIONS

An analytical and numerical study was made of oblique-shock-wave reflection in air in pseudo-stationary flow. The domains and transition boundaries between the various types of reflection (RR, SMR, CMR and DMR) were established using the transition criteria in Refs. 1-3, up to $M_s = 20$ for both perfect and imperfect air. Additional calculations were made for perfect gases with differing γ in order to clarify the effect of the specific-heat ratio γ on the shock-wave configurations. The transition boundary lines significantly shift downwards with decreasing γ, as for real gases. It was verified that the reflection angle ω' was a very sensitive function of γ. A decrease in γ lowered the value of ω' significantly. A decrease in γ shifted the value of ω' towards negative values under certain conditions. For a perfect gas with $\gamma = 1.67$ or 1.40, it was not possible to have a negative value of ω'. It was found that ω' could be positive or negative for imperfect air at higher M_s.

Transition boundaries predicted on the basis of a perfect gas with $\gamma = 1.40$ agree, in general, with the available experimental data for air and nitrogen. However, RR persists below the perfect termination line determined by the detachment criterion, and SMR and DMR can sometimes occur outside their analytically predicted domains. The experimental data used in the present study was checked in relation to the relaxation lengths behind the shock waves, which are good indicators for estimating the states of the gas immediately behind the shock waves. It was clarified that the flow states at the shock fronts were frozen or nearly frozen regarding vibrational excitation and dissociation. Consequently, it can be concluded that, within the limit of the available experimental data, the various wave systems are determined at the frozen shock fronts and, in general, the perfect-gas analysis predicts well the shock-wave configurations. The discrepancies between the present analysis and experiment are probably due to the basic assumptions and the transition criteria themselves.

Four outstanding problems remain for future consideration:

1. Improved criteria for all transition lines. This could explain the "von Neumann paradox" and improve the agreement between analysis and experiment.

2. To determine experimentally the persistence of RR over a significant range of $3 \leq M_s \leq 10$.

3. A detailed analysis of the boundary-layer growth on the wedge surface and a comparison with experimental data for persistence of RR and the measured reflected wave angle ω'.

4. To resolve some of the remaining problems such as: a better analytical method for predicting the first triple-point trajectory angle χ for very small wedge angle ($\theta_w \leq 5°$), and the location of the kink K (or the second triple point T') for large wedge angle ($\theta_w \geq 40°$).

Some of these problems have already been considered in some detail and will be reported on in Ref. 36, in the very near future.

REFERENCES

1. Ben-Dor, G., "Regions and Transitions of Non-Stationary Oblique Shock Wave Diffractions in Perfect and Imperfect Gases", UTIAS Report No. 232, 1978.

2. Ben-Dor, G., Glass, I. I., "Domains and Boundaries of Non-Stationary Oblique Shock-Wave Reflexions. 1. Diatomic Gas", J. Fluid Mech., Vol. 92, 1979, p. 459.

3. Ben-Dor, G., Glass, I. I., "Domains and Boundaries of Non-Stationary Oblique Shock-Wave Reflexions. 2. Monatomic Gas", J. Fluid Mech., Vol. 96, 1980, p. 735.

4. Griffith, W. C., "Shock Waves", J. Fluid Mech., Vol. 106, 1981, p. 81.

5. von Neumann, J., "Oblique Reflection of Shocks", Explosives Research Report No. 12, Navy Dept., Bureau of Ordnance, Re2C, Washington, D.C., 1943.

6. Henderson, L. F., Lozzi, A., "Experiments on Transition of Mach Reflection", J. Fluid Mech., Vol. 68, 1975, p. 139.

7. Hornung, H. G., Oertel, H., Sandeman, R. J., "Transition to Mach Reflexion of Shock Waves in Steady and Pseudosteady Flow with and without Relaxation", J. Fluid Mech., Vol. 90, 1979, p. 541.

8. Ames Research Staff, "Equations, Tables, and Charts for Compressible Flow", NACA Report 1135, 1953.

9. Smith, L. G., "Photographic Investigation of the Reflection of Plane Shocks in Air", OSRD Report No. 6271, 1945.

10. White, D. R., "An Experimental Survey of the Mach Reflection of Shock Waves", 2nd Mid-western Conf. on Fluid Mech., 1952.

11. Bleakney, W., Taub, A. H., "Interaction of Shock Waves", Rev. Mod. Phys., Vol. 21, 1949, p. 584.

12. Henderson, L. F., Siegenthaler, A., "Experiments on the Diffraction of Weak Blast Waves: the von Neumann Paradox", Proc. R. Soc., A369, 1980, p. 573.

13. Ando, S., "Pseudo-Stationary Oblique Shock-Wave Reflection in Carbon Dioxide – Domains and Boundaries", UTIAS Tech. Note No. 231, 1981.

14. Ben-Dor, G., Takayama, K., Kawauchi, T., "The Transition from Regular to Mach Reflexion and from Mach to Regular Reflexion in Truly Non-Stationary Flows", J. Fluid Mech., Vol. 100, 1980, p. 147.

15. Itoh, S., Okazaki, N., Itaya, M., "On the Transition Between Regular and Mach Reflection in Truly Non-Stationary Flows", J. Fluid Mech., Vol. 108, 1981, p. 383.

16. Gvozdeva, L. G., Bazhenova, T. V., Predvoditeleva, O. A., Fokeev, V. P., "Mach Reflection of Shock Waves in Real Gases", Astronautica Acta., Vol. 14, 1969, p. 503.

17. Gvozdeva, L. G., Bazhenova, T. V., Predvoditeleva, O. A., "Pressure and Temperature at the Wedge Surface for Mach Reflection of Strong Shock Waves", Astronautica Acta., Vol. 15, 1970, p. 503.

18. Bazhenova, T. V., Fokeev, V. P., Gvozdeva, L. G., "Regions of Various Forms of Mach Reflection and Its Transition to Regular Reflection", Astronautica Acta., Vol. 3, 1976, p. 131.

19. Law, C. K., Glass, I. I., "Diffraction of Strong Shock Waves by a Sharp Compressive Corner", CASI Trans., Vol. 4, No. 1, 1971.

20. Ando, S., Glass, I. I., "Domains and Boundaries of Pseudostationary Oblique-Shock-Wave Reflections in Carbon Dioxide", Proc. 7th Int. Symp. on the Military Applications of Blast Simulation, 1981.

21. Auld, D. J., Bird, G. A., "The Reflection from Regular to Mach Reflection", AIAA Paper No. 76-322, 1976.

22. Schneyer, G. P., "Numerical Simulation of Regular and Mach Reflections", Phys. Fluids, Vol. 18, No. 9, 1975, p. 1119.

23. Kutler, P., Shankar, V. S., "Diffraction of a Shock Wave by a Compression Corner: I. Regular Reflection", AIAA J., Vol. 15, No. 2, 1977, p. 197.

24. Shankar, V. S., Kutler, P., Anderson, D., "Diffraction of Shock Waves by a Compression Corner, II. Single Mach Reflection", AIAA Paper No. 77-89, 1977.

25. Booen, W. B., Needham, C. E., "Two Dimensional HULL Code Simulation of Complex and Double Mach Reflections", AFWL Tech. Note No. NTE-TN-81-001, 1980.

26. Book, D., Boris, J., Kuhl, A., Oran, E., Picone, M., Zalensak, S., "Simulation of Complex Shock Reflections from Wedges in Inert and Reactive Gases Mixtures", Proc. 7th Int. Conf. on Numerical Methods in Fluid Dynamics, 1980.

27. Glaz, H. M., Naval Surface Weapons Center, Dahlgren, Virginia, 1982 (private communication).

28. Champney, J. M., Chaussee, D. S., Kutler, P., "Computation of Blast Wave-Obstacle Interactions", AIAA Paper No. 82-0227, 1982.

29. Ben-Dor, G., Glass, I. I., "Nonstationary Oblique Shock-Wave Reflections: Actual Isopycnics and Numerical Experiments", AIAA J., Vol. 16, No. 11, 1978, p. 1146.

30. Hansen, C. F., "Approximations for the Thermodynamic and Transport Properties of High Temperature Air", NASA TR R-50, 1959.

31. Gilmore, F. R., "Equilibrium Composition and Thermodynamic Properties of Air to 24,000°K", The Rand Corporation RM-1543, 1955.

32. Laird, J. D., Heron, K., "Shock Tube Gas Dynamics Charts, Part I: Equilibrium Argon-Free Air from 3,000 to 40,000°K", Avco Corporation RAD-TM-64-12, 1964.

33. Lewis, C. H., Burgess, E. G. III, "Charts of Normal Shock Wave Properties in Imperfect Air", AEDC-TDR-64-43, 1964.

34. Lewis, C. H., Burgess, E. G. III, "Charts of Normal Shock Wave Properties in Imperfect Nitrogen", AEDC-TDR-64-104, 1964.

35. Liepmann, H. W., Roshko, A., "Elements of Gasdynamics", John Wiley, New York, 1957, p.87.

36. Shirouzu, M., Glass, I. I., "An Assessment of Recent Results on Pseudo-Stationary Oblique-Shock-Wave Reflections", UTIAS Report No. 264, 1982.

37. Hansen, C. F., "Molecular Physics of Equilibrium Gases: A Handbook for Engineers", NASA SP-3096, 1976.

38. Ben-Dor, G., "Analytical Solution of Double-Mach Reflection", AIAA J., Vol. 18, No. 9, 1980, p. 1036.

39. Deschambault, R., UTIAS, M.A.Sc. Thesis (to be published).

40. Ben-Dor, G., "Nonstationary Oblique-Shock-Wave Reflections in Nitrogen and Argon: Experimental Results", UTIAS Report No. 237, 1978.

41. Vincenti, W. G., Kruger, C. H. Jr., "Introduction to Physical Gas Dynamics", John Wiley, New York, 1965, p. 436.

42. Gaydon, A. G., Hurle, I. G., "Measurement of Times of Vibrational Relaxation and Dissociation Behind Shock Waves in N_2, O_2, Air, CO, CO_2 and H_2", 8th Int. Symp. on Comb., 1962, p. 309.

43. Logan, J. G. Jr., "Relaxation Phenomena in Hypersonic Aerodynamics", IAS Preprint No. 728, presented at the 25th Annual Meeting, 1957.

44. Schulz-Grunow, F., "Structure of Shock Waves Including Dissociation and Ionization", Z. Flugwiss., 23, Heft 2, 1975, p. 51.

Table 1

Degree of dissociation in states (1) to (3) for oblique shock-wave reflections for imperfect air at P_o = 15 torr and T_o = 300 K

(a) M_s=5.0	θ'_w	θ_w	χ	state (1)		state (2)		state (3)	
				α_{O_2}	α_{N_2}	α_{O_2}	α_{N_2}	α_{O_2}	α_{N_2}
Line H (M_1=1.0 line)	22.2	-	-	0.0	0.0	-	-	-	-
Line B ($\theta_1+\theta 2_m$=0 line)	47.0	47.0	0.0	0.0	0.0	0.01	0.0	-	-
Line D (M_{2K}=1.0 line)	33.2	24.7	8.5	0.0	0.0	0.0	0.0	0.0	0.0
Line F (M_{2T}=1.0 line)	24.6	9.1	15.5	0.0	0.0	0.0	0.0	0.0	0.0

(b) M_s=10.0	θ'_w	θ_w	χ	state (1)		state (2)		state (3)	
				α_{O_2}	α_{N_2}	α_{O_2}	α_{N_2}	α_{O_2}	α_{N_2}
Line H	17.9	-	-	0.49	0.0	-	-	-	-
Line B	43.4	43.4	0.0	0.49	0.0	1.00	0.01	-	-
Line D	22.9	13.0	9.9	0.49	0.0	0.51	0.0	0.65	0.0
Line F	18.6	4.1	14.5	0.49	0.0	0.50	0.0	0.54	0.0

(c) M_s=15.0	θ'_w	θ_w	χ	state (1)		state (2)		state (3)	
				α_{O_2}	α_{N_2}	α_{O_2}	α_{N_2}	α_{O_2}	α_{N_2}
Line H	16.6	-	-	1.00	0.085	-	-	-	-
Line B	41.6	41.6	0.0	1.00	0.085	1.00	0.313	-	-
Line D	20.1	9.9	10.2	1.00	0.085	1.00	0.096	1.00	0.128
Line F	17.0	2.9	14.1	1.00	0.085	1.00	0.087	1.00	0.099

(d) M_s=20.0	θ'_w	θ_w	χ	state (1)		state (2)			state (3)	
				α_{O_2}	α_{N_2}	α_{O_2}	α_{N_2}	β	α_{O_2}	α_{N_2}
Line H	15.3	-	-	1.00	0.383	-	-	-	-	-
Line B	45.1	45.1	0.0	1.00	0.383	1.00	1.00	0.025	-	-
Line D	17.9	7.6	10.3	1.00	0.383	1.00	0.394	0.0	1.00	0.434
Line F	15.7	3.0	12.7	1.00	0.383	1.00	0.389	0.0	1.00	0.404

Table 2

Shock Mach number corresponding to $\omega'=0$ for CO_2, SF_6 and imperfect air

θ_w	M_s		
	$\gamma=1.093$	$\gamma=1.290$	Imperfect air
20°	3.40	-	7.90
25°	3.10	7.25	7.12
30°	2.93	5.60	6.50
35°	2.81	5.00	5.95
40°	2.75	4.75	5.75
45°	2.77	4.85	5.80

Table 3

Initial conditions and experimental results in air

Exp. Ref.39	θ_w	M_s	P_o (torr)	T_o (°C)	χ	χ'	ω'	Type
639	2	1.21	752.0	26.1	25.7	-	73.0	SMR
638	2	1.37	749.0	24.2	26.8	-	70.0	SMR
637	2	1.40	750.5	25.0	27.0	-	73.3	SMR
640	2	3.93	15.0	24.5	-	-	-	SMR
910	10	2.04	50.0	23.4	18.7	-	66.8	SMR
911	10	3.05	25.0	24.6	18.1	-	47.3	SMR
912	10	3.89	15.0	24.2	17.3	-	33.0	SMR
913	10	4.76	15.0	23.5	17.0	-	29.0	SMR
914	10	6.41	15.0	22.7	16.5	-	22.2	SMR
618	10	7.85	55.0	24.4	15.8	-	23.8	CMR
615	10	8.99	30.8	21.6	15.0	-	17.3	CMR
416	10	10.32	44.3	24.9	13.4	-	14.0	CMR
942	20	3.00	150.0	25.3	12.1	-	30.0	SMR
943	20	3.60	60.0	25.1	12.6	-	23.1	CMR
936	20	7.63	60.0	25.4	11.5	-	14.9	CMR
975	20	8.85	30.8	23.5	-	-	-	DMR
974	20	10.18	15.0	23.1	-	-	-	DMR
931	27	1.90	80.0	25.8	9.0	-	46.8	SMR
63	27	2.04	50.0	24.9	9.0	-	40.8	SMR
53	27	2.04	250.0	26.0	9.0	-	43.5	SMR
932	27	2.81	25.0	24.1	9.1	-	26.9	CMR
673	27	3.84	45.0	23.4	-	-	-	DMR
65	27	4.77	15.0	25.1	10.0	12.0	10.4	DMR
934	27	5.65	150.0	24.5	9.5	11.1	7.2	DMR
66	27	7.87	5.0	24.7	8.6	9.6	3.0	DMR
56	27	8.89	30.8	26.0	7.7	8.8	4.9	DMR
944	30	1.98	125.0	24.4	7.3	-	35.5	SMR
945	30	2.86	125.0	24.4	8.7	-	24.8	CMR
946	30	3.79	45.0	23.6	9.1	11.4	14.6	DMR
660	30	4.68	42.0	25.0	-	-	-	DMR
951	40	1.24	750.0	24.8	0.7	-	65.9	SMR
953	40	2.88	125.0	24.4	4.5	8.1	19.7	DMR
952	40	5.50	10.0	24.8	4.8	5.5	4.8	DMR

Continued...

Table 3 - Continued

Initial conditions and experimental results in air

Exp. Ref.39	θ_w	M_s	P_o (torr)	T_o (°C)	χ	χ'	ω'	Type
947	45	1.26	758.5	23.9	-	-	52.1	RR
948	45	1.50	380.0	25.3	-	-	-	SMR
950	45	2.88	125.0	24.3	-	-	-	DMR
922	47	1.41	740.0	22.7	-	-	54.1	RR
923	47	1.54	380.0	21.3	-	-	48.0	SMR
924	47	1.63	250.0	23.2	0.4	-	43.0	SMR
925	47	1.90	80.0	27.5	0.9	-	35.9	CMR
926	47	2.08	50.0	26.0	1.5	-	26.0	CMR
976	47	2.40	150.0	23.6	-	-	-	DMR
927	47	3.03	25.0	25.4	2.1	5.2	26.0	DMR
928	47	3.82	15.0	25.6	2.4	5.3	9.1	DMR
929	47	4.78	15.0	26.4	1.6	2.5	6.0	DMR
930	47	5.59	10.0	23.7	-	-	32.2	RR
620	47	7.78	55.0	24.7	-	-	18.9	RR
621	47	10.17	15.0	23.3	-	-	15.1	RR
961	49	1.62	250.0	24.6	-	-	-	RR
964	49	1.89	160.0	23.4	-	-	-	CMR
965	49	2.08	125.0	23.3	-	-	-	DMR
963	49	2.31	150.0	23.4	-	-	-	DMR
962	49	2.61	100.0	24.0	-	-	-	DMR
967	49	3.08	67.0	22.6	-	-	-	DMR
966	49	3.71	45.0	22.1	-	-	-	DMR
968	49	4.48	15.0	22.4	-	-	-	RR
668	49	4.77	15.0	22.4	-	-	-	RR
955	50	1.60	250.0	24.8	-	-	-	RR
956	50	2.06	125.0	24.3	-	-	-	RR
957	50	2.82	125.0	23.2	-	-	-	RR
958	50	3.69	45.0	23.3	-	-	-	RR
959	50	4.61	15.0	23.0	-	-	-	RR
67	60	2.05	50.0	24.4	-	-	21.0	RR
61	60	4.61	15.0	23.4	-	-	13.5	RR
935	60	4.72	46.0	25.3	-	-	13.0	RR
69	63.4	2.02	50.0	24.4	-	-	18.0	RR
59	63.4	2.05	250.0	25.0	-	-	-	RR

*Note: Where data are blank, precise measurements could not be made.

Table 4

Relaxation lengths (ℓ^*) in mm behind incident shock waves in air for given initial pressures p_o at 300 K

Exp. Ref.39	θ_w	M_s	P_o (torr)	$\ell^*_{O_2 vib}$	$\ell^*_{O_2 dis}$	$\ell^*_{N_2 vib}$	$\ell^*_{N_2 dis}$	$\ell^*_{air\ overall}$
914	10	6.41	15.0	2.7	-	-	-	-
618	10	7.85	55.0	0.16	-	7.1	-	18.2
615	10	8.00	30.8	0.15	32.5	6.8	-	5.2
416	10	10.32	44.3	0.05	3.16	2.4	-	0.5
936	20	7.63	60.0	0.23	-	9.3	-	-
975	20	8.85	30.8	0.17	39.0	7.5	-	6.5
974	20	10.18	15.0	0.15	10.7	7.5	-	1.7
934	27	5.65	150.0	0.73	-	24.0	-	-
66	27	7.87	5.0	2.2	-	90.0	-	-
56	27	8.89	30.8	0.16	35.7	7.1	-	5.8
952	40	5.50	10.0	13.0	-	-	-	-
930	47	5.59	10.0	12.0	-	-	-	-
620	47	7.78	55.0	0.22	-	7.8	-	36.4
621	47	10.17	15.0	0.15	10.0	7.3	-	1.7

Table 5

Vibrational relaxation length ($\ell^*_{N_2 vib}$) in mm behind incident shock waves in nitrogen for given initial pressures P_o at 300 K

Exp. Ref.40	θ_w	M_s	P_o (torr)	$\ell^*_{N_2 vib}$
33	5	5.85	15.2	184
34	5	6.01	15.2	158
35	5	6.86	10.0	100
36	5	7.51	5.2	117
42	10	5.92	15.3	170
43	10	6.79	10.2	103
44	10	7.58	5.1	116
47	20	6.27	15.3	118
46	20	6.87	10.1	99
45	20	7.71	5.1	104
102	26.56	8.06	5.1	78
54	30	5.93	15.2	165
55	30	6.96	10.1	93
56	30	7.97	5.0	86
60	40	6.17	15.3	137
59	40	6.97	10.3	91
57	40	7.78	5.0	98
58	40	7.95	5.0	86
124	50	6.22	15.3	124
123	50	7.29	10.2	69

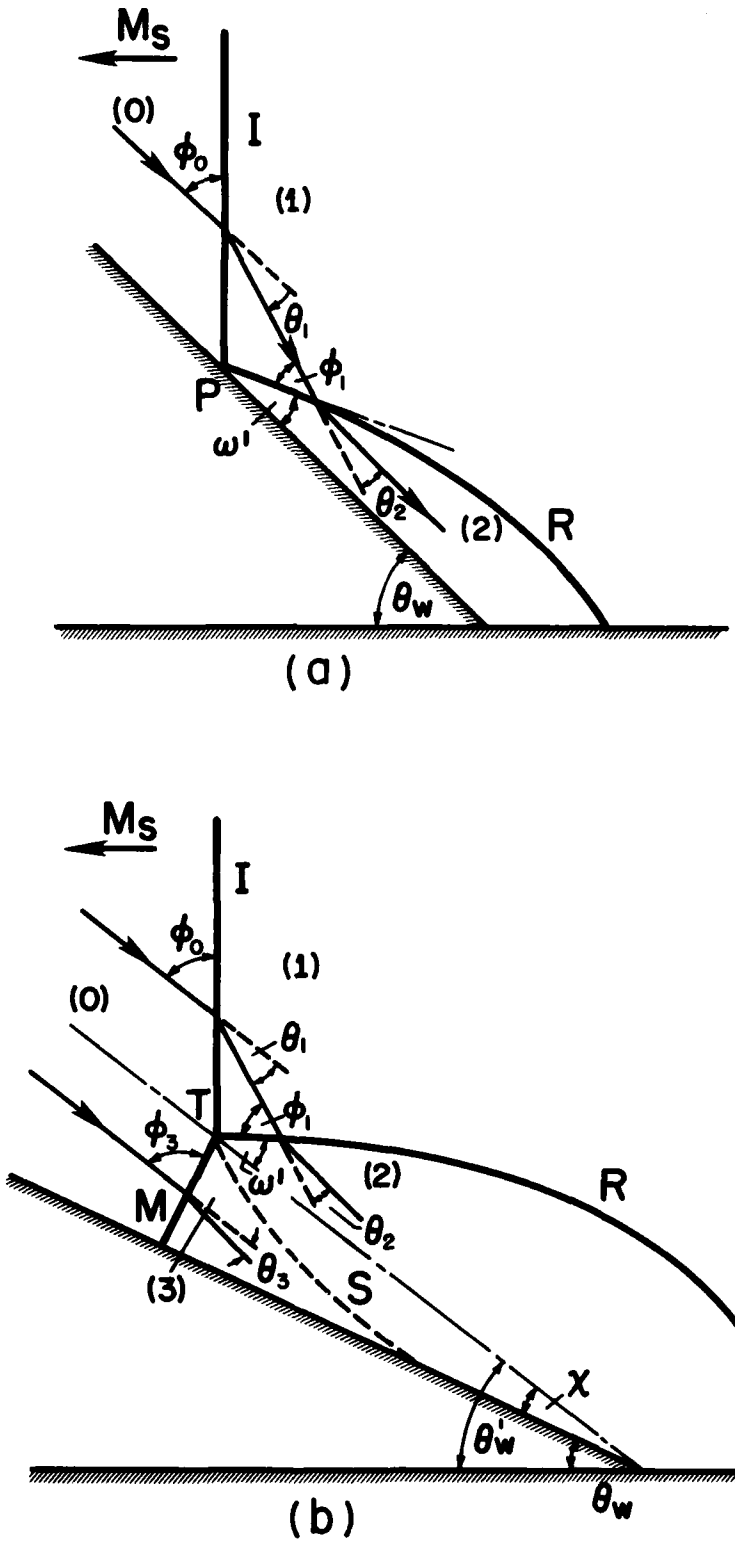

FIG. 1 SCHEMATIC DIAGRAM OF REGULAR AND SIMPLE MACH REFLECTIONS: (a) REGULAR REFLECTION (RR), (b) SINGLE MACH REFLECTION (SMR).

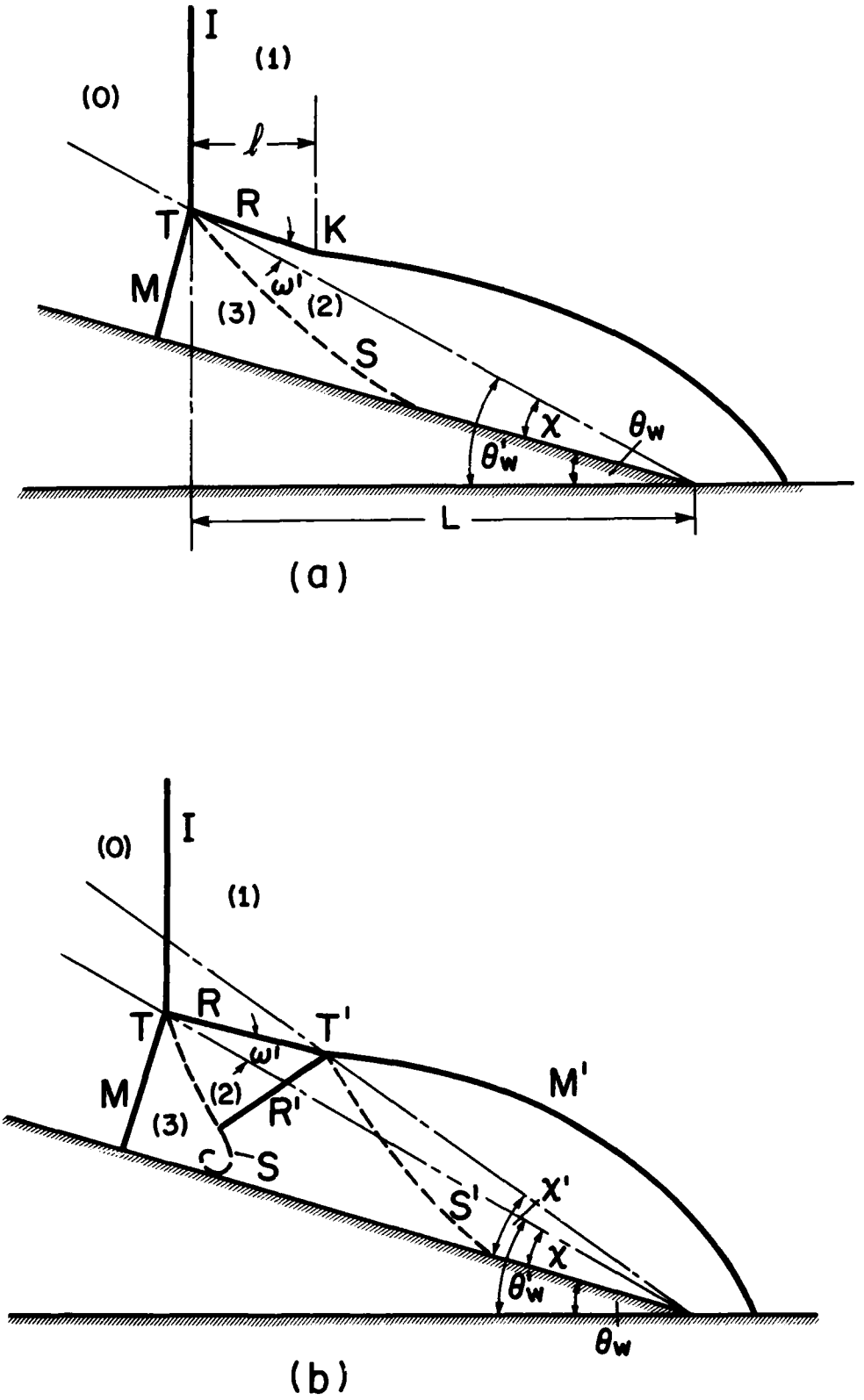

FIG. 2 SCHEMATIC DIAGRAM OF COMPLEX AND DOUBLE MACH REFLECTIONS:
(a) COMPLEX MACH REFLECTION (CMR), (b) DOUBLE MACH REFLECTION (DMR).

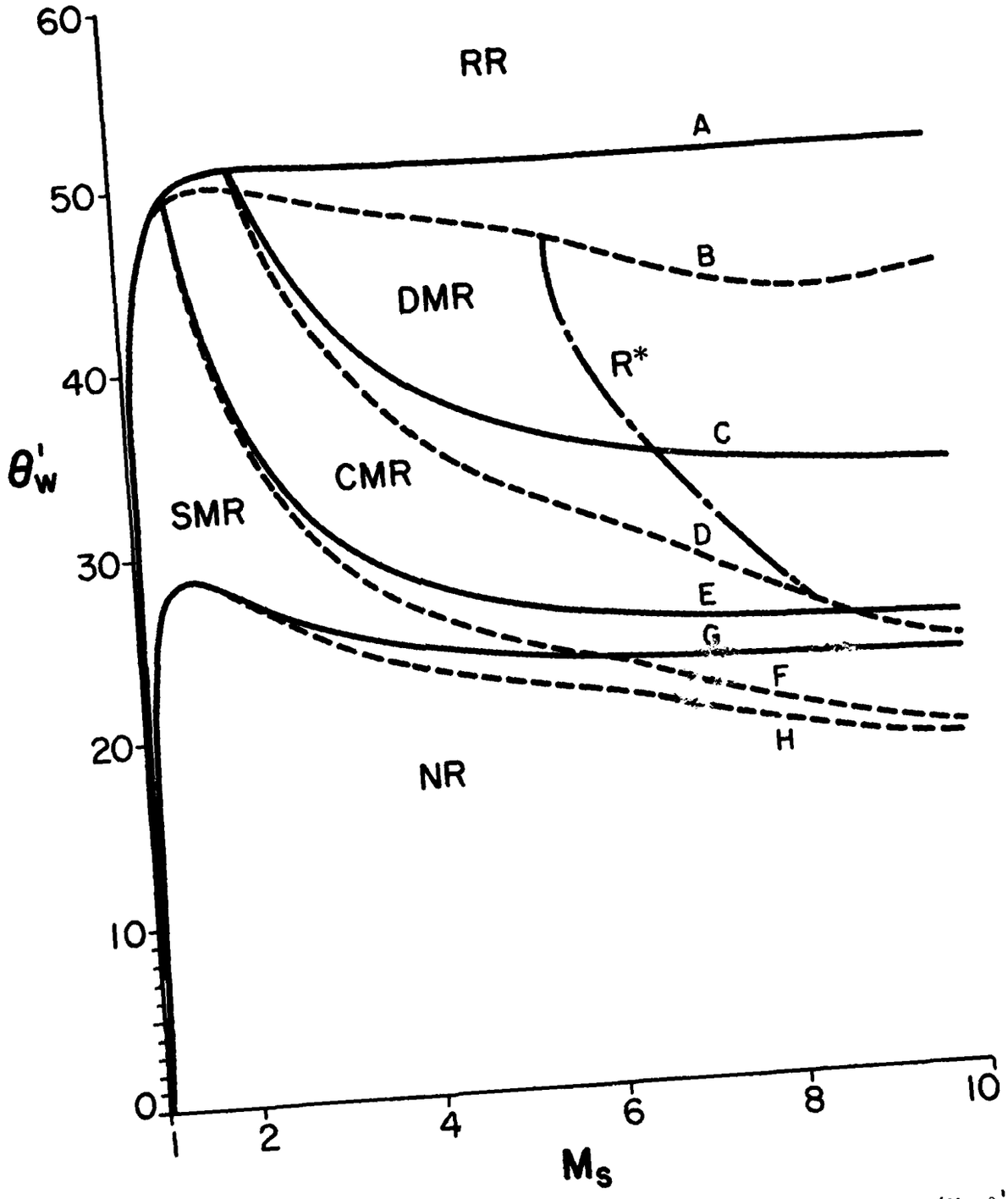

FIG. 3(a) REGIONS OF VARIOUS TYPES OF SHOCK-WAVE REFLECTION IN (M_s-θ'_w) PLANE SOLID LINES ARE FOR PERFECT AIR WITH γ = 1.40; DASHED LINES ARE FOR IMPERFECT AIR AT P_o = 15 TORR AND T_o = 300 K, $\theta'_w = \theta_w + \chi$.

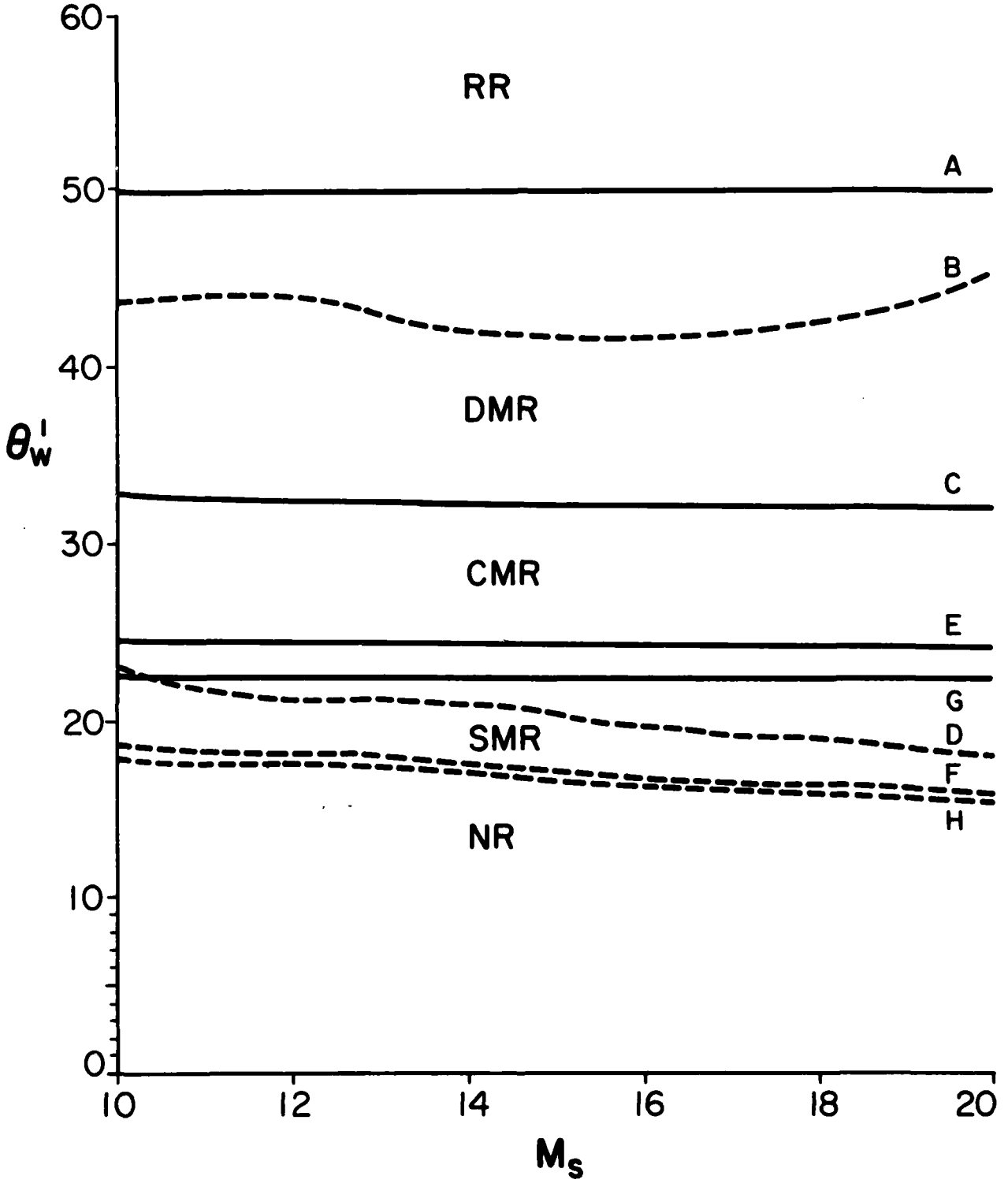

FIG. 3(b) REGIONS OF VARIOUS TYPES OF SHOCK-WAVE REFLECTION IN (M_s-θ_w') PLANE. SOLID LINES ARE FOR PERFECT AIR WITH γ = 1.40; DASHED LINES ARE FOR IMPERFECT AIR AT P_o = 15 TORR AND T_o = 300 K, $\theta_w' = \theta_w + \chi$ (CONTINUED).

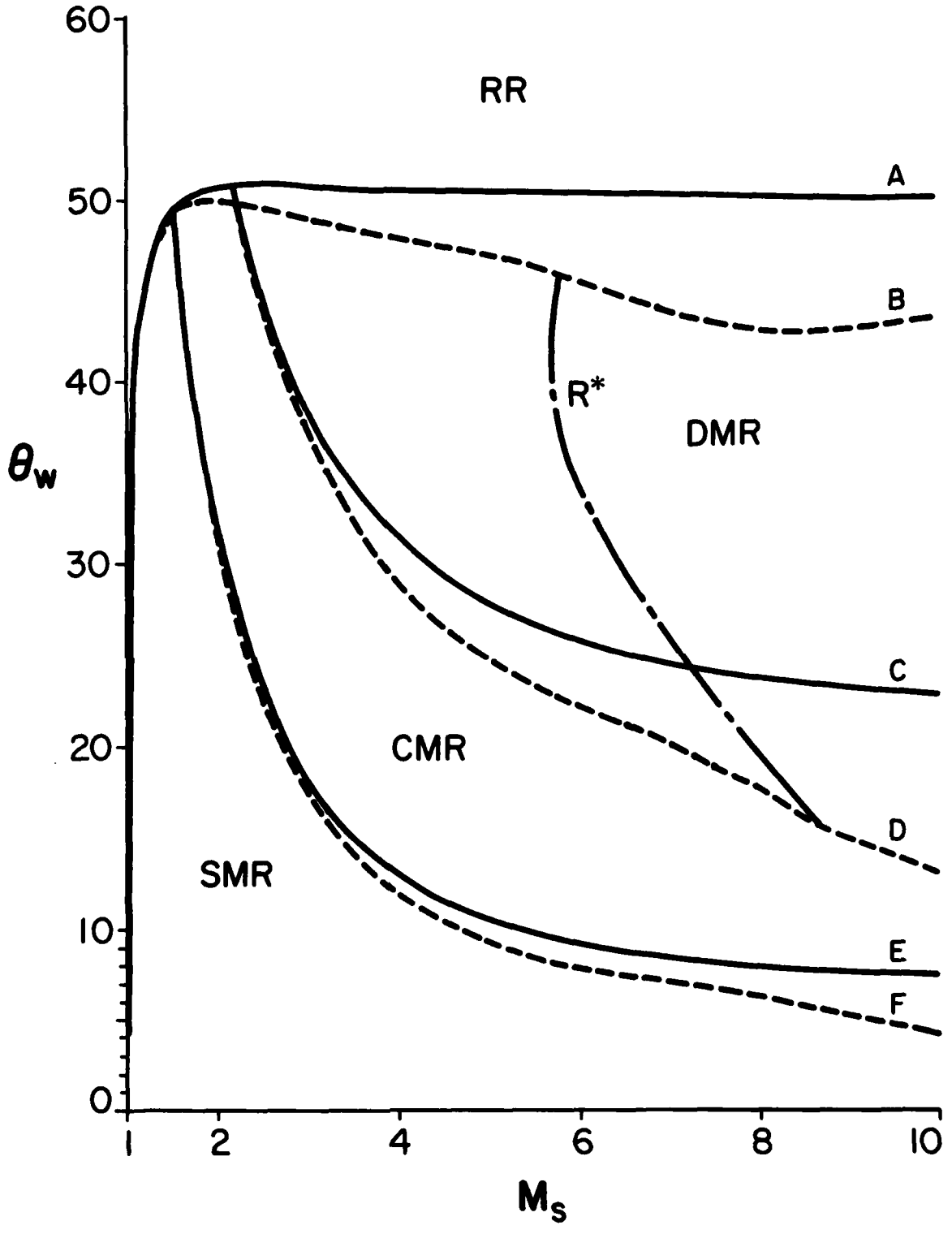

FIG. 4(a) REGIONS OF VARIOUS TYPES OF SHOCK-WAVE REFLECTION IN (M_s-θ_w) PLANE. SOLID LINES ARE FOR PERFECT AIR WITH γ = 1.40; DASHED LINES ARE FOR IMPERFECT AIR AT P_o = 15 TORR AND T_o = 300 K.

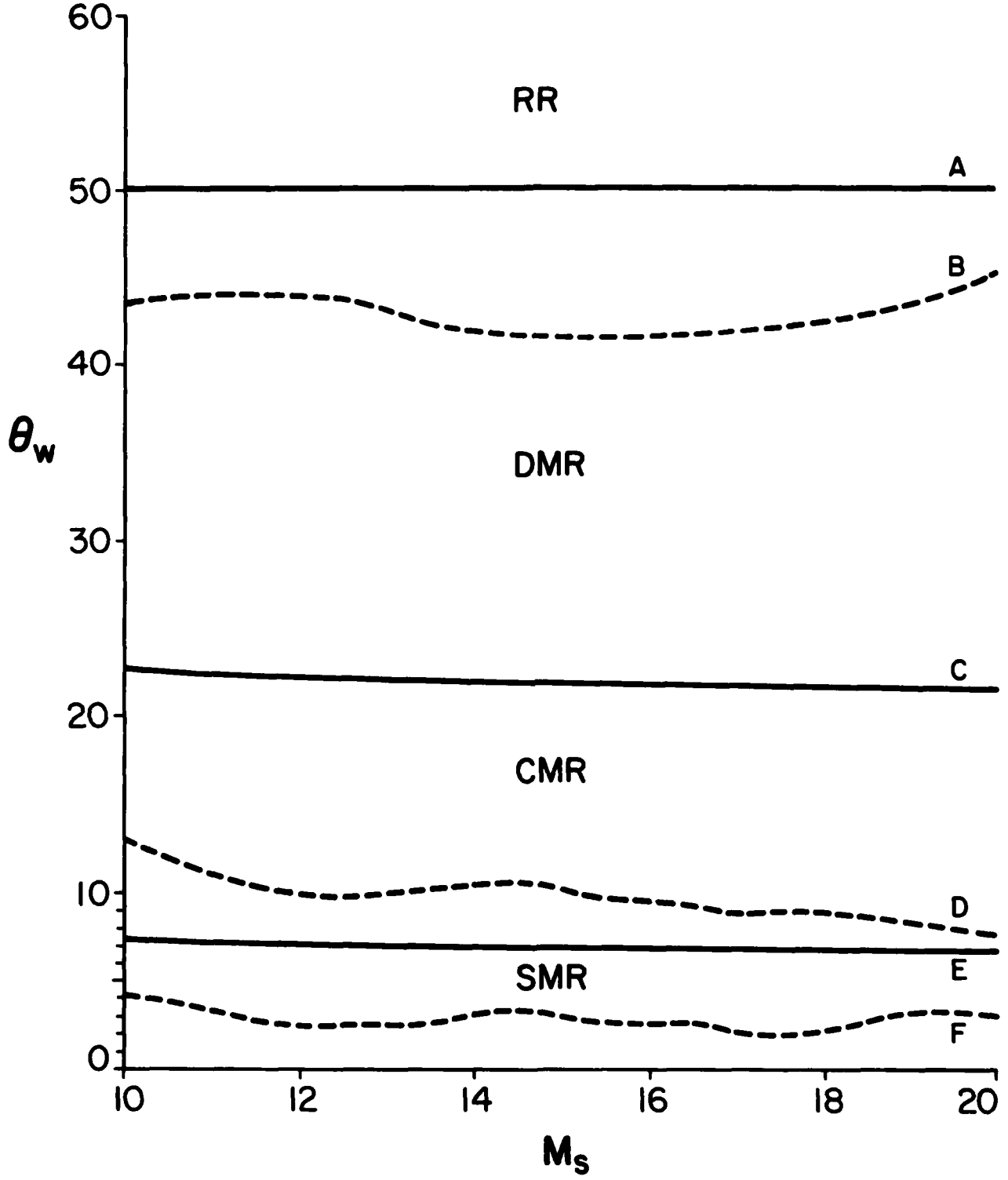

FIG. 4(b) REGIONS OF VARIOUS TYPES OF SHOCK-WAVE REFLECTION IN (M_s-θ_w) PLANE. SOLID LINES ARE FOR PERFECT AIR WITH γ = 1.40; DASHED LINES ARE FOR IMPERFECT AIR AT P_o = 15 TORR AND T_o = 300 K (CONTINUED).

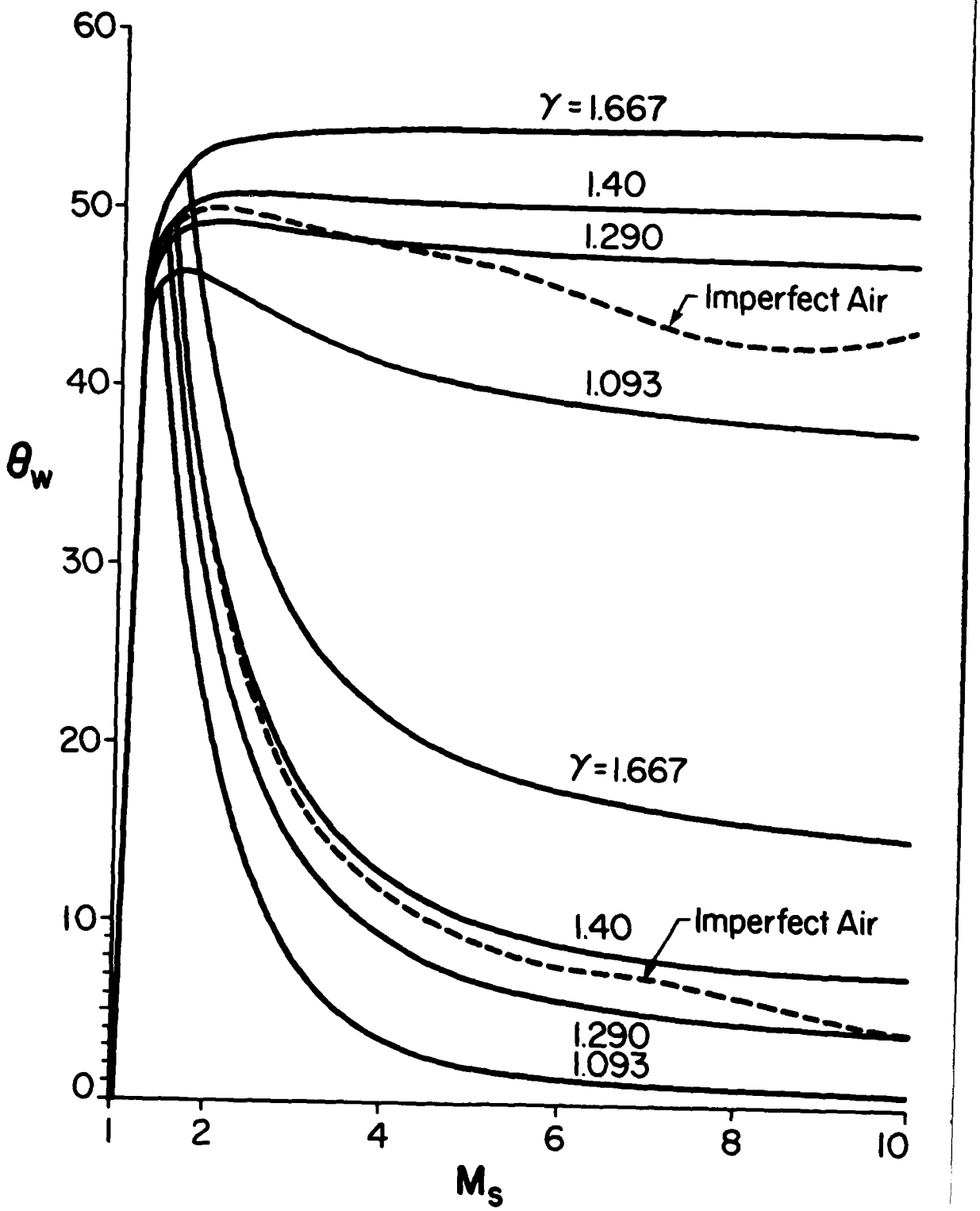

FIG. 5 TRANSITION LINES FOR RR ≷ MR AND SMR ≷ CMR FOR PERFECT GASES WITH DIFFERENT γ AND IMPERFECT AIR.

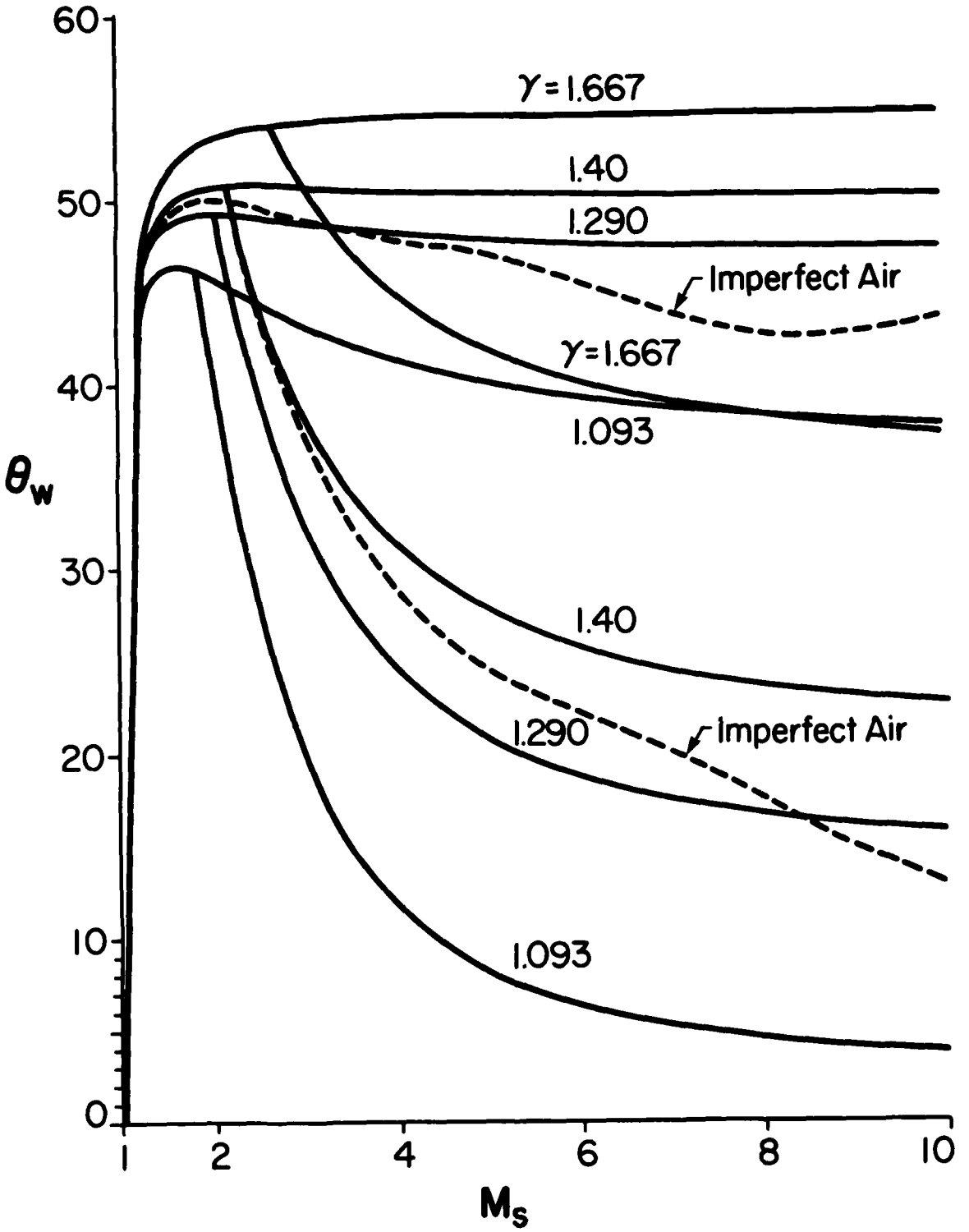

FIG. 6 TRANSITION LINES FOR RR ≷ MR AND CMR ≷ DMR FOR PERFECT GASES WITH DIFFERENT γ AND IMPERFECT AIR.

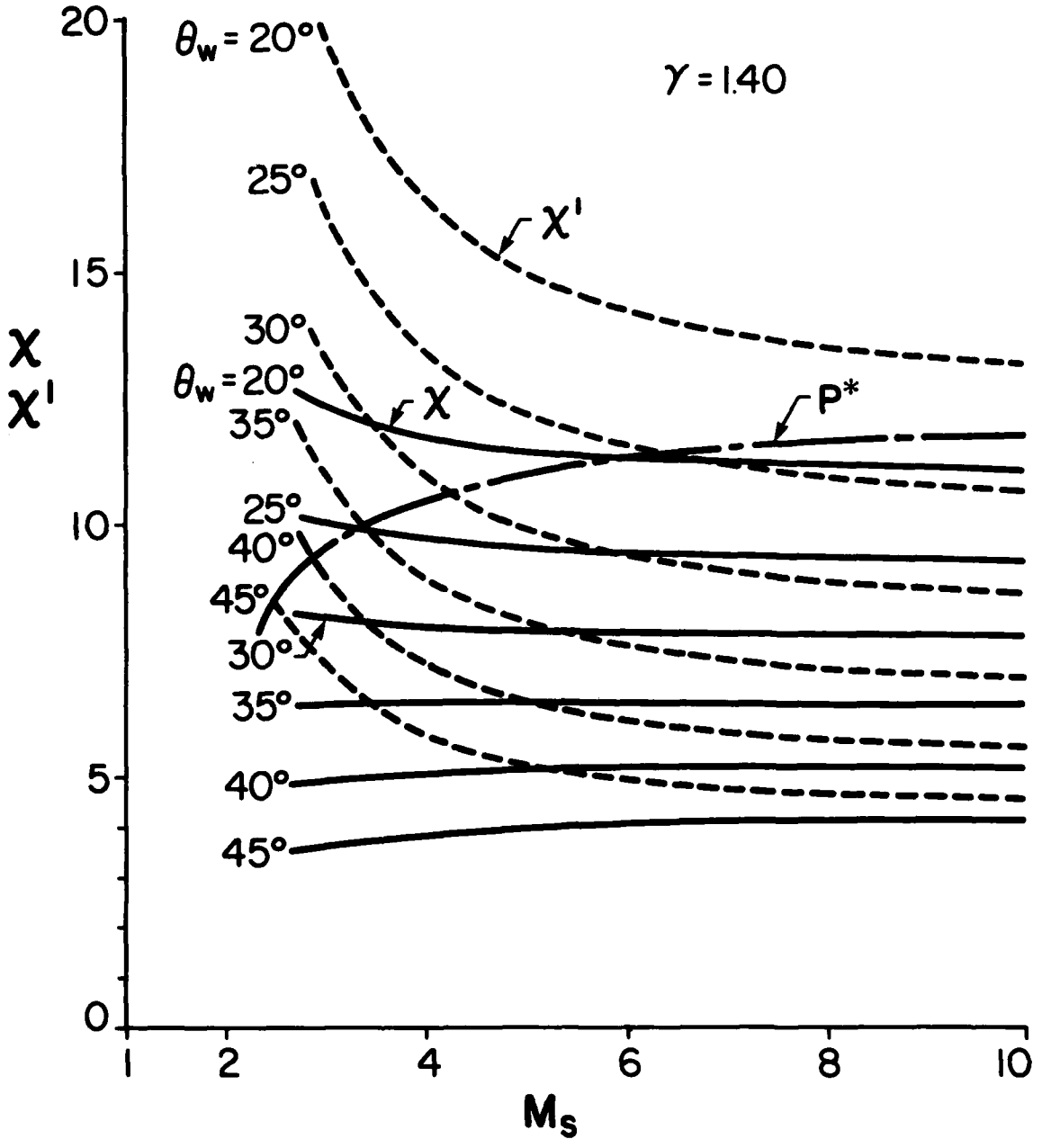

FIG. 7(a) VARIATION OF χ AND χ' WITH M_S FOR GIVEN θ_w (PERFECT AIR WITH γ = 1.40).

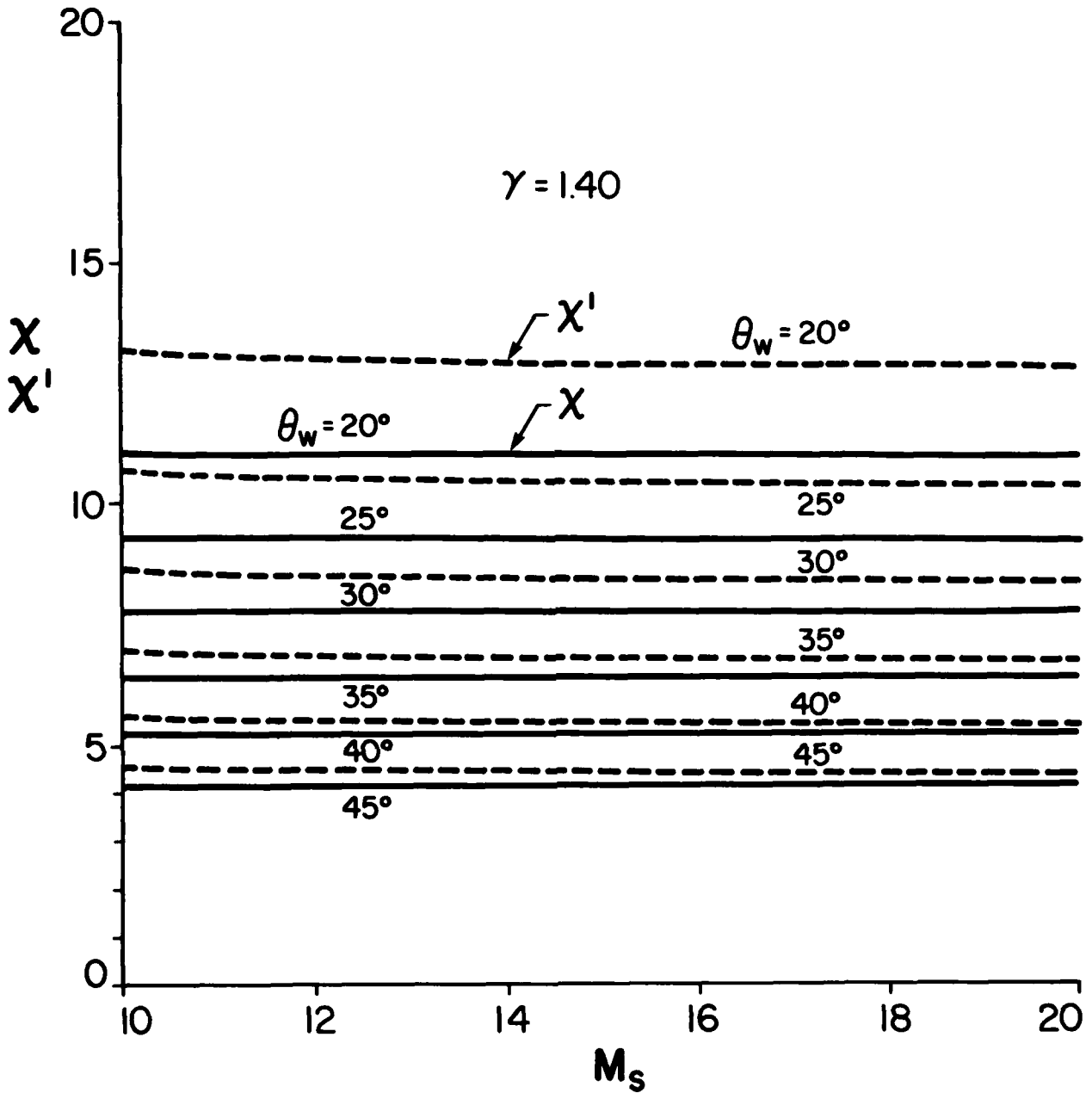

FIG. 7(b) VARIATION OF χ AND χ' WITH M_S FOR GIVEN θ_w (PERFECT AIR WITH γ = 1.40) (CONTINUED).

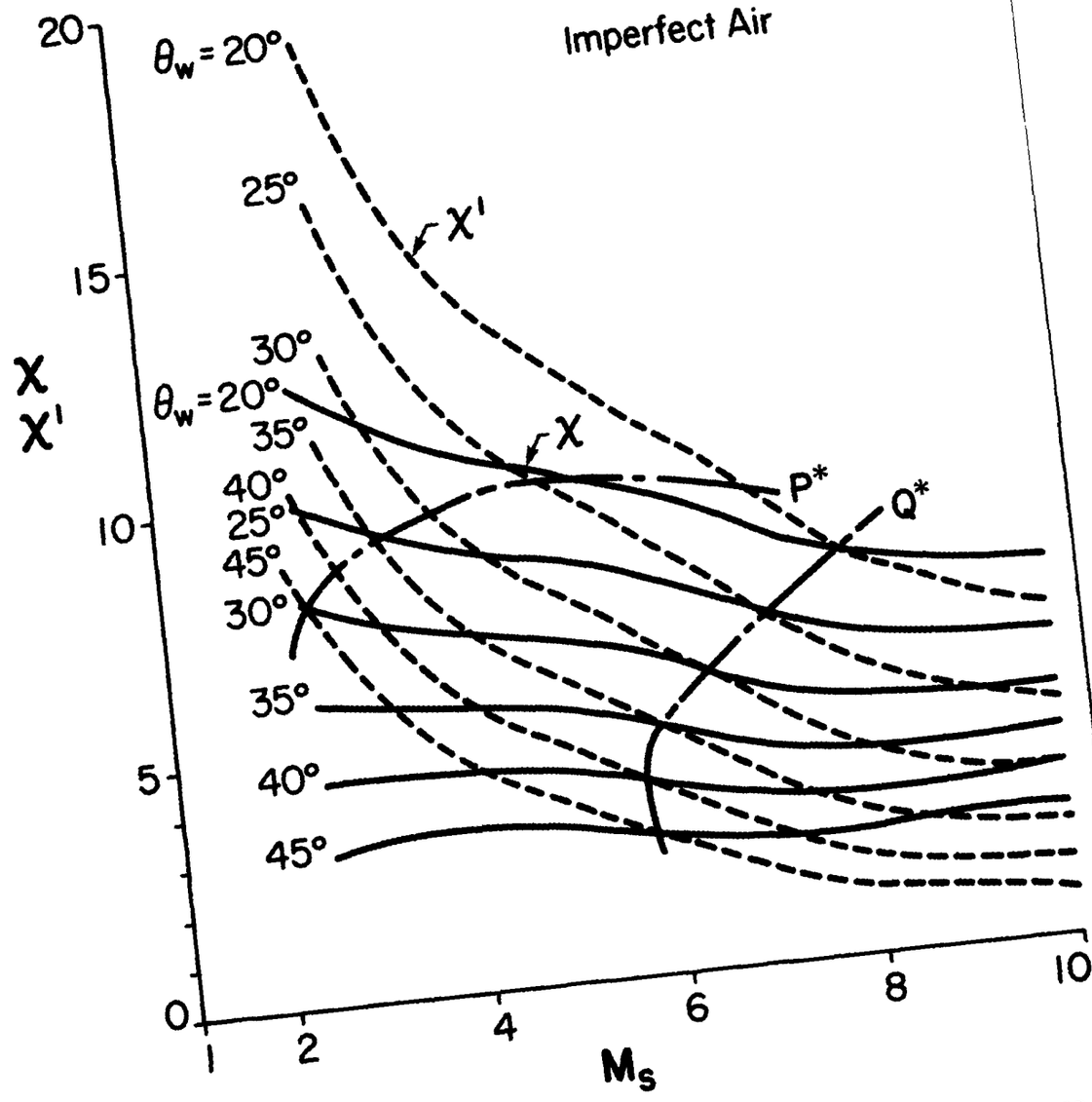

FIG. 8(a) VARIATION OF χ AND χ' WITH M_s FOR GIVEN θ_w (IMPERFECT AIR AT P_o = 15 TORR AND T_o = 300 K).

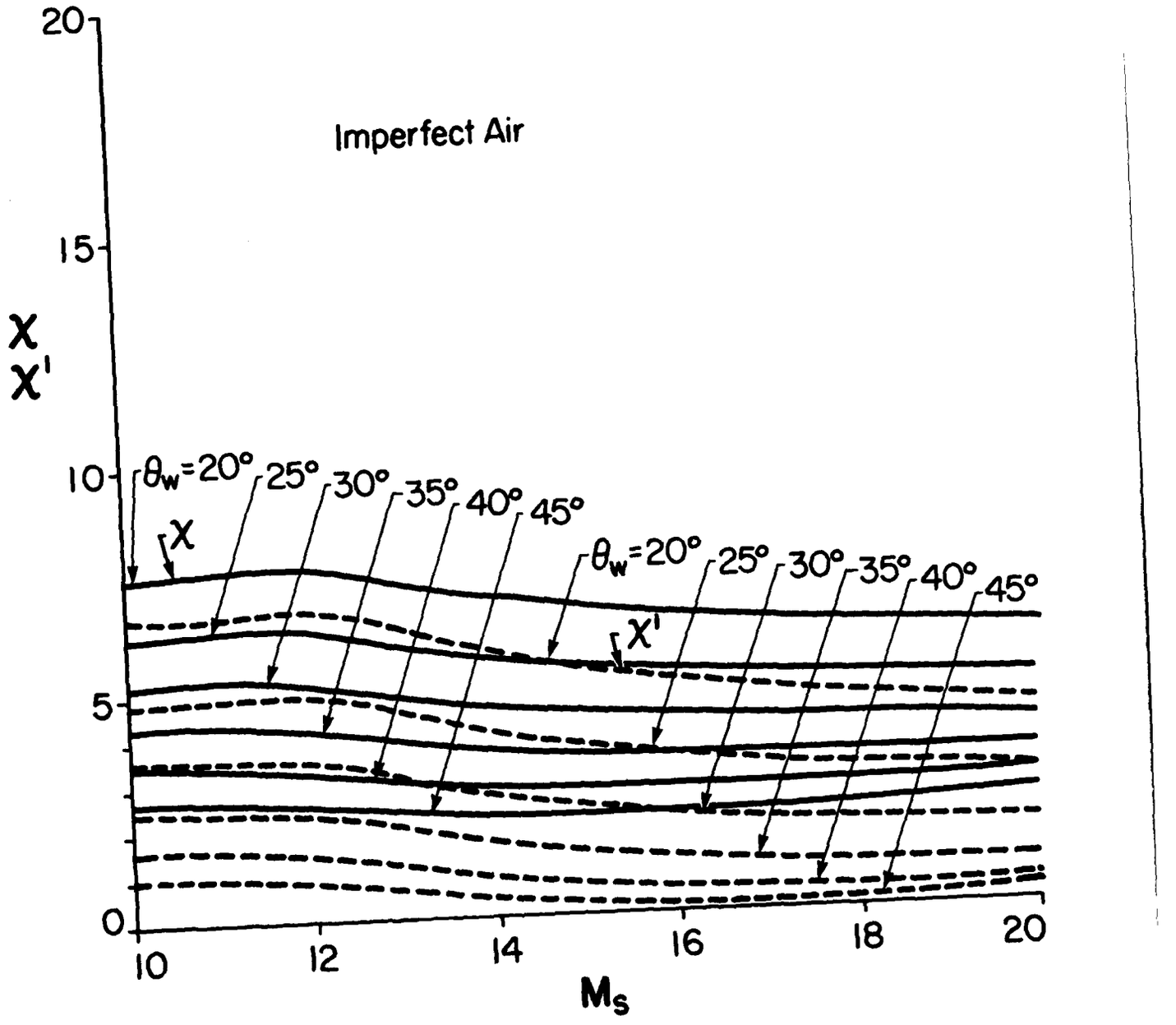

FIG. 8(b) VARIATION OF χ AND χ' WITH M_s FOR GIVEN θ_w (IMPERFECT AIR AT P_o = 15 TORR AND T_o = 300 K) (CONTINUED).

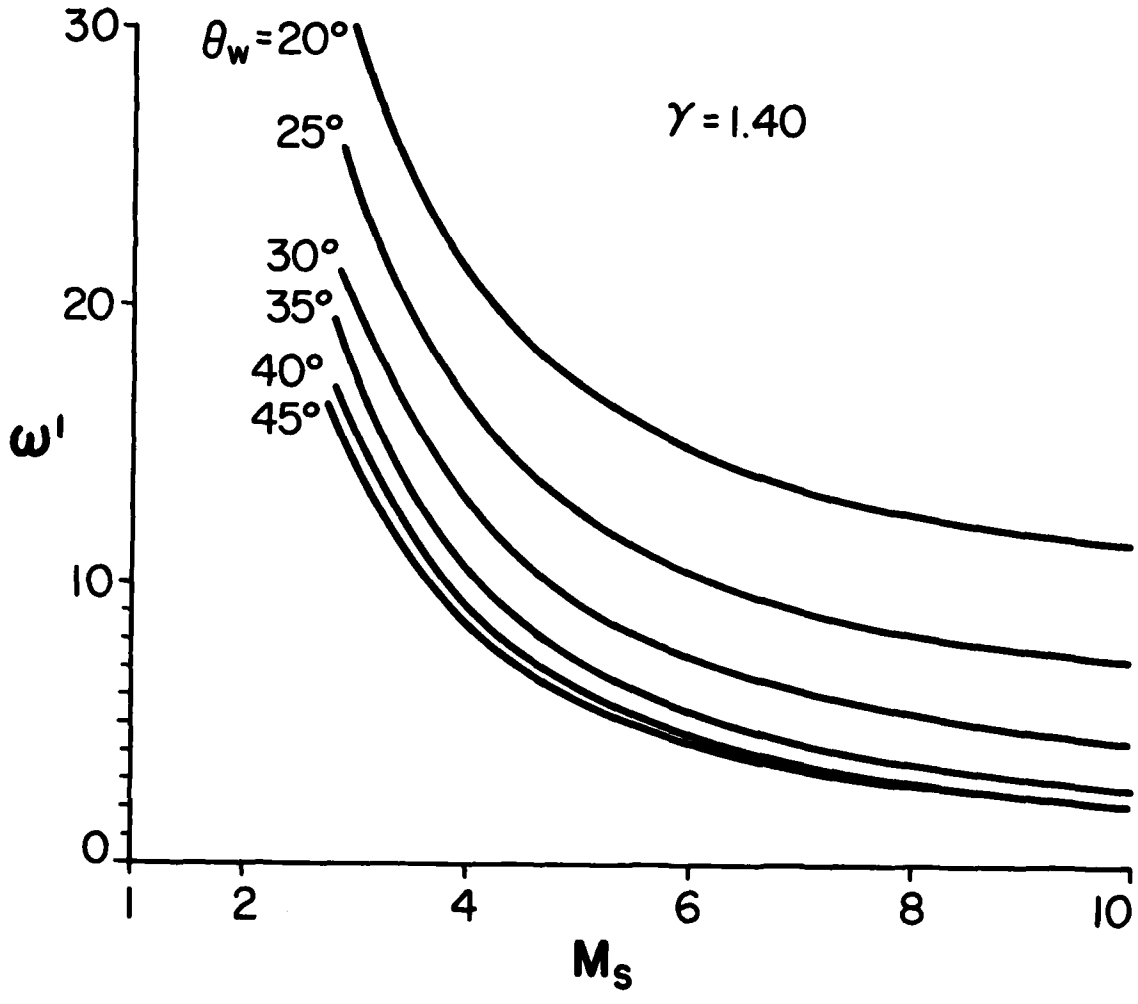

FIG. 9(a) VARIATION OF REFLECTION ANGLE ω' WITH M_S FOR GIVEN θ_w (PERFECT AIR WITH $\gamma = 1.40$).

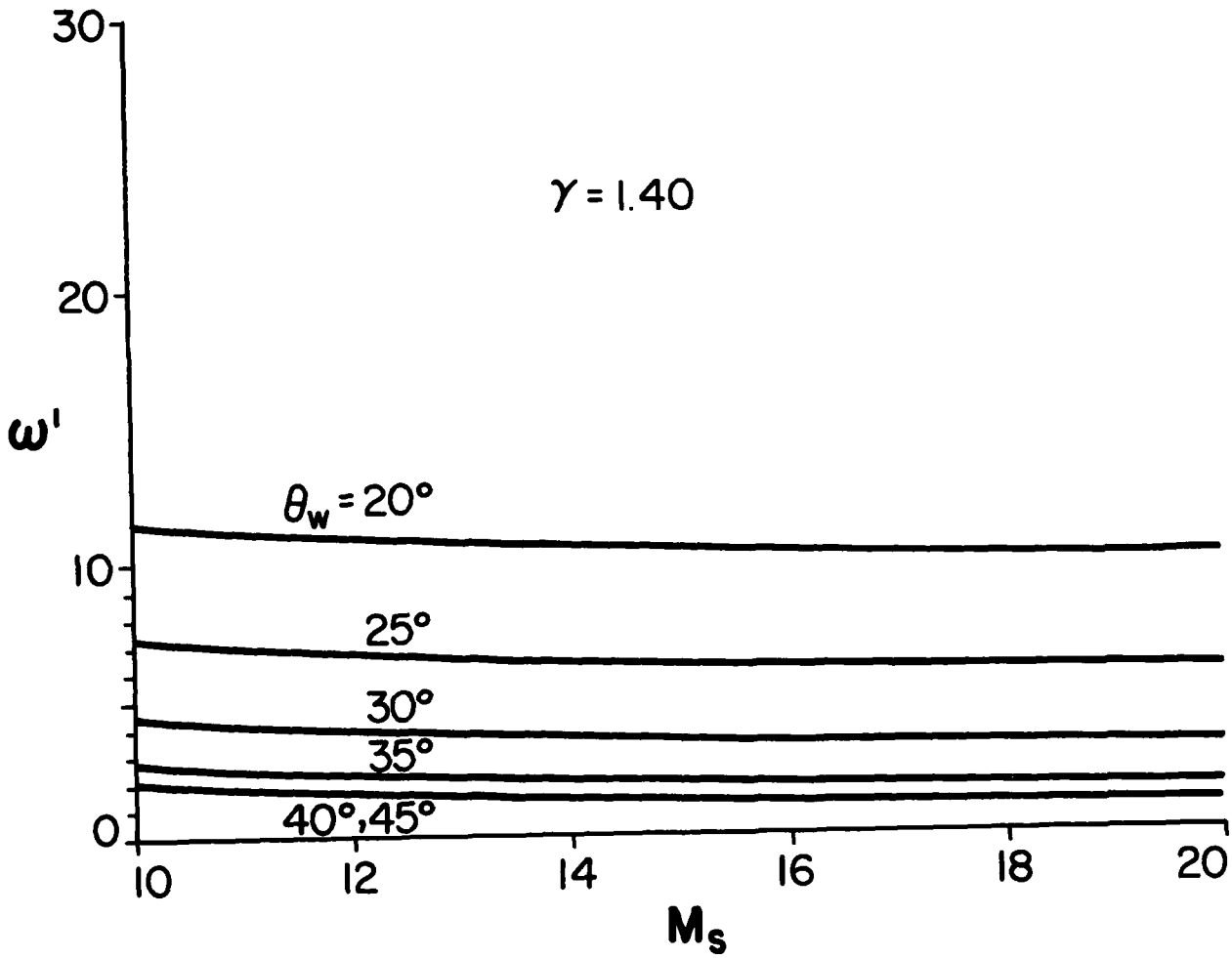

FIG. 9(b) VARIATION OF REFLECTION ANGLE ω' WITH M_S FOR GIVEN θ_w (PERFECT AIR WITH γ = 1.40) (CONTINUED).

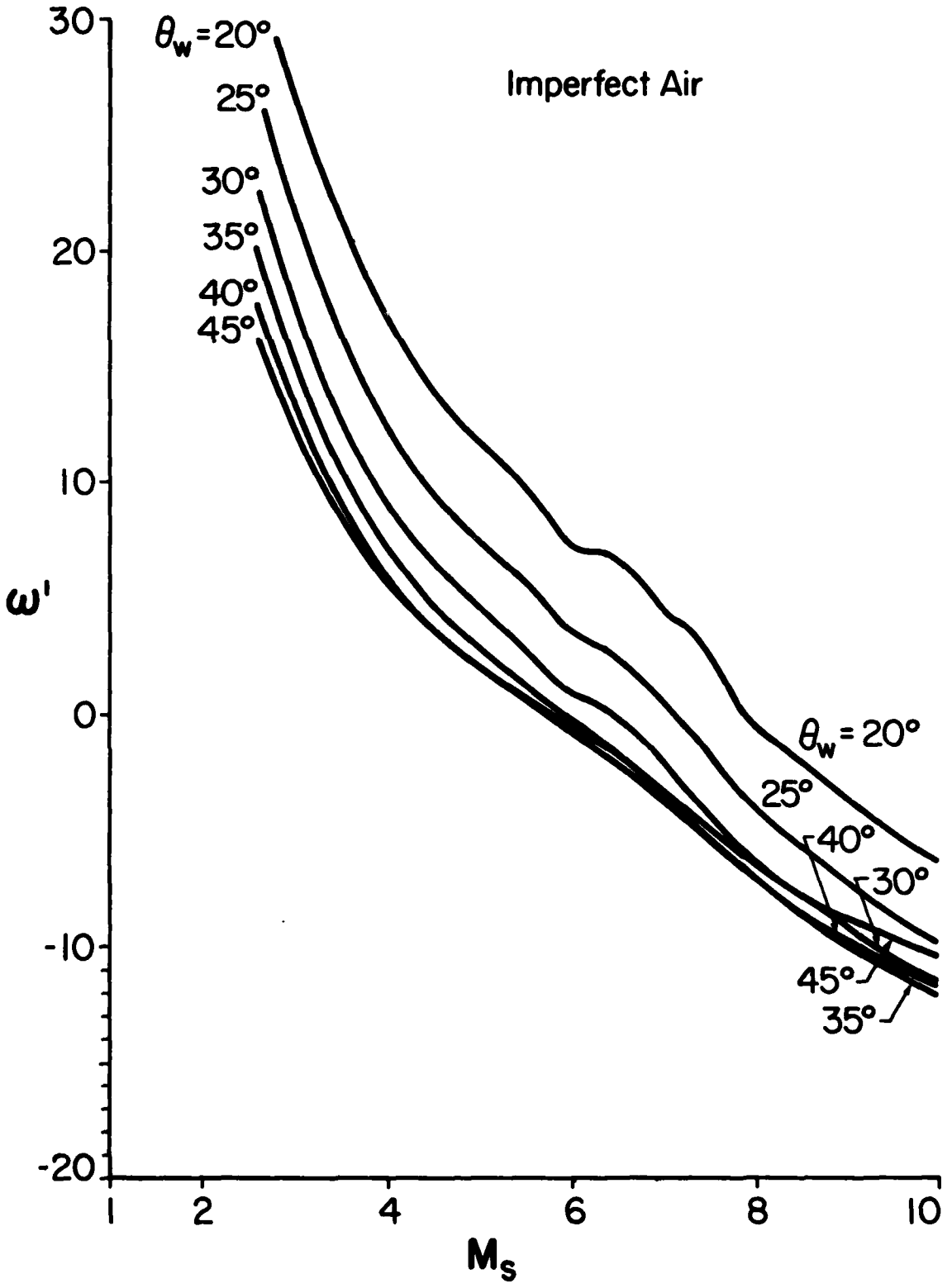

FIG. 10(a) VARIATION OF REFLECTION ANGLE ω' WITH M_S FOR GIVEN θ_w (IMPERFECT AIR AT P_o = 15 TORR AND T_o = 300 K).

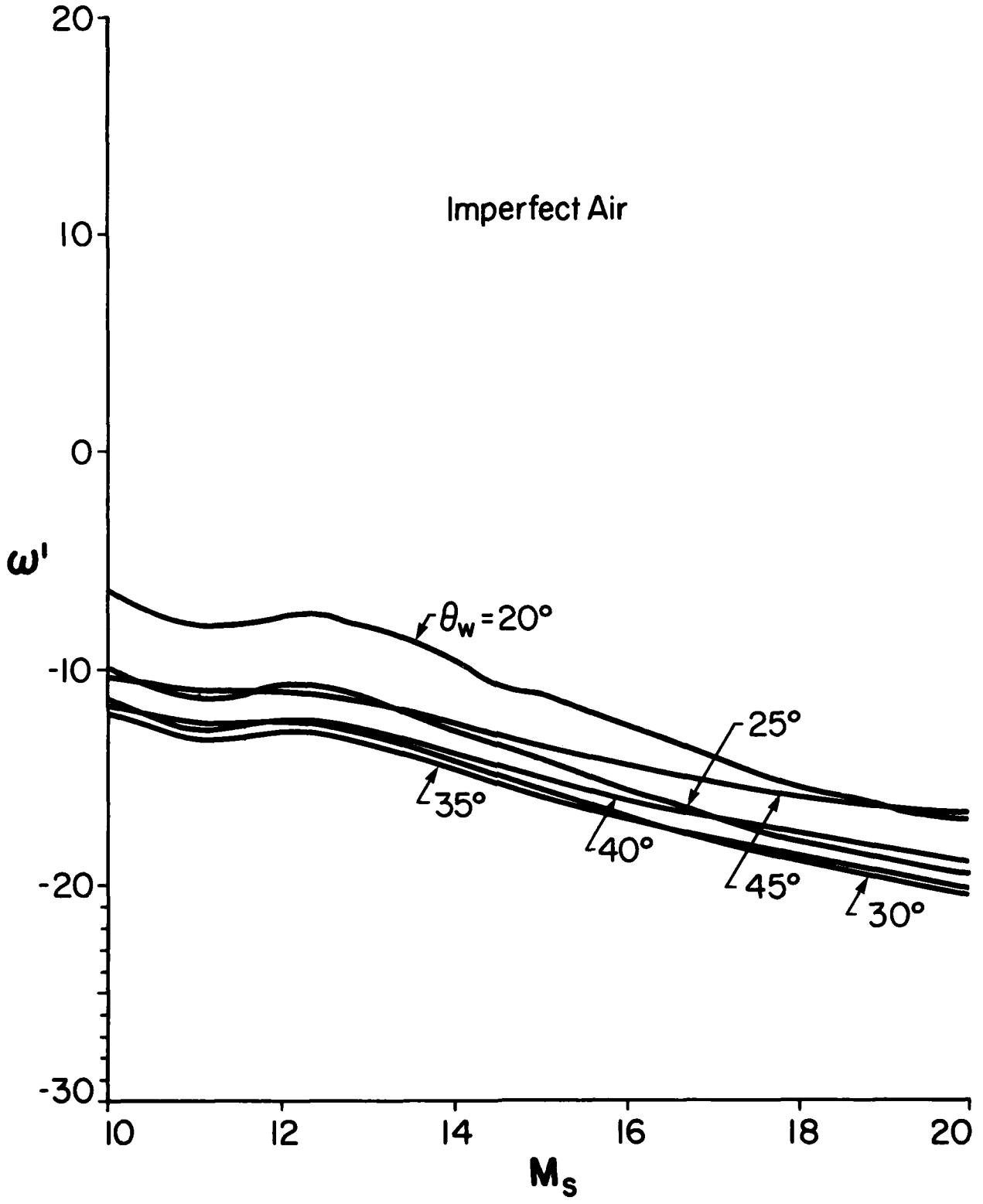

FIG. 10(b) VARIATION OF REFLECTION ANGLE ω' WITH M_S FOR GIVEN θ_w (IMPERFECT AIR AT P_0 = 15 TORR AND T_0 = 300 K) (CONTINUED).

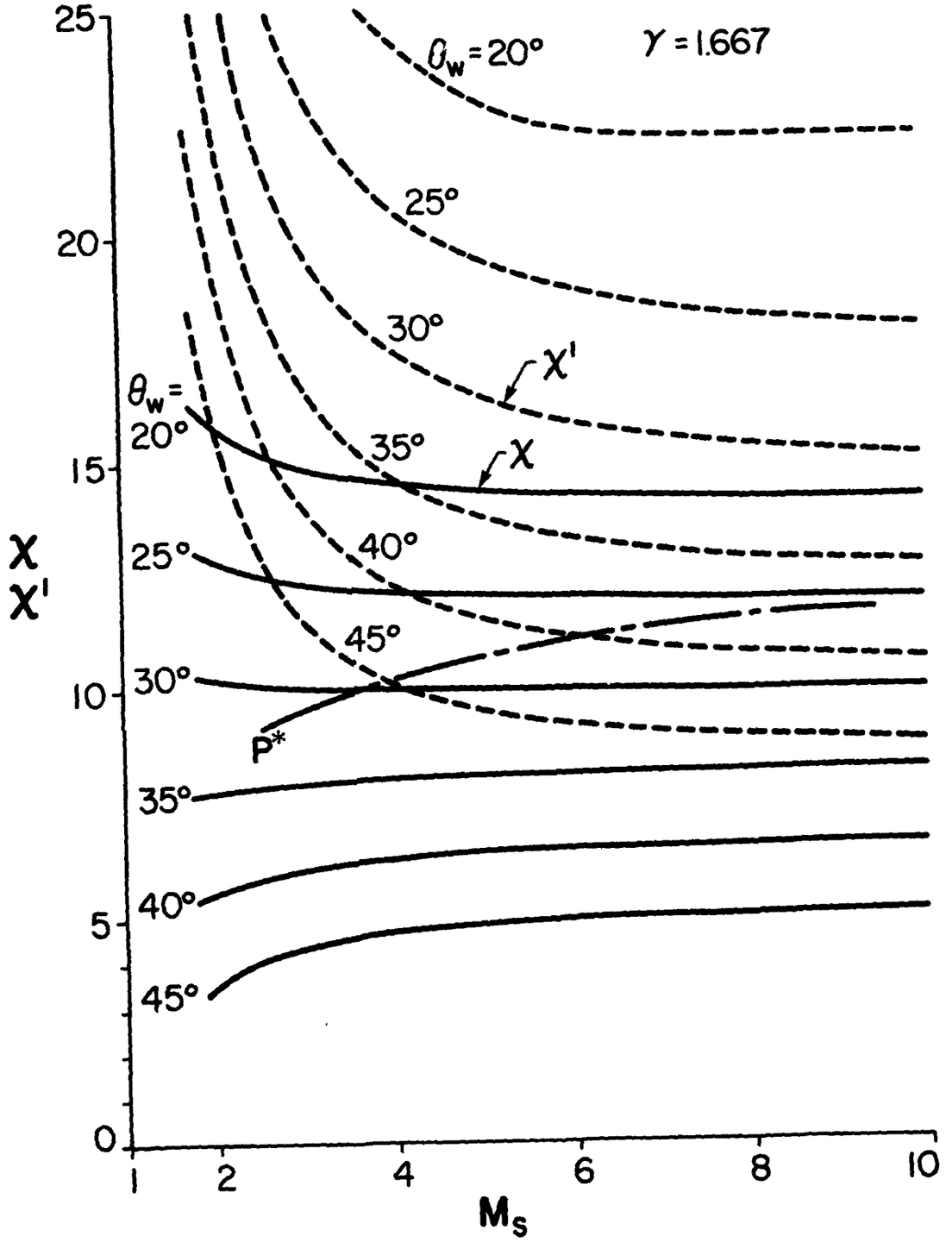

FIG. 11 VARIATION OF χ AND χ' WITH M_S FOR GIVEN θ_w (MONATOMIC GAS WITH γ = 1.667).

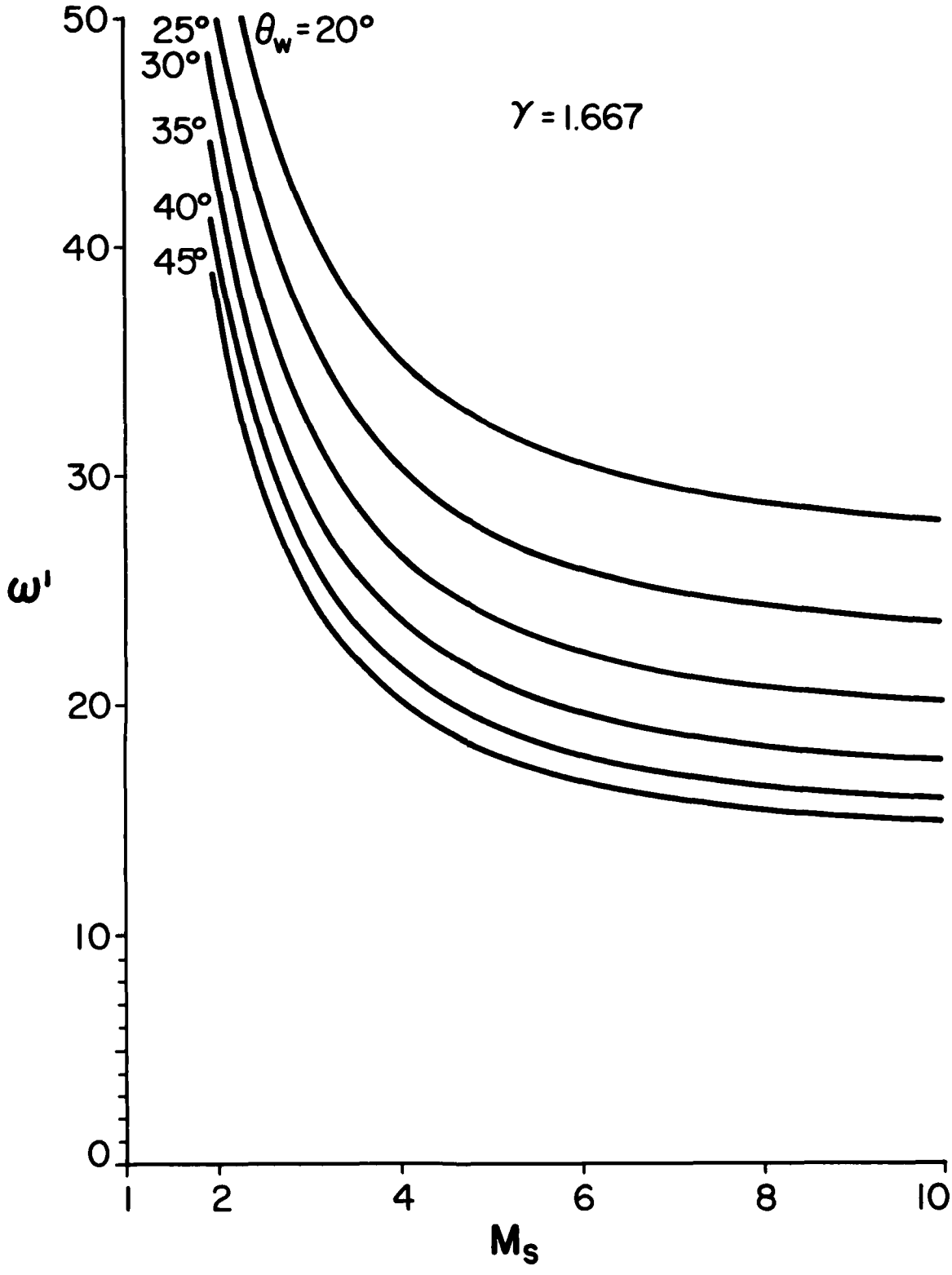

FIG. 12 VARIATION OF REFLECTION ANGLE ω' WITH M_S FOR GIVEN θ_W (MONATOMIC GAS WITH $\gamma = 1.667$).

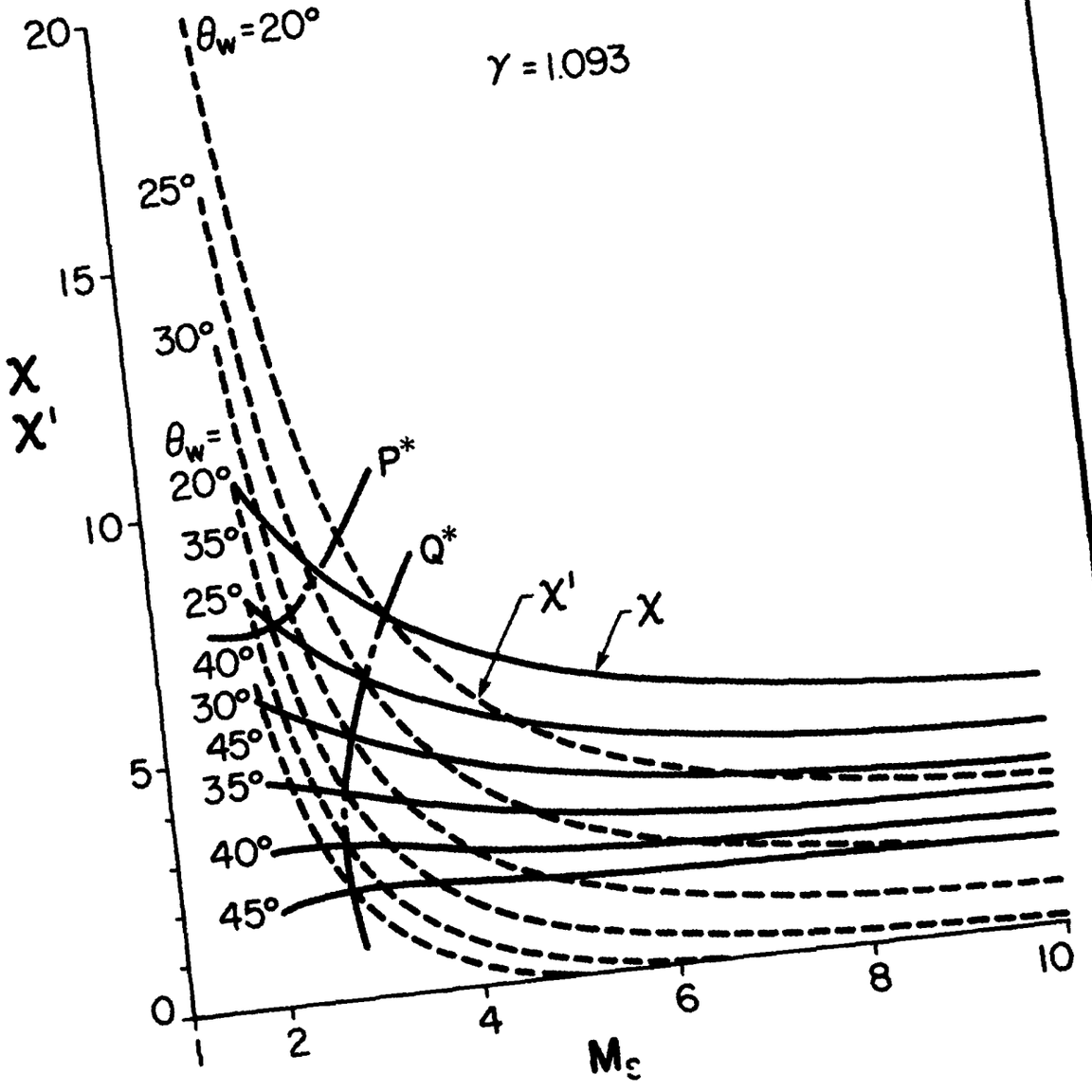

FIG. 15 VARIATION OF χ AND χ' WITH M_s FOR GIVEN θ_w (POLYATOMIC GAS - SF_6 WITH $\gamma = 1.093$).

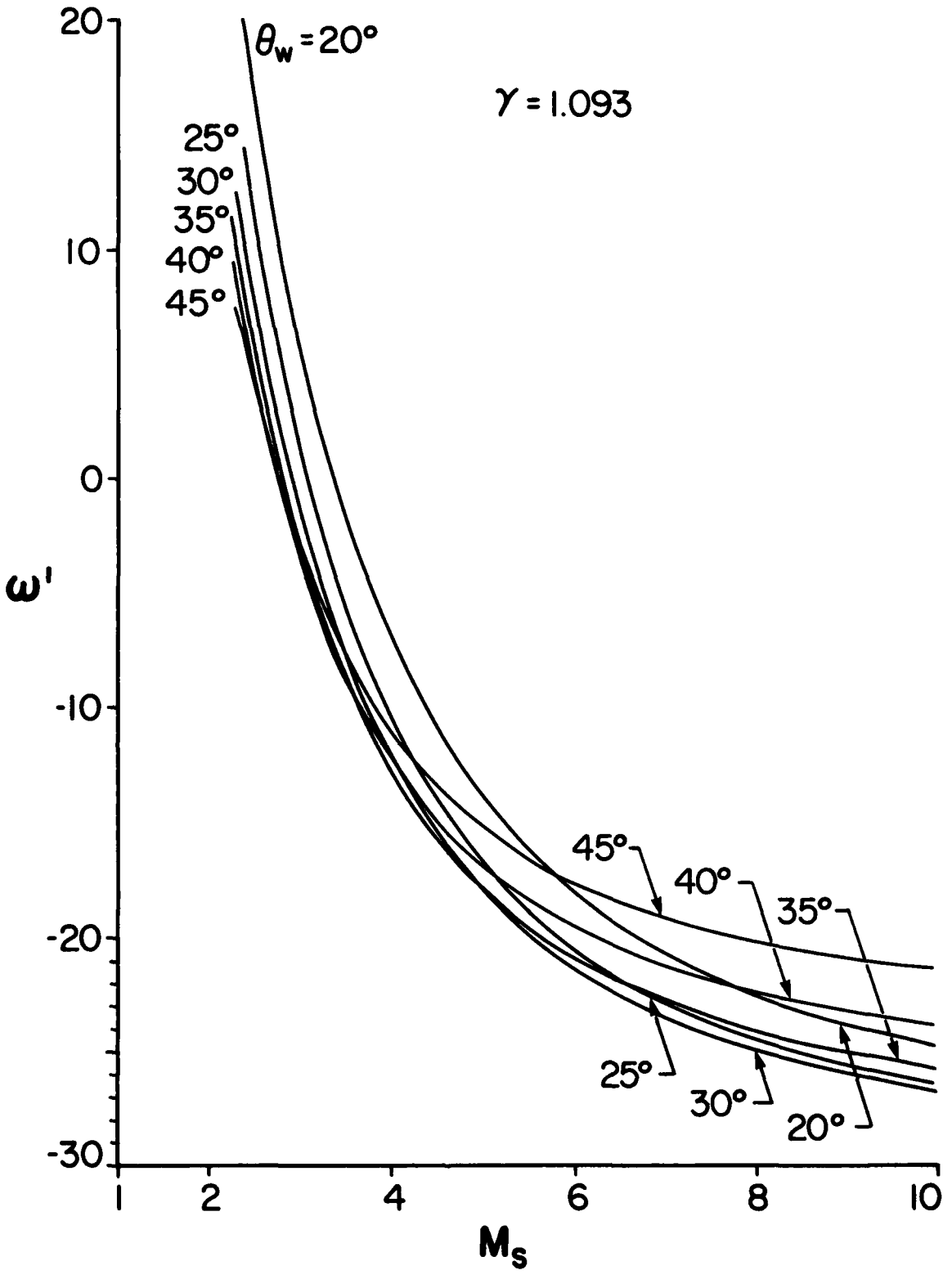

FIG. 16 VARIATION OF REFLECTION ANGLE ω' WITH M_s FOR GIVEN θ_w (POLYATOMIC GAS - SF_6 WITH $\gamma = 1.093$).

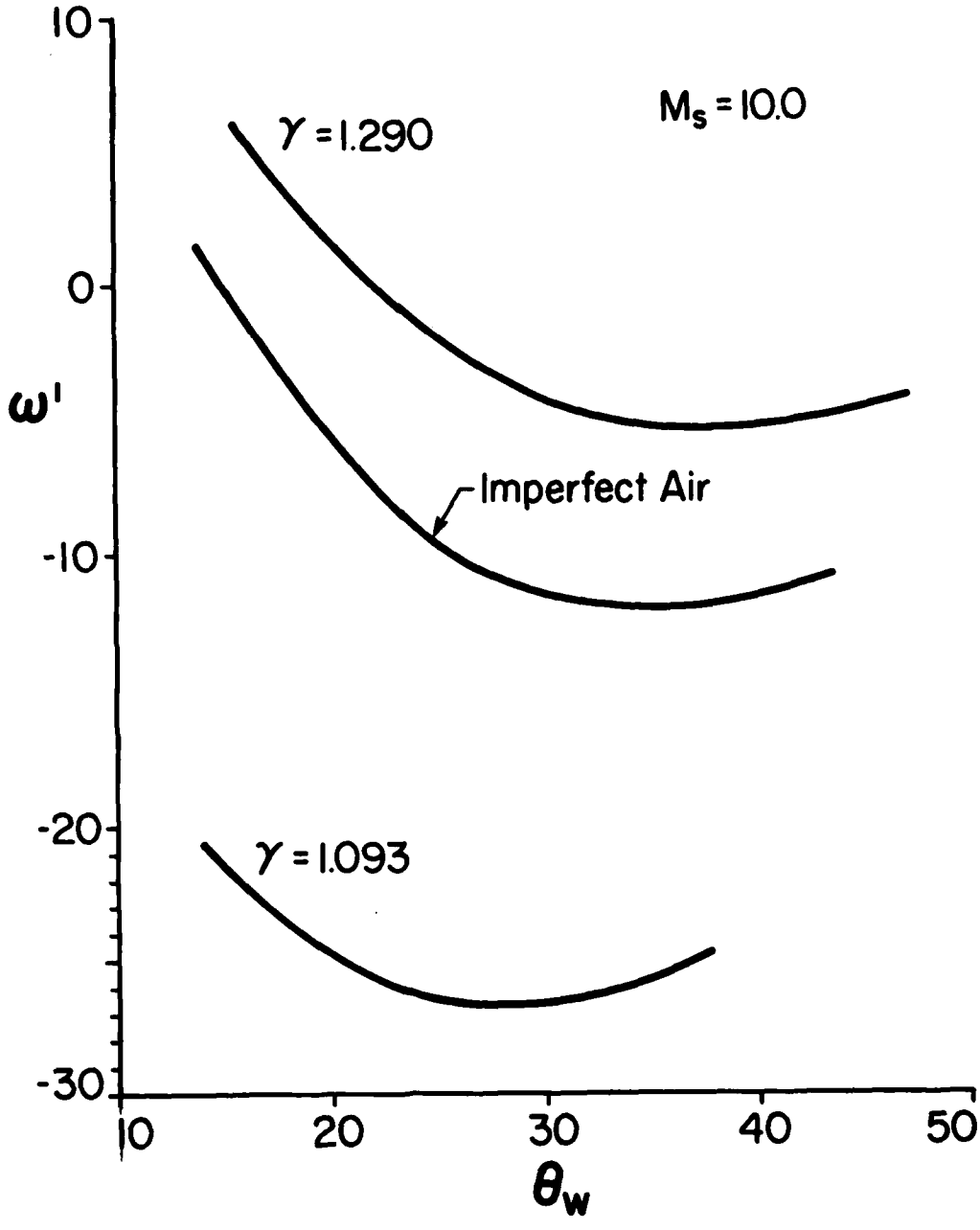

FIG. 17 VARIATION OF REFLECTION ANGLE ω' WITH θ_w AT CONSTANT M_s.

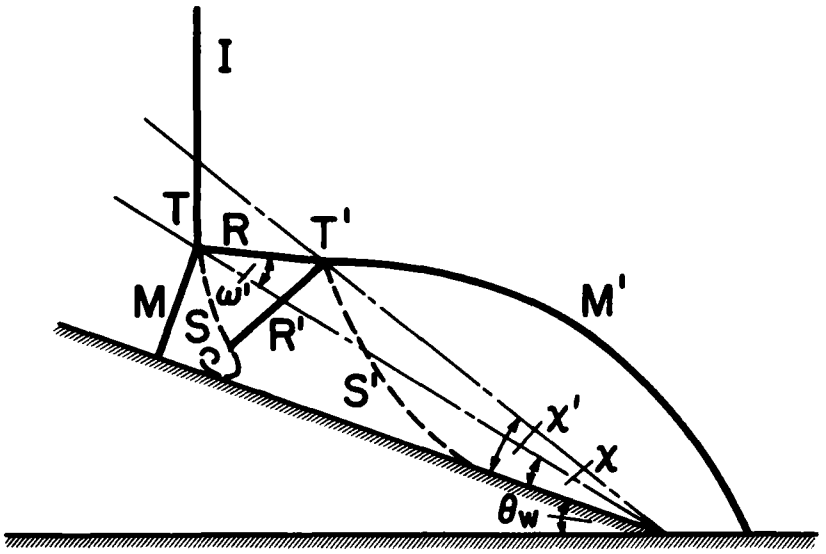

(a) $\chi' > \chi$, $\omega' > 0$

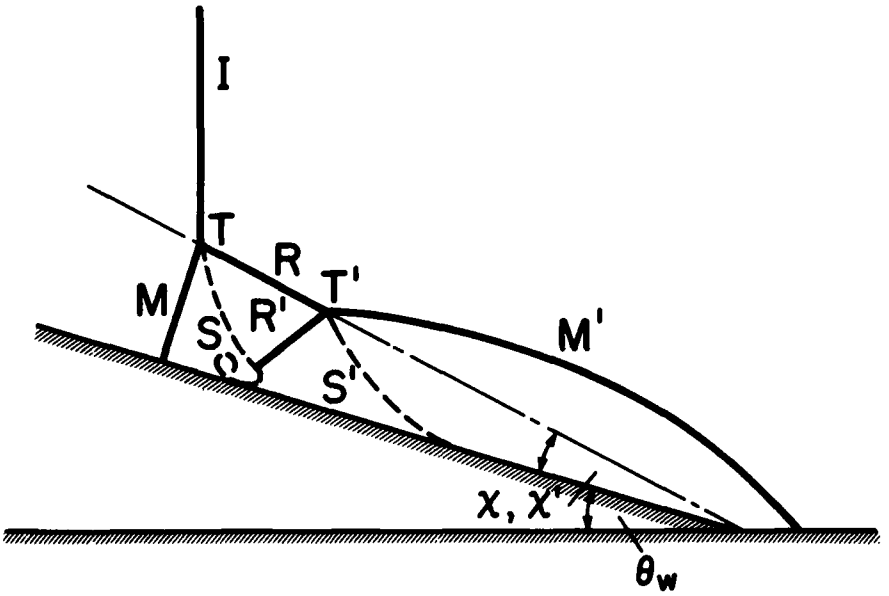

(b) $\chi' = \chi$, $\omega' = 0$

FIG. 18 SEVERAL PATTERNS OF DOUBLE MACH REFLECTION; CASE (d) IS HYPOTHETICAL.

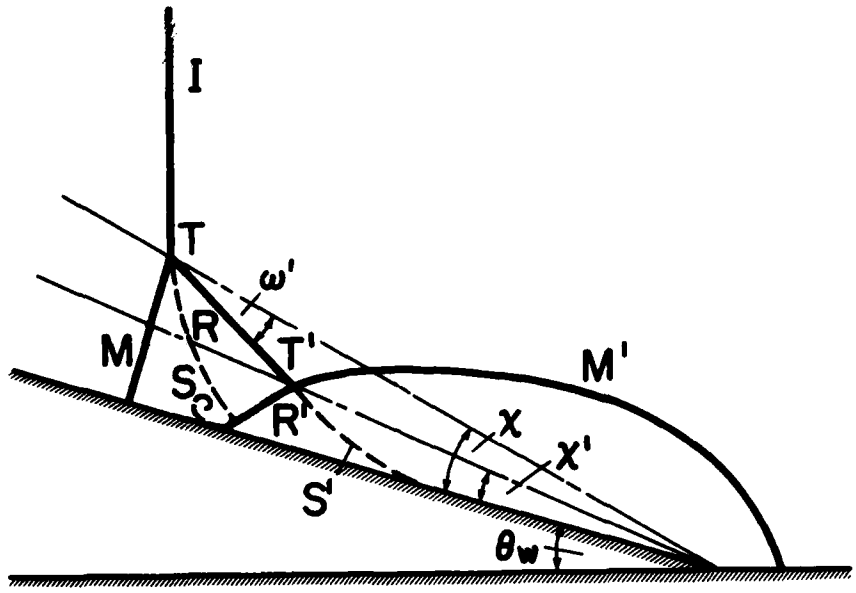

(c) $\chi' < \chi$, $\omega' < 0$

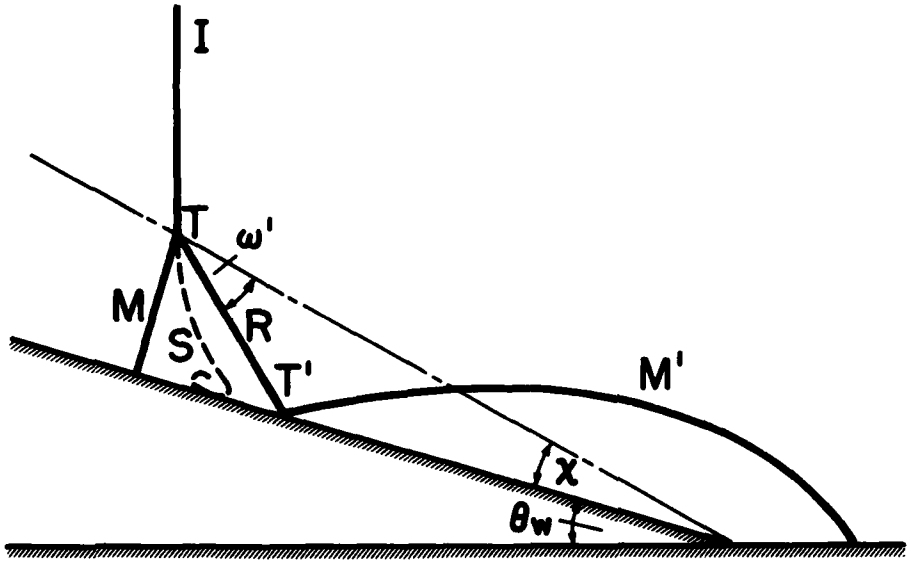

(d) $\chi' = 0$, $\omega' < 0$

FIG. 18 - CONTINUED - SEVERAL PATTERNS OF DOUBLE MACH REFLECTION: CASE (d) IS HYPOTHETICAL.

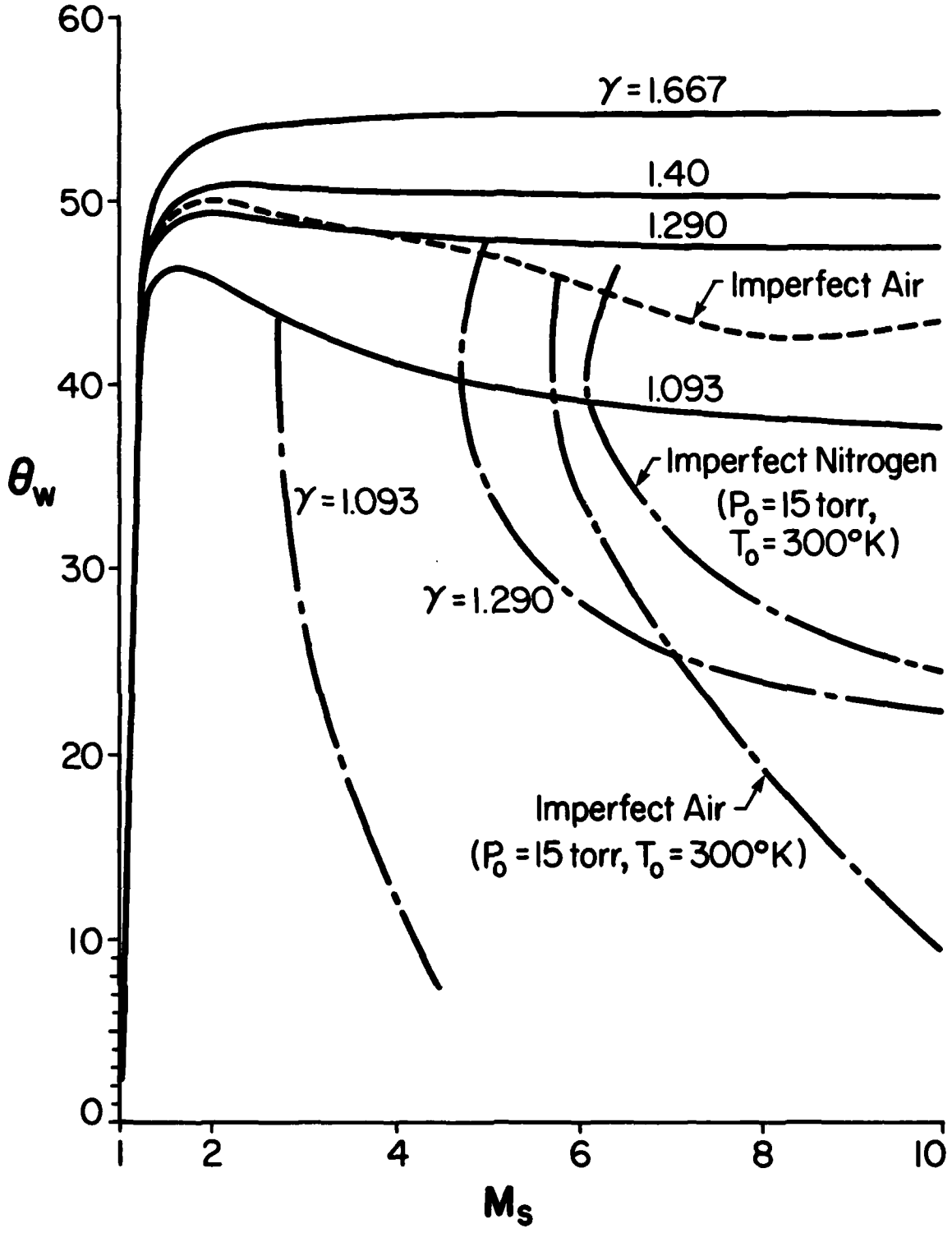

FIG. 19 TRANSITION LINES FOR $DMR^+ \gtrless DMR^-$ ($\omega' = 0$) FOR CO_2, SF_6, IMPERFECT AIR AND IMPERFECT NITROGEN.

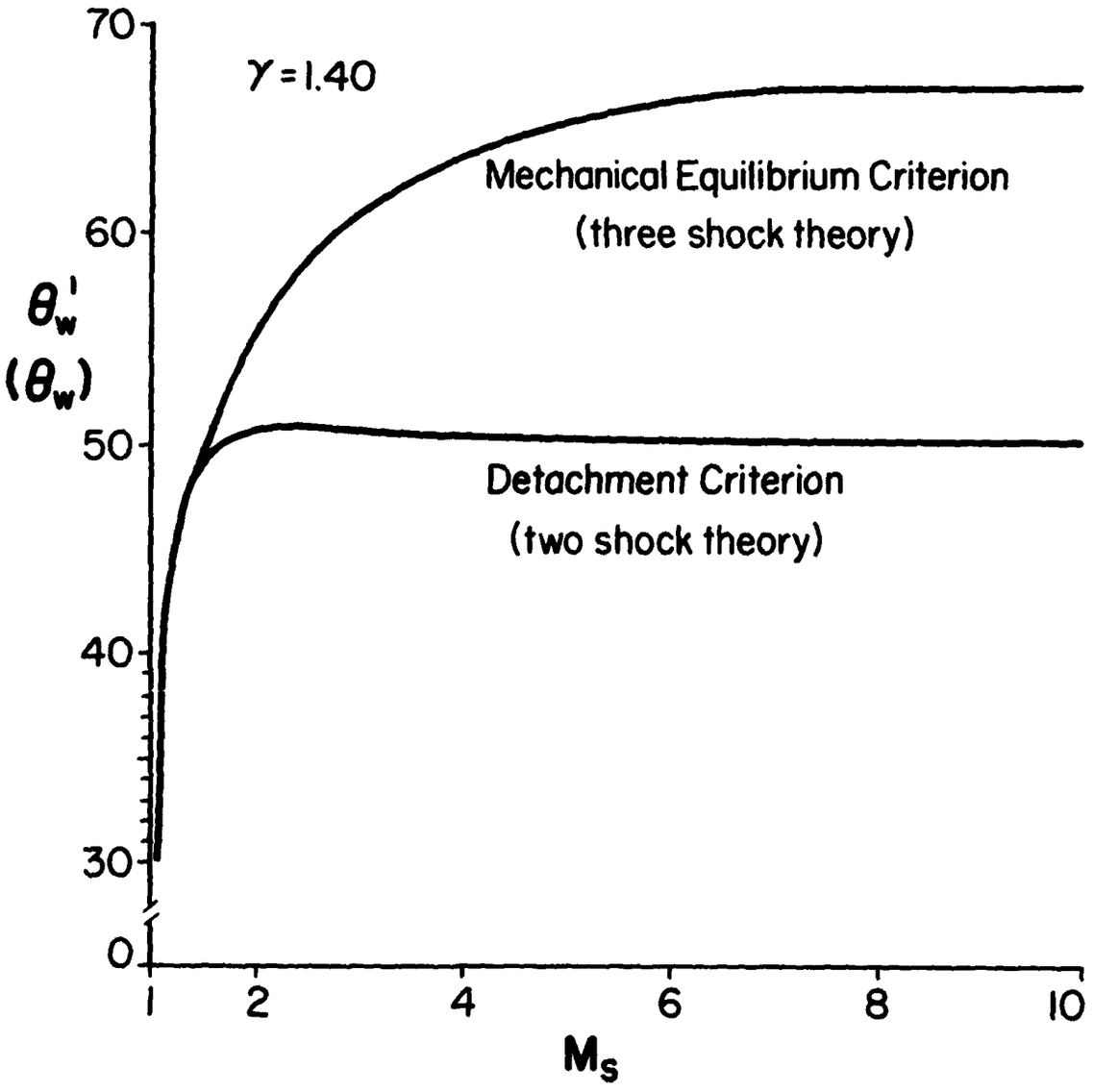

FIG. 20 DETACHMENT AND MECHANICAL EQUILIBRIUM CRITERIA FOR MR(RR) TERMINATION, $\gamma = 1.40$.

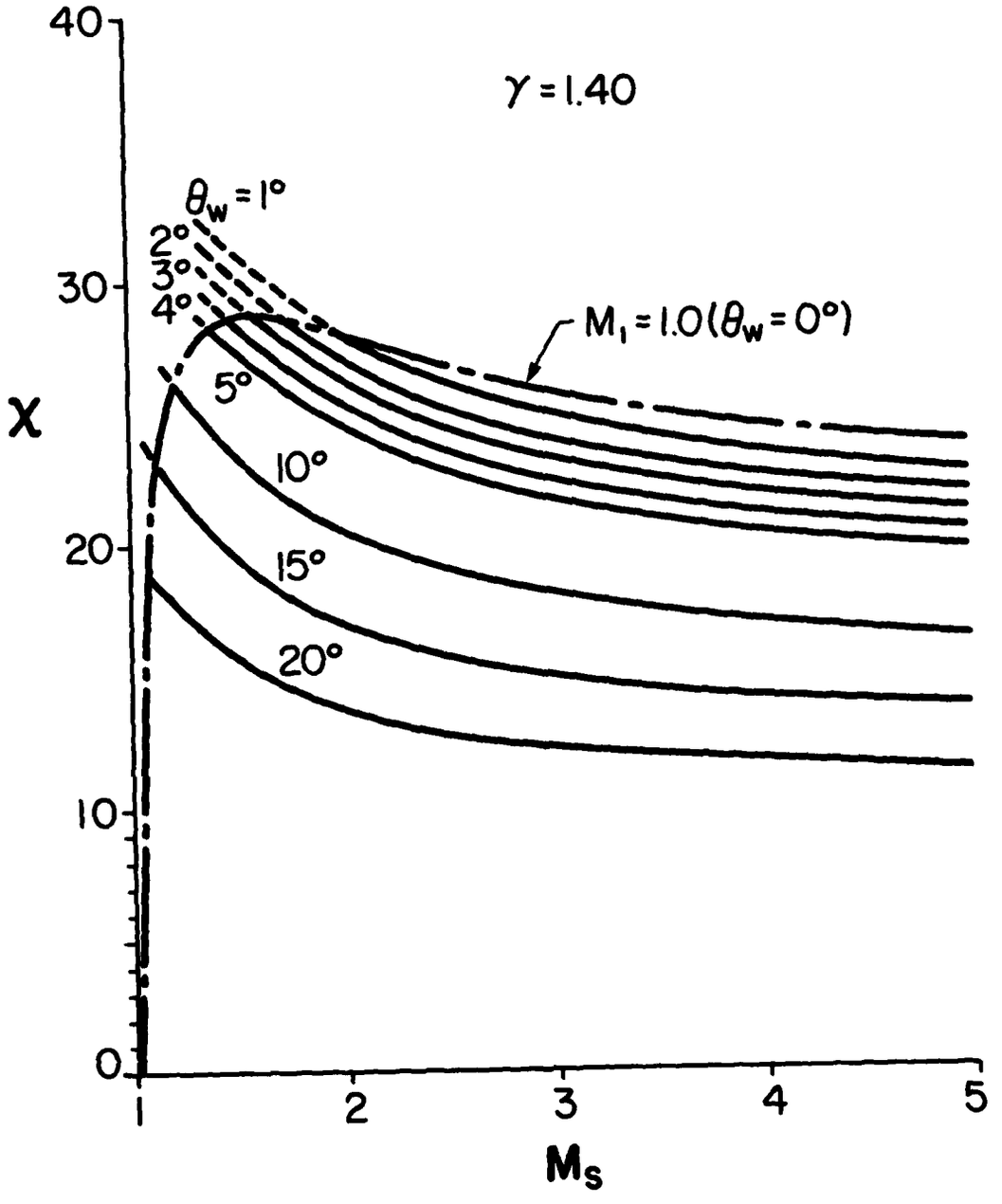

FIG. 21 VARIATION OF χ WITH M_s FOR VERY SMALL WEDGE ANGLES.

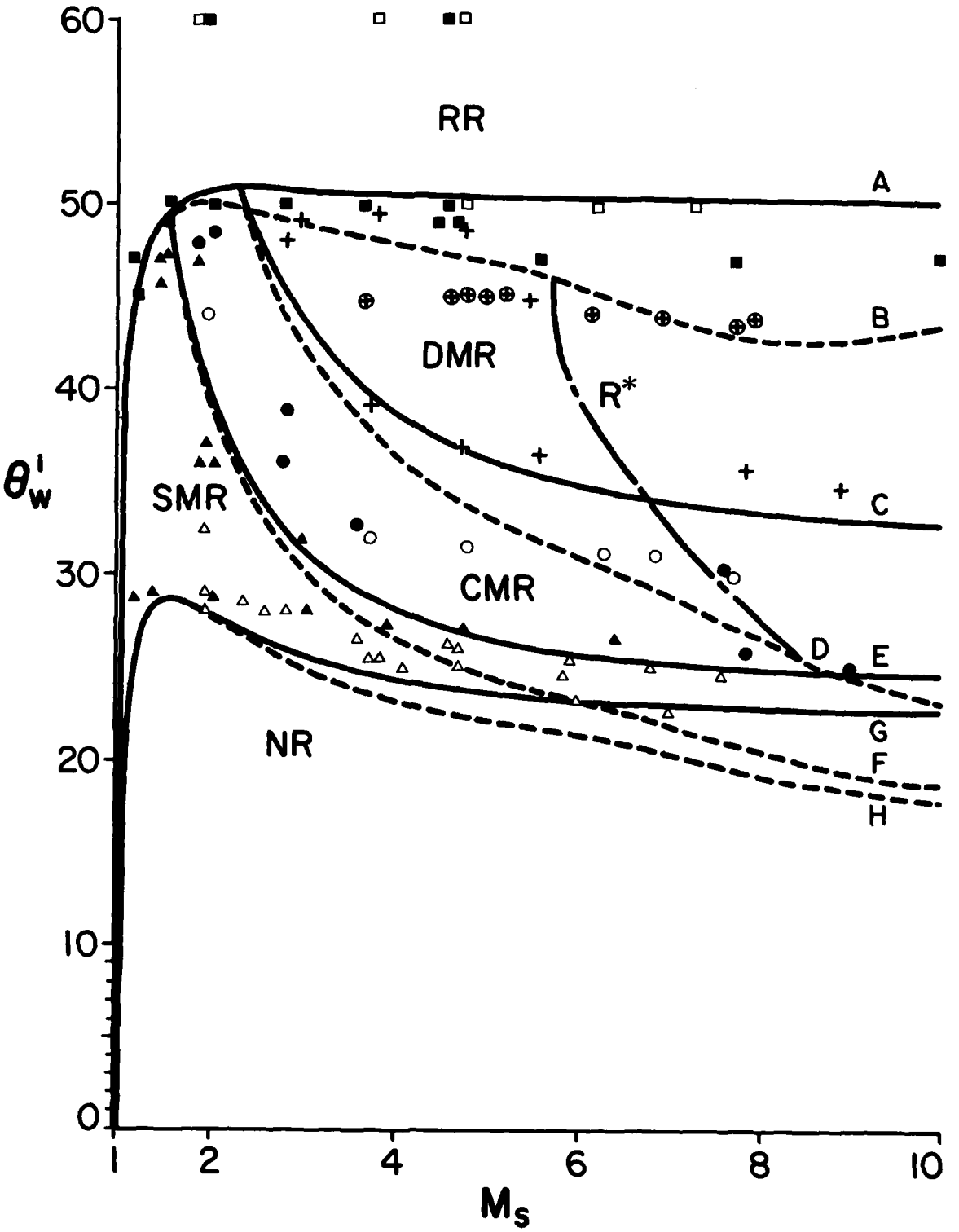

FIG. 22 COMPARISON OF PREDICTED DOMAINS OF VARIOUS TYPES OF REFLECTION AND EXPERIMENTAL RESULTS IN THE (M_s-θ_w') PLANE. SOLID LINES ARE FOR PERFECT AIR WITH γ = 1.40. DASHED LINES ARE FOR IMPERFECT AIR AT P_o = 15 TORR AND T_o = 300 K. SOLID SYMBOLS ARE AIR DATA FROM DESCHAMBAULT [REF. 39]. OPEN SYMBOLS ARE N_2 DATA FROM BEN-DOR [REF. 40]. RR □ ■, SMR △ ▲, CMR ○ ●, DMR ⊕ +.

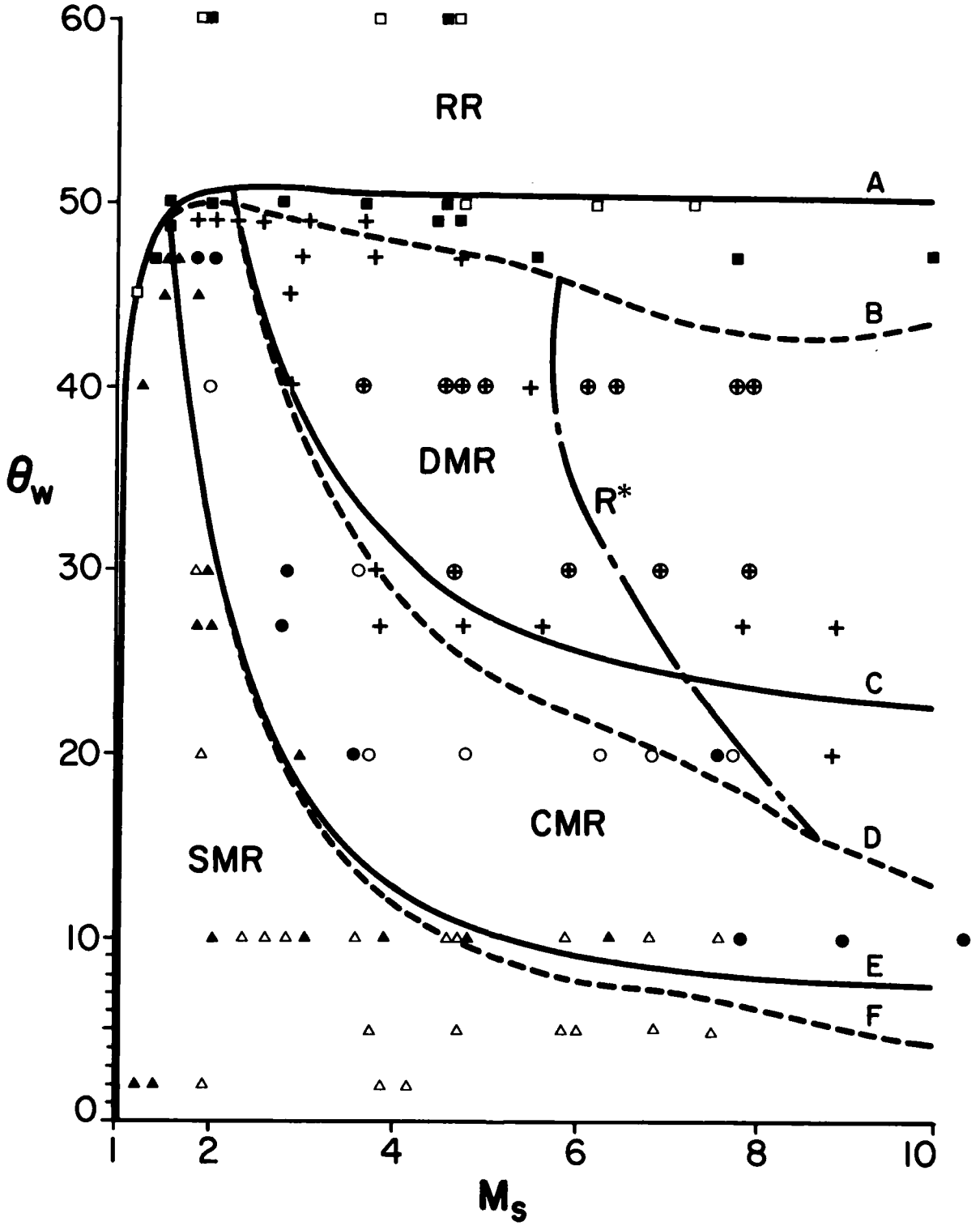

FIG. 23 COMPARISON OF PREDICTED DOMAINS OF VARIOUS TYPES OF REFLECTION AND THE EXPERIMENT IN THE (M_S-θ_W) PLANE. SOLID LINES ARE FOR PERFECT AIR WITH γ = 1.40. DASHED LINES ARE FOR IMPERFECT AIR AT P_O = 15 TORR AND T_O = 300 K. SOLID SYMBOLS ARE AIR DATA FROM DESCHAMBAULT [REF. 39]. OPEN SYMBOLS ARE N_2 DATA FROM BEN-DOR [REF. 40]. RR □■ , SMR △▲ , CMR O ●, DMR ⊕ +.

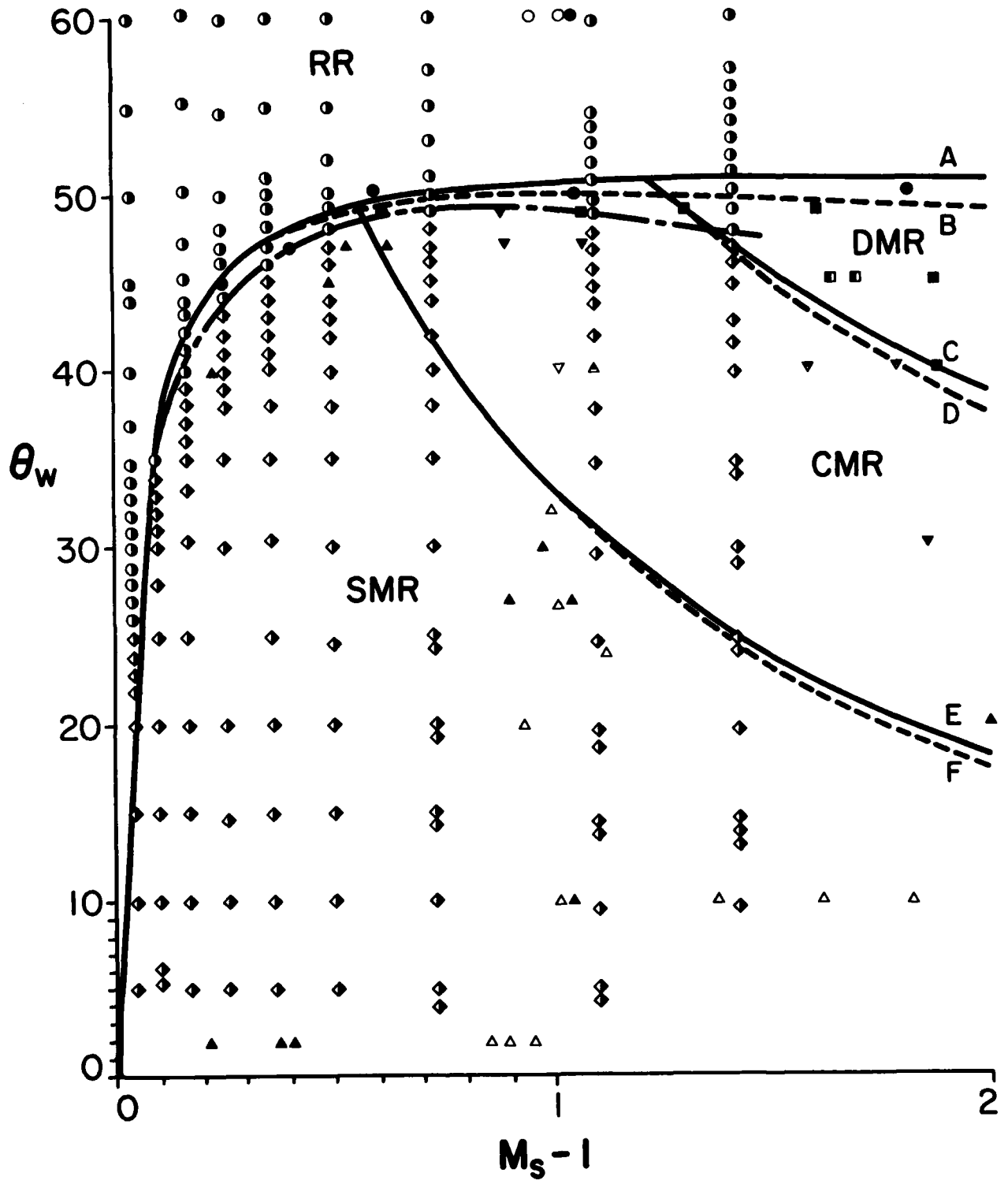

FIG. 24 COMPARISON OF PREDICTED DOMAINS OF VARIOUS TYPES OF REFLECTION AND THE EXPERIMENT IN THE (M_S-θ_W) PLANE IN THE RANGE $1.0 < M_S \leq 3.0$. SOLID LINES ——— ARE FOR PERFECT AIR WITH $\gamma = 1.40$. DASHED LINES ----- ARE FOR IMPERFECT AIR AT $P_0 = 15$ TORR AND $T_0 = 300$ K. DASH-DOT LINE —·—·— SHOWS PERSISTENCE OF REGULAR REFLECTION RR. EXPERIMENTAL DATA — AIR: SMITH ◐ ◆ [REF. 9], BAZHENOVA ET AL ◧ [REF. 18], DESCHAMBAULT ● ▲ ▼ ■ [REF. 39]; NITROGEN: BAZHENOVA ET AL ◬ [REF. 18], BEN-DOR ○ △ ▽ [REF. 40]; OXYGEN: LAW AND GLASS ▲ ▽ [REF. 19]. RR ◐ ○ SMR ▲ △ ◬ ▲ , CMR ▼ ▽ ▼ , DMR ■ ◧ , MR ◆.

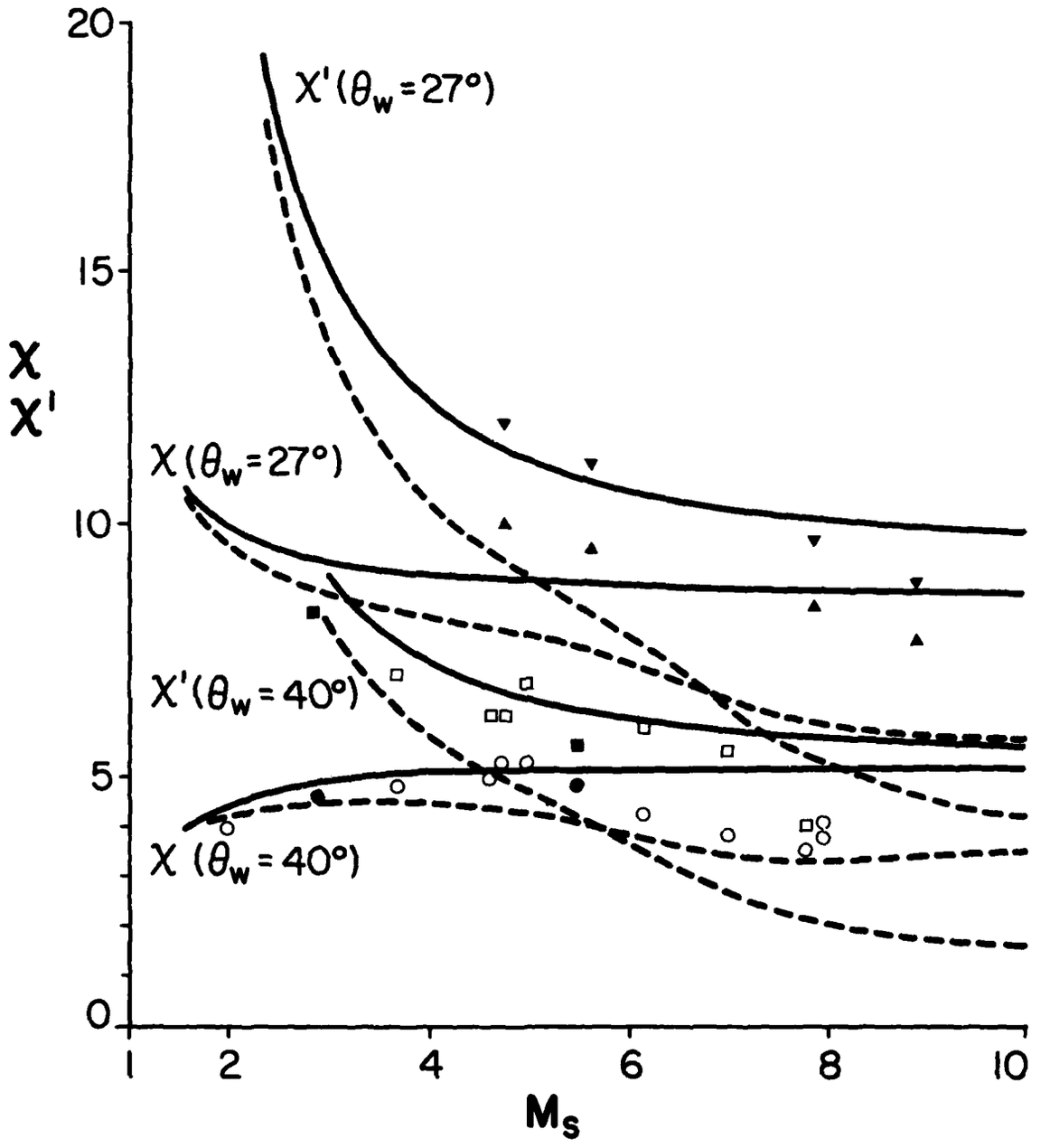

FIG. 25 EXPERIMENTAL COMPARISON OF χ AND χ' WITH M_S FOR GIVEN θ_w. SOLID LINES SHOW PERFECT AIR WITH $\gamma = 1.40$. DASHED LINES SHOW IMPERFECT AIR AT P_0 = 15 TORR AND T_0 = 300 K. SOLID SYMBOLS ARE AIR DATA FROM DESCHAMBAULT [REF. 39]. OPEN SYMBOLS ARE N_2 DATA FROM BEN-DOR [REF. 40]. ▼: χ' (θ_w = 27°), ■□: χ' (θ_w = 40°), ▲: χ (θ_w = 27°), ● 0: χ (θ_w = 40°).

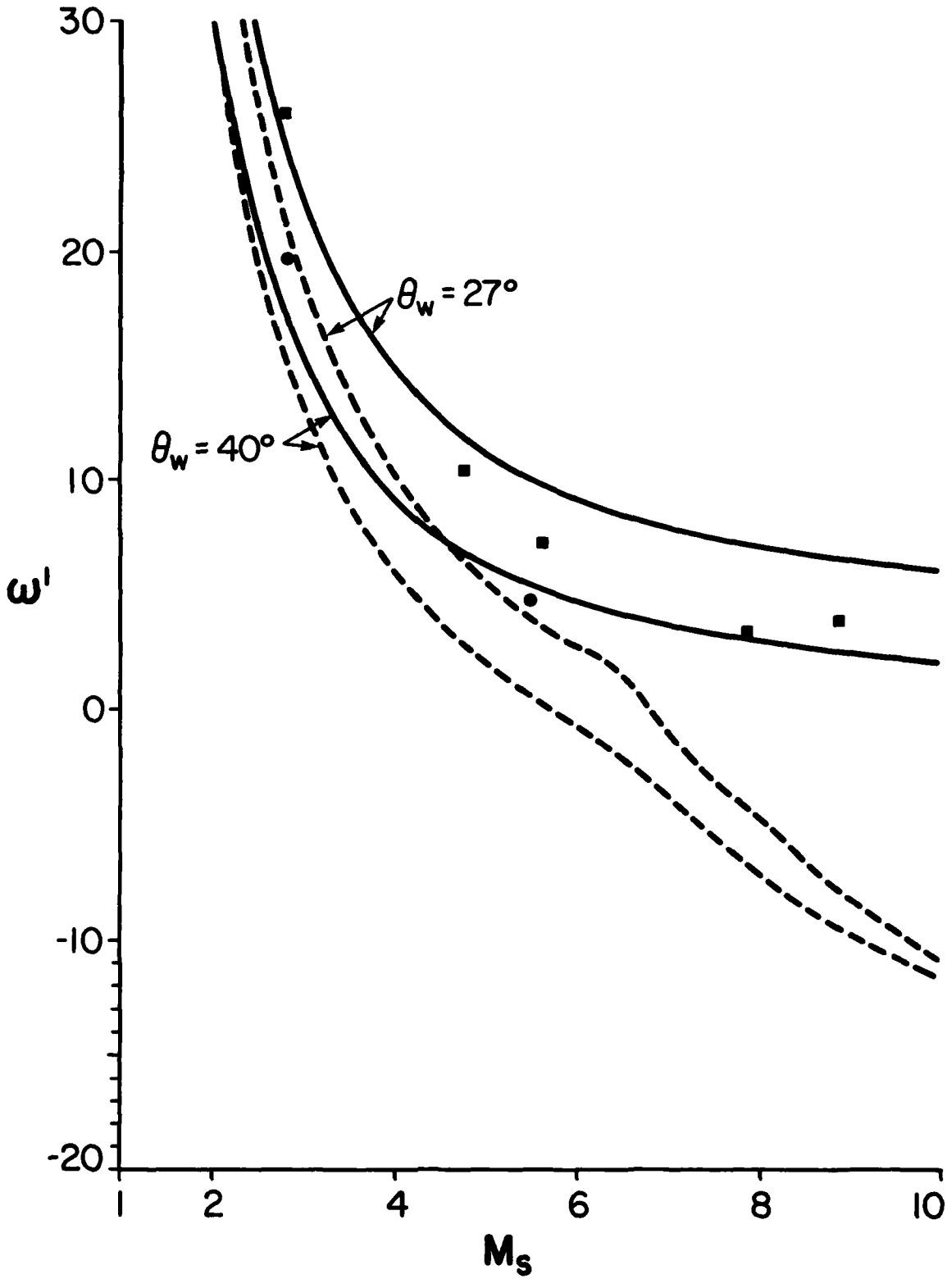

FIG. 26 EXPERIMENTAL COMPARISON OF REFLECTION ANGLE ω' WITH M_S FOR GIVEN θ_W. ■: $\theta_W = 27°$, ●: $\theta_W = 40°$, ——— AIR $\gamma = 1.40$, ----- EQUILIBRIUM AIR, $P_O = 15$ TORR, $T_O = 300$ K.

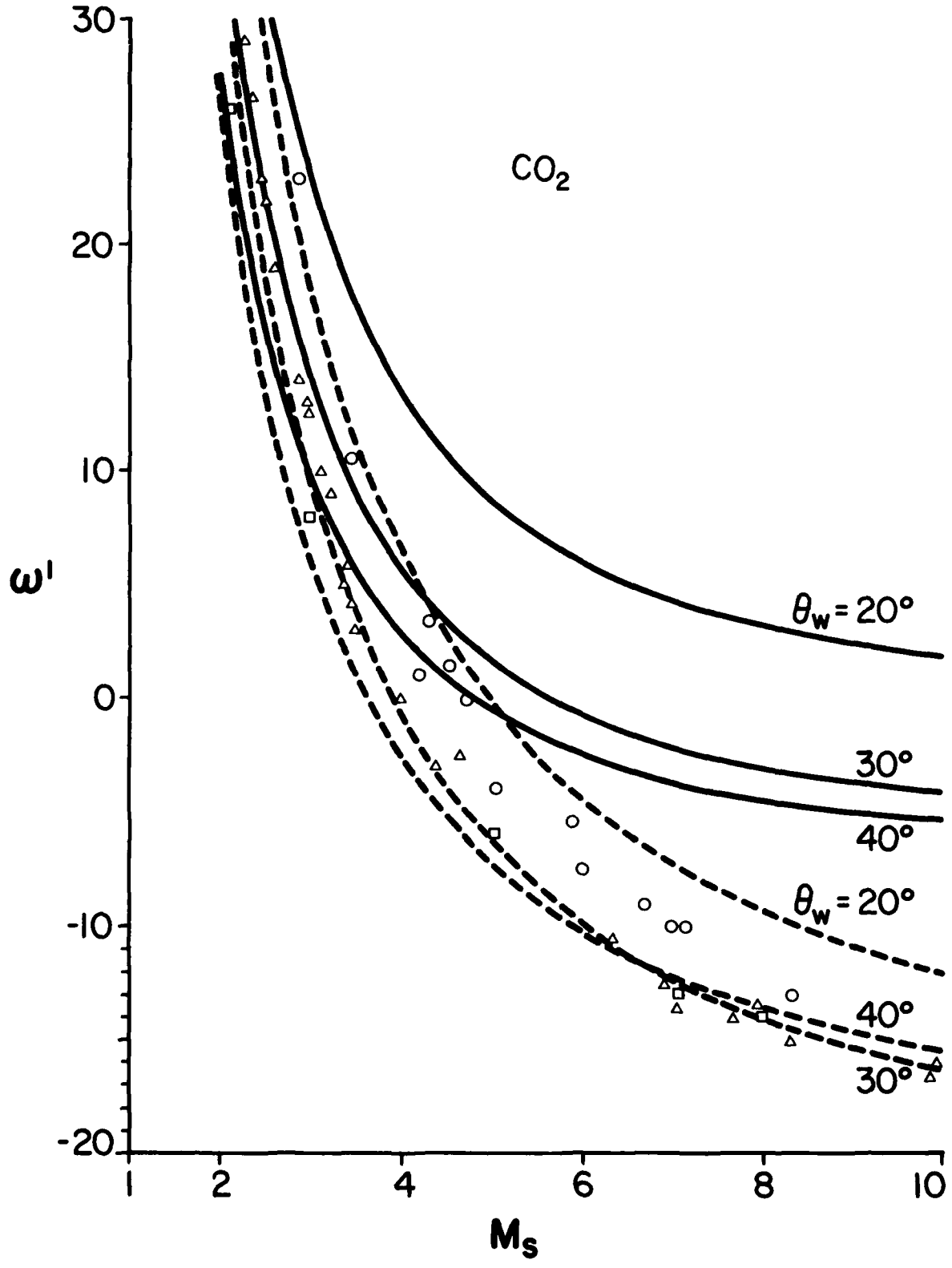

FIG. 27 COMPARISON OF REFLECTION ANGLE ω' WITH SHOCK MACH NUMBER M_S FOR GIVEN WEDGE ANGLE θ_W WITH EXPERIMENTS IN CO_2 FROM REF. 13. O: $\theta_W = 20°$, △: $\theta_W = 30°$, □: $\theta_W = 40°$, —— $\gamma = 1.29$, ------ VIBRATIONAL EQUILIBRIUM.

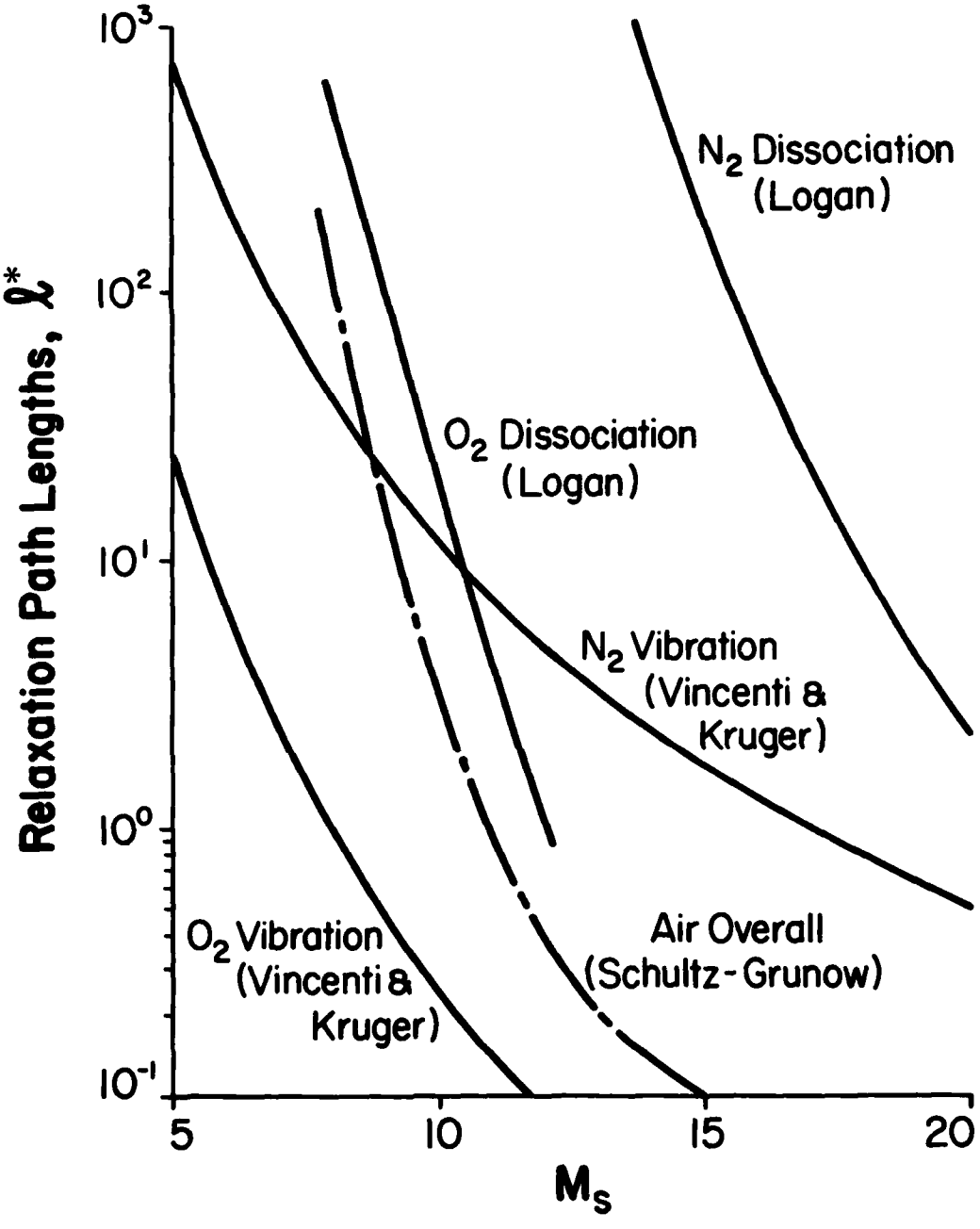

FIG. 28 RELAXATION LENGTHS ℓ^* BEHIND NORMAL SHOCK WAVE VERSUS M_S FOR INITIAL CONDITIONS OF P_O = 10 TORR, T_O = 300 K [AFTER REFS. 41, 43, 44]. NOTE THAT THE VARIOUS ℓ^*'s DEPEND ON THE ACTUAL P AND T BEHIND SHOCK WAVE.

UTIAS Report No. 262
Institute for Aerospace Studies, University of Toronto (UTIAS)
4925 Dufferin Street, Downsview, Ontario, Canada, M3H 5T6

DOMAINS AND BOUNDARIES OF PSEUDO-STATIONARY OBLIQUE SHOCK-WAVE REFLECTIONS IN AIR

Lee, J.-H., Glass, I. I.

1. Oblique shock-wave reflections; 2. Domains and transition boundaries;
3. Perfect and real-gas effects; 4. Shock-tube flows.

I. Lee, J.-H., Glass, I. I. II. UTIAS Report No. 262

The reflection of oblique shock waves in air in pseudo-stationary flow was investigated analytically and numerically. The transition boundaries between the four types of shock-wave reflection (regular RR, single Mach SMR, complex Mach CMR and double Mach DMR) were established up to $M_s = 20$ for both perfect and imperfect air in thermodynamic equilibrium (rotation-vibration coupling, vibrational excitation, dissociation, electronic excitation and ionization). In addition, an analysis was made for perfect gases with differing γ, in order to clarify the effects of the specific-heat ratio γ, on the shock-wave configurations. It was verified that the reflected wave angle ω' was a very sensitive function of γ, and a decrease in γ lowered the value of ω' significantly and even shifted the value of ω' towards negative values under certain conditions of Mach reflection. This phenomenon occurred in a perfect gas with γ less than 1.4 and in imperfect air. However, it was absent in perfect air with $\gamma = 1.4$. An examination of the perfect and imperfect air results shows no crossings of transition lines and removes the conjecture of possible triple-Mach reflection. The present analytical results were compared with the available experimental data for air and nitrogen for shock Mach numbers up to 10. From the available experimental cases, it was clarified, by examining the relaxation lengths behind the shock waves, that the flow states behind the shock fronts, which determined the wave systems for the shock-wave reflection, were frozen or nearly frozen regarding vibrational excitation and dissociation. Consequently, in general, the present perfect-gas analysis agreed with experiment. However, RR persisted, to some extent, below the perfect-gas termination line determined by the detachment criterion, and SMR and DMR did sometimes occur outside their analytically predicted domains. The development of more accurate transition criteria, improvements in the methods of predicting the first triple-point trajectory angle, accurate locations of the kink and triple points along with possible boundary-layer effects on the persistence of regular reflection are problems to be resolved in the future.

Available copies of this report are limited. Return this card to UTIAS if you require a copy.

UTIAS Report No. 262
Institute for Aerospace Studies, University of Toronto (UTIAS)
4925 Dufferin Street, Downsview, Ontario, Canada, M3H 5T6

DOMAINS AND BOUNDARIES OF PSEUDO-STATIONARY OBLIQUE SHOCK-WAVE REFLECTIONS IN AIR

Lee, J.-H., Glass, I. I.

1. Oblique shock-wave reflections; 2. Domains and transition boundaries;
3. Perfect and real-gas effects; 4. Shock-tube flows.

I. Lee, J.-H., Glass, I. I. II. UTIAS Report No. 262

The reflection of oblique shock waves in air in pseudo-stationary flow was investigated analytically and numerically. The transition boundaries between the four types of shock-wave reflection (regular RR, single Mach SMR, complex Mach CMR and double Mach DMR) were established up to $M_s = 20$ for both perfect and imperfect air in thermodynamic equilibrium (rotation-vibration coupling, vibrational excitation, dissociation, electronic excitation and ionization). In addition, an analysis was made for perfect gases with differing γ, in order to clarify the effects of the specific-heat ratio γ, on the shock-wave configurations. It was verified that the reflected wave angle ω' was a very sensitive function of γ, and a decrease in γ lowered the value of ω' significantly and even shifted the value of ω' towards negative values under certain conditions of Mach reflection. This phenomenon occurred in a perfect gas with γ less than 1.4 and in imperfect air. However, it was absent in perfect air with $\gamma = 1.4$. An examination of the perfect and imperfect air results shows no crossings of transition lines and removes the conjecture of possible triple-Mach reflection. The present analytical results were compared with the available experimental data for air and nitrogen for shock Mach numbers up to 10. From the available experimental cases, it was clarified, by examining the relaxation lengths behind the shock waves, that the flow states behind the shock fronts, which determined the wave systems for the shock-wave reflection, were frozen or nearly frozen regarding vibrational excitation and dissociation. Consequently, in general, the present perfect-gas analysis agreed with experiment. However, RR persisted, to some extent, below the perfect-gas termination line determined by the detachment criterion, and SMR and DMR did sometimes occur outside their analytically predicted domains. The development of more accurate transition criteria, improvements in the methods of predicting the first triple-point trajectory angle, accurate locations of the kink and triple points along with possible boundary-layer effects on the persistence of regular reflection are problems to be resolved in the future.

Available copies of this report are limited. Return this card to UTIAS if you require a copy.

UTIAS Report No. 262
Institute for Aerospace Studies, University of Toronto (UTIAS)
4925 Dufferin Street, Downsview, Ontario, Canada, M3H 5T6

DOMAINS AND BOUNDARIES OF PSEUDO-STATIONARY OBLIQUE SHOCK-WAVE REFLECTIONS IN AIR

Lee, J.-H., Glass, I. I.

1. Oblique shock-wave reflections; 2. Domains and transition boundaries;
3. Perfect and real-gas effects; 4. Shock-tube flows.

I. Lee, J.-H., Glass, I. I. II. UTIAS Report No. 262

The reflection of oblique shock waves in air in pseudo-stationary flow was investigated analytically and numerically. The transition boundaries between the four types of shock-wave reflection (regular RR, single Mach SMR, complex Mach CMR and double Mach DMR) were established up to $M_s = 20$ for both perfect and imperfect air in thermodynamic equilibrium (rotation-vibration coupling, vibrational excitation, dissociation, electronic excitation and ionization). In addition, an analysis was made for perfect gases with differing γ, in order to clarify the effects of the specific-heat ratio γ, on the shock-wave configurations. It was verified that the reflected wave angle ω' was a very sensitive function of γ, and a decrease in γ lowered the value of ω' significantly and even shifted the value of ω' towards negative values under certain conditions of Mach reflection. This phenomenon occurred in a perfect gas with γ less than 1.4 and in imperfect air. However, it was absent in perfect air with $\gamma = 1.4$. An examination of the perfect and imperfect air results shows no crossings of transition lines and removes the conjecture of possible triple-Mach reflection. The present analytical results were compared with the available experimental data for air and nitrogen for shock Mach numbers up to 10. From the available experimental cases, it was clarified, by examining the relaxation lengths behind the shock waves, that the flow states behind the shock fronts, which determined the wave systems for the shock-wave reflection, were frozen or nearly frozen regarding vibrational excitation and dissociation. Consequently, in general, the present perfect-gas analysis agreed with experiment. However, RR persisted, to some extent, below the perfect-gas termination line determined by the detachment criterion, and SMR and DMR did sometimes occur outside their analytically predicted domains. The development of more accurate transition criteria, improvements in the methods of predicting the first triple-point trajectory angle, accurate locations of the kink and triple points along with possible boundary-layer effects on the persistence of regular reflection are problems to be resolved in the future.

Available copies of this report are limited. Return this card to UTIAS if you require a copy.

UTIAS Report No. 262
Institute for Aerospace Studies, University of Toronto (UTIAS)
4925 Dufferin Street, Downsview, Ontario, Canada, M3H 5T6

DOMAINS AND BOUNDARIES OF PSEUDO-STATIONARY OBLIQUE SHOCK-WAVE REFLECTIONS IN AIR

Lee, J.-H., Glass, I. I.

1. Oblique shock-wave reflections; 2. Domains and transition boundaries;
3. Perfect and real-gas effects; 4. Shock-tube flows.

I. Lee, J.-H., Glass, I. I. II. UTIAS Report No. 262

The reflection of oblique shock waves in air in pseudo-stationary flow was investigated analytically and numerically. The transition boundaries between the four types of shock-wave reflection (regular RR, single Mach SMR, complex Mach CMR and double Mach DMR) were established up to $M_s = 20$ for both perfect and imperfect air in thermodynamic equilibrium (rotation-vibration coupling, vibrational excitation, dissociation, electronic excitation and ionization). In addition, an analysis was made for perfect gases with differing γ, in order to clarify the effects of the specific-heat ratio γ, on the shock-wave configurations. It was verified that the reflected wave angle ω' was a very sensitive function of γ, and a decrease in γ lowered the value of ω' significantly and even shifted the value of ω' towards negative values under certain conditions of Mach reflection. This phenomenon occurred in a perfect gas with γ less than 1.4 and in imperfect air. However, it was absent in perfect air with $\gamma = 1.4$. An examination of the perfect and imperfect air results shows no crossings of transition lines and removes the conjecture of possible triple-Mach reflection. The present analytical results were compared with the available experimental data for air and nitrogen for shock Mach numbers up to 10. From the available experimental cases, it was clarified, by examining the relaxation lengths behind the shock waves, that the flow states behind the shock fronts, which determined the wave systems for the shock-wave reflection, were frozen or nearly frozen regarding vibrational excitation and dissociation. Consequently, in general, the present perfect-gas analysis agreed with experiment. However, RR persisted, to some extent, below the perfect-gas termination line determined by the detachment criterion, and SMR and DMR did sometimes occur outside their analytically predicted domains. The development of more accurate transition criteria, improvements in the methods of predicting the first triple-point trajectory angle, accurate locations of the kink and triple points along with possible boundary-layer effects on the persistence of regular reflection are problems to be resolved in the future.

Available copies of this report are limited. Return this card to UTIAS if you require a copy.